DYNAMIC FUNCTIONAL CONNECTIVITY IN NEUROPSYCHIATRIC DISORDERS: METHODS AND APPLICATIONS

EDITED BY: Wenbin Guo, Feng Liu and Zaixu Cui
PUBLISHED IN: Frontiers in Neuroscience, Frontiers in Psychiatry and Frontiers in Neurology

frontiers Research Topics

frontiers

ISSN 1664-8714
ISBN 978-2-88966-195-4
DOI 10.3389/978-2-88966-195-4

About Frontiers

Frontiers is more than just an open-access publisher of scholarly articles: it is a pioneering approach to the world of academia, radically improving the way scholarly research is managed. The grand vision of Frontiers is a world where all people have an equal opportunity to seek, share and generate knowledge. Frontiers provides immediate and permanent online open access to all its publications, but this alone is not enough to realize our grand goals.

Frontiers Journal Series

The Frontiers Journal Series is a multi-tier and interdisciplinary set of open-access, online journals, promising a paradigm shift from the current review, selection and dissemination processes in academic publishing. All Frontiers journals are driven by researchers for researchers; therefore, they constitute a service to the scholarly community. At the same time, the Frontiers Journal Series operates on a revolutionary invention, the tiered publishing system, initially addressing specific communities of scholars, and gradually climbing up to broader public understanding, thus serving the interests of the lay society, too.

Dedication to Quality

Each Frontiers article is a landmark of the highest quality, thanks to genuinely collaborative interactions between authors and review editors, who include some of the world's best academicians. Research must be certified by peers before entering a stream of knowledge that may eventually reach the public - and shape society; therefore, Frontiers only applies the most rigorous and unbiased reviews.
Frontiers revolutionizes research publishing by freely delivering the most outstanding research, evaluated with no bias from both the academic and social point of view. By applying the most advanced information technologies, Frontiers is catapulting scholarly publishing into a new generation.

What are Frontiers Research Topics?

Frontiers Research Topics are very popular trademarks of the Frontiers Journals Series: they are collections of at least ten articles, all centered on a particular subject. With their unique mix of varied contributions from Original Research to Review Articles, Frontiers Research Topics unify the most influential researchers, the latest key findings and historical advances in a hot research area! Find out more on how to host your own Frontiers Research Topic or contribute to one as an author by contacting the Frontiers Editorial Office: researchtopics@frontiersin.org

DYNAMIC FUNCTIONAL CONNECTIVITY IN NEUROPSYCHIATRIC DISORDERS: METHODS AND APPLICATIONS

Topic Editors:
Wenbin Guo, Central South University, China
Feng Liu, Tianjin Medical University General Hospital, China
Zaixu Cui, University of Pennsylvania, United States

Citation: Guo, W., Liu, F., Cui, Z., eds. (2020). Dynamic Functional Connectivity in Neuropsychiatric Disorders: Methods and Applications. Lausanne: Frontiers Media SA. doi: 10.3389/978-2-88966-195-4

Table of Contents

frontiers in Neuroscience

EDITORIAL
published: 20 April 2020
doi: 10.3389/fnins.2020.00332

Editorial: Dynamic Functional Connectivity in Neuropsychiatric Disorders: Methods and Applications

Xiaoya Fu[1,2], *Feng Liu*[3], *Zaixu Cui*[4] *and Wenbin Guo*[1,2]*

[1] Department of Psychiatry, The Second Xiangya Hospital of Central South University, Changsha, China, [2] National Clinical Research Center on Mental Disorders, Changsha, China, [3] Department of Radiology, Tianjin Medical University General Hospital, Tianjin, China, [4] Department of Psychiatry, Perelman School of Medicine, University of Pennsylvania, Philadelphia, PA, United States

Keywords: functional magnetic resonance imaging, dynamic functional connectivity, neuropsychiatric disorders, cognitive deficits, regional homogeneity, amplitude of low-frequency fluctuations

Editorial on the Research Topic

Dynamic Functional Connectivity in Neuropsychiatric Disorders: Methods and Applications

Resting-state functional magnetic resonance imaging (RS-fMRI), a non-invasive measurement of spontaneous brain activity, has greatly broadened our understanding of neural substrate underlying neuropsychiatric disorders over the last several decades. Since Biswal et al. discovered synchronized brain activity in different brain areas even without any tasks or stimuli (Biswal, 2012), numerous studies have investigated resting-state coupling (i.e., functional connectivity, FC) between different brain areas in neuropsychiatric disorders (Guo et al., 2015; Zhu et al., 2018).

FC can be defined as a temporal correlation of blood-oxygen-level dependent (BOLD) signal between spatially distributed brain regions (Biswal et al., 1997). Most previous RS-fMRI studies assumed that FC was constant throughout the observation period of task-free experiments (Hutchison et al., 2013). Recently, several studies have demonstrated the feasibility of dynamic methods in characterization of functional brain changes, such as dynamic FC (dFC) investigated by the sliding-window method, which provide novel insights into underlying neural activity (Chang and Glover, 2010; Liu et al., 2017; Duan et al., 2019). However, window size, window stepsize, and window type are open areas of research and important parameters to capture the resting-state FC dynamics. Sliding-window and time-frequency analyses are the two frequently used dynamic functional analyses (Hutchison et al., 2013). Apart from dFC, dynamic amplitude of low frequency fluctuations (dALFF) and dynamic regional homogeneity (dReHo) are also widely used (Deng et al., 2016; Fu et al., 2018). Both static and dynamic functional metrics provide great insight into understanding functional deficits of neuropsychiatric disorders (Biswal, 2012; Hutchison et al., 2013). Therefore, deep and detailed understanding of the method and application of dynamic functional metrics in neuropsychiatric disorders is critical.

This special issue focuses on the recent developments in dynamic functional analyses and their applications in neuropsychiatric disorders. A total of 7 articles were included in this Research Topic.

POSTTRAUMATIC STRESS DISORDER (PTSD)

Fu et al. applied dReHo and dFC to investigate both local and large-scale functional coupling in patients with PTSD. Results indicated increased dReHo in the left precuneus in patients with PTSD. Also, the left precuneus exhibited increased dFC with the left insula and decreased dFC with the left inferior parietal lobe and right precuneus, suggesting that the left precuneus might be critical for the pathophysiology of PTSD.

OPEN ACCESS

Edited and reviewed by:
Vince D. Calhoun,
Georgia State University,
United States

***Correspondence:**
Wenbin Guo
guowenbin76@csu.edu.cn

Specialty section:
This article was submitted to Brain Imaging Methods, a section of the journal Frontiers in Neuroscience

Received: *26 December 2019*
Accepted: *20 March 2020*
Published: *20 April 2020*

Citation:
Fu X, Liu F, Cui Z and Guo W (2020) Editorial: Dynamic Functional Connectivity in Neuropsychiatric Disorders: Methods and Applications. Front. Neurosci. 14:332. doi: 10.3389/fnins.2020.00332

GENERALIZED ANXIETY DISORDER (GAD)

Brain signal variability (BSV) is a method to measure the temporal variability of standard variation of BOLD signal, which reflects capacity of transition between brain states and processing various external stimuli. Li L. et al. evaluated the changes of BSV in patients with GAD and found that extensive brain regions exhibited decreased BSV in patients with GAD compared to healthy controls (HCs), suggesting that the brain of patients with GAD may be in a less flexible state compared to HCs.

EARLY BLIND

Dynamic causal modeling (DCM) is an approach to measure causal functional interactions among neuronal populations, i.e., effective connectivity. Li, Wang et al. used spectral DCM to investigate whether early visual deprivation had an impact on the dynamic causal interactions among regions within the default mode network, salience network, and dorsal attention network in patients with early blind. Abnormal patterns of effective connectivity within all these three networks were found in patients with early blind compared to HCs, which might imply the effect of early sensory deprivation on brain plasticity.

PARKINSON'S DISEASE (PD)

Li, Xiong et al. recruited 62 participants with PD and demonstrated that dynamic nodal efficiency measurement, which was calculated from RS-fMRI brain network and sliding-window analysis, could be used to predict the severity level of PD after drug therapy. Hippocampus, post-central gyrus, cingulate gyrus, and orbital gyrus were the contributed regions for the prediction. This study offered an example of using RS-fMRI data to predict the treatment effect in patients with PD.

Another study on PD by Zhang C. et al. used dALFF to explore the feasibility of differentiating patients with PD from HCs. Increased coefficient of variation in the left precuneus was observed in patients with PD. Moreover, coefficient of variation of dALFF in the left precuneus was positively correlated with disease duration in the patients. These findings were likely to provide a new direction for diagnosis of PD.

SUBACUTE STROKE

Chen et al. explored abnormal dynamic characteristics in patients with subacute stroke. Results of both dALFF and dReHo showed significant intergroup differences of regional brain activity. Fugl-Meyer assessment, an index for evaluating the degree of motor deficit, exhibited a positive correlation with dALFF variability in supplementary motor area (SMA) and a negative correlation with dReHo variability in ipsilesional middle frontal gyrus (MFG). The receiver operating characteristic analysis suggested that dALFF in SMA and dReHo in ipsilesional MFG might be potential markers to distinguish patients with subacute stroke from HCs. Therefore, dALFF and dReHo have the potential for evaluating the motor function in patients with subacute stroke.

SCHIZOPHRENIA

Zhang Y. et al. focused dReHo and dynamic fALFF to investigate abnormal dynamic local functional activity in schizophrenia. Results revealed deficits in the sensory and perception functional networks and a positive relationship between dReHo of the thalamus and the severity of symptoms in the patients, which highlighted the importance of the sensorimotor networks in the physiopathology of schizophrenia.

Taken together, all studies in this special issue suggested progress in the methodology and application of dynamic functional properties in neuropsychiatric disorders. These advances would promote better understanding in the temporal evolution of brain functional activity and provide valuable insight into the development of objective neuro-biomarker of neuropsychiatric disorders. Clinicians will be benefit from this topic in regard to theoretical, experimental and clinical questions related to the nature and origins of dFC in neuropsychiatric disorders.

AUTHOR CONTRIBUTIONS

WG has contributed to the conception and design of the editorial. XF has not contributed to the conception or design of the editorial, yet contributed considerably to the writing. FL and ZC contributed to the revision of the editorial.

FUNDING

This study was supported by grants from the National Key R&D Program of China (Grant No. 2016YFC1307100), the National Natural Science Foundation of China (Grant No. 81771447), and the Natural Science Foundation of Tianjin (Grant No. 18JCQNJC10900).

REFERENCES

Biswal, B. B. (2012). Resting state fMRI: a personal history. *Neuroimage* 62, 938–944. doi: 10.1016/j.neuroimage.2012.01.090

Biswal, B. B., Van Kylen, J., and Hyde, J. S. (1997). Simultaneous assessment of flow and BOLD signals in resting-state functional connectivity maps. *NMR Biomed.* 10, 165–170. doi: 10.1002/(sici)1099-1492(199706/08)10:4/5<165::aid-nbm454>3.0.co;2-7

Chang, C., and Glover, G. H. (2010). Time–frequency dynamics of resting-state brain connectivity measured with fMRI. *Neuroimage* 50, 81–98. doi: 10.1016/j.neuroimage.2009.12.011

Deng, L., Sun, J., Cheng, L., and Tong, S. (2016). Characterizing dynamic local functional connectivity in the human brain. *Sci. Rep.* 6:26976. doi: 10.1038/srep26976

Duan, X., Hu, M., Huang, X., Su, C., Zong, X., Dong, X., et al. (2019). Effect of risperidone monotherapy on dynamic functional connectivity of insular

subdivisions in treatment-naive, first-episode schizophrenia. *Schizophr. Bull.* doi: 10.1093/schbul/sbz087. [Epub ahead of print].

Fu, Z., Tu, Y., Di, X., Du, Y., Pearlson, G. D., Turner, J. A., et al. (2018). Characterizing dynamic amplitude of low-frequency fluctuation and its relationship with dynamic functional connectivity: an application to schizophrenia. *Neuroimage* 180, 619–631. doi: 10.1016/j.neuroimage.2017.09.035

Guo, W., Liu, F., Liu, J., Yu, L., Zhang, J., Zhang, Z., et al. (2015). Abnormal causal connectivity by structural deficits in first-episode, drug-naive schizophrenia at rest. *Schizophr. Bull.* 41, 57–65. doi: 10.1093/schbul/sbu126

Hutchison, R. M., Womelsdorf, T., Allen, E. A., Bandettini, P. A., Calhoun, V. D., Corbetta, M., et al. (2013). Dynamic functional connectivity: Promise, issues, and interpretations. *Neuroimage* 80, 360–378. doi: 10.1016/j.neuroimage.2013.05.079

Liu, F., Wang, Y., Li, M., Wang, W., Li, R., Zhang, Z., et al. (2017). Dynamic functional network connectivity in idiopathic generalized epilepsy with generalized tonic-clonic seizure: dynamic FNC in IGE-GTCS. *Hum. Brain Mapp.* 38, 957–973. doi: 10.1002/hbm.23430

Zhu, F., Liu, F., Guo, W., Chen, J., Su, Q., Zhang, Z., et al. (2018). Disrupted asymmetry of inter- and intra-hemispheric functional connectivity in patients with drug-naive, first-episode schizophrenia and their unaffected siblings. *EBiomedicine* 36, 429–435. doi: 10.1016/j.ebiom.2018.09.012

Conflict of Interest: The authors declare that the research was conducted in the absence of any commercial or financial relationships that could be construed as a potential conflict of interest.

frontiers in Neuroscience

ORIGINAL RESEARCH
published: 07 January 2019
doi: 10.3389/fnins.2018.00994

Dynamic Alterations in Spontaneous Neural Activity in Multiple Brain Networks in Subacute Stroke Patients: A Resting-State fMRI Study

Jing Chen[1†], Dalong Sun[2†], Yonghui Shi[1], Wei Jin[1], Yanbin Wang[3], Qian Xi[3] and Chuancheng Ren[1,4]*

[1] Department of Neurology, Shanghai Fifth People's Hospital, Fudan University, Shanghai, China, [2] Division of Gastroenterology, Department of Internal Medicine, Zhongshan Hospital, Fudan University, Shanghai, China, [3] Department of Radiology, Shanghai East Hospital, Tongji University, Shanghai, China, [4] Department of Neurology, Shanghai East Hospital, Tongji University, Shanghai, China

Objective: To examine whether subacute stroke patients would exhibit abnormal dynamic characteristics of brain activity relative to healthy controls (HC) and to investigate whether the altered dynamic regional indexes were associated with clinical behavior in stroke patients.

Methods: The dynamic amplitude of low-frequency fluctuations (dALFF) and dynamic regional homogeneity (dReHo) in 42 subacute stroke patients and 55 healthy controls were compared. Correlation analyses between dALFF and dReHo in regions showing significant intergroup differences and clinical scores (i.e., the National Institutes of Health Stroke Scale, Fugl-Meyer assessment and lesion volume size) were conducted in stroke patients. Receiver operating characteristic (ROC) curve analysis was used to determine the potential value of altered dynamic regional indexes to identify stroke patients.

Results: Significantly dALFF in the bilateral cerebellum posterior lobe (CPL), ipsilesional superior parietal lobe, ipsilesional inferior temporal gyrus (ITG), the midline supplementary motor area (SMA), ipsilesional putamen and lentiform nucleus were detected in stroke patients compared to HC. Relative to the HC group, the stroke patients showed significant differences in dReHo in the contralesional rectal gyrus, contralesional ITG, contralesional pons, ipsilesional middle frontal gyrus (MFG). Significant correlations between dALFF variability in midline SMA and Fugl-Meyer assessment (FMA) scores or between dReHo variability in the ipsilesional MFG and FMA scores were detected in stroke patients. Furthermore, the ROC curve revealed that dynamic ALFF at SMA and ReHo at ipsilesional MFG might have the potential to distinguish stroke patients.

Conclusion: The pattern of intrinsic brain activity variability is altered in stroke patients compared with HC, and dynamic ALFF/ReHo might be potential tools to assess stroke patients' motor function.

Keywords: stroke, dynamic intrinsic brain activity, resting-state fMRI, amplitude of low-frequency fluctuations, regional homogeneity

OPEN ACCESS

Edited by:
Zaixu Cui,
University of Pennsylvania, United States

Reviewed by:
Yang Yu,
Second Affiliated Hospital, Zhejiang University School of Medicine, China
Songran Yang,
Sun Yat-sen Memorial Hospital, China

***Correspondence:**
Chuancheng Ren
rccfns17@sina.com

[†] These authors have contributed equally to this work

Specialty section:
This article was submitted to Brain Imaging Methods, a section of the journal Frontiers in Neuroscience

Received: *28 August 2018*
Accepted: *11 December 2018*
Published: *07 January 2019*

Citation:
Chen J, Sun D, Shi Y, Jin W, Wang Y, Xi Q and Ren C (2019) Dynamic Alterations in Spontaneous Neural Activity in Multiple Brain Networks in Subacute Stroke Patients: A Resting-State fMRI Study. Front. Neurosci. 12:994. doi: 10.3389/fnins.2018.00994

INTRODUCTION

Stroke is the most common cause leading to varying degrees of neurological dysfunction with a very high likelihood of long-term disability (Liu et al., 2011; Yang et al., 2013). Movement disorders are the major common conditions of stroke-induced disability, and motor functional recovery remains highly variable. Although the exact mechanism of motor deficits and motor recovery are still under investigation, recent advances in neuroimaging have expanded our understanding. Resting-state functional magnetic resonance imaging (fMRI), which is operationally defined as task-independent spatiotemporal correlations within functionally related regions of the brain (Biswal et al., 1995), has been extensively used to delineate neural function abnormalities in stroke patients.

Resting-state fMRI measures spontaneous brain activity in low-frequency fluctuations which can be reflected by the blood oxygen level dependent (BOLD) signal. An increasingly large body of resting-state fMRI studies in stroke patients has focused on the characteristics of within-region or inter-region functional connectivity, such as connections within motor networks or between motor networks and non-motor networks (Wang et al., 2010; Grefkes and Fink, 2014; Wu et al., 2015). However, few studies have examined regional brain activities in patients with stroke. Neural regional properties are crucial for a better understanding of the neurophysiological and neuropathological conditions, such as regional abnormal energy consumption suggesting excessive or decreased resting metabolic rates (Raichle, 2006; Fox and Raichle, 2007). Currently, one of the methods to measure regional properties of the BOLD signal is the amplitude of low-frequency fluctuations (ALFF), which measures the signal strength in low-frequency oscillations of spontaneous neural activity (Zang et al., 2007). The ALFF is correlated with field potential activity in local brain regions (Logothetis et al., 2001), and the amplitude of oscillations can be applied as an index to examine alterations in neural function (Mohamed et al., 2004). Another approach is regional homogeneity (ReHo), which reflects the statistical similarity of local neural activity among spatially adjacent regions (Zang et al., 2004). These two approaches have been widely adopted for evaluating local neural function in neurologic disorders and neuropsychiatric diseases (Qiu et al., 2011; Li et al., 2012; Liu et al., 2012, 2013).

It has been reported that ALFF or ReHo were altered under resting conditions in stroke patients with movement disorders (Skidmore et al., 2013; Tsai et al., 2014) and that the ALFF value or ReHo value in certain brain regions were associated with the severity of motor deficits (Liu et al., 2015; Zhu et al., 2015). However, the aforementioned investigations of regional brain activities assumed that the BOLD signal is stationary during the entire fMRI scan, ignoring the characteristics of dynamic changes of brain spontaneous activity over time. Indeed, evidence has accumulated that brain responds to internal or external stimuli by dynamic integration or adjustment over multiple time scales (Abrams et al., 2013; Yin et al., 2013). Fortunately, the dynamic nature of brain activity may be detected by task manipulations using methods such as electroencephalography and can also be informed by the lower temporal resolution of resting-state fMRI (Calhoun et al., 2008). In recent years, sliding window approaches to functional connectivity have effectively examined abnormal brain function in stroke (Duncan and Small, 2017). Nevertheless, it is not enough to merely focus on time-varying dynamic functional connectivity, since evidence from neuroimaging techniques of high spatiotemporal resolution has verified that local brain activity itself exists with substantial fluctuations (Liao et al., 2015; Fu et al., 2017), and until now, no study explored the dynamic characteristics of local brain activity indexes in stroke patients. These dynamic local approaches are expected to explore the variability of the oscillation amplitudes and regional synchronization of spontaneous brain activity and to advance our understanding of brain function by identifying specific pathophysiological function signatures and our ability to decipher the neural underpinnings of normal or abnormal human behaviors.

Hence, the present study applied resting-state fMRI to investigate whether subacute stroke patients would exhibit abnormal dynamic characteristics of spontaneous brain activity by calculating regional indexes, ALFF and ReHo, compared with healthy controls (HC). Furthermore, another goal was to explore whether the altered dynamic ALFF (dALFF) and dynamic ReHo (dReHo) were correlated with the clinical behavior of the stroke patients. In the current study, we included subacute stroke patients for two reasons. First, the condition of stroke patients at the subacute stage is relatively stable than acute stroke patients, and the patients' compliance is relatively high, facilitating the smooth progress of the current study. Second, we enrolled stroke patients within 1–3 weeks after symptom onset, and this period is well within the recovery window. A period of dramatic changes in functional and structural reorganization may provide more information of spontaneous neural activity. We hypothesized that variability of regional brain activity was altered in patients with stroke-induced motor deficits compared with HC and that dynamic regional indexes in certain regions detected to be associated with the Fugl-Meyer assessment (FMA) scores could provide more information for evaluating of motor function in stroke patients.

MATERIALS AND METHODS

Subjects

This study was part of an integrated stroke and rehabilitation project at Shanghai 5th People's Hospital affiliated with Fudan University and was approved by the local ethical committee of Shanghai 5th People's Hospital affiliated with Fudan University. Written informed consent was obtained from all subjects before participating according to the Declaration of Helsinki. A total of 45 subacute stroke patients were recruited. Additionally, 55 HC, who were right-handed and matched for age, gender and education, were recruited from the local communities. The inclusion criteria for stroke patients were as follows: (1) they were aged 40–80 years; (2) it was a first-onset stroke with a single lesion in right-side subcortical regions as verified by diffusion-weighted imaging (DWI); (3) they were examined within 1–3 weeks after stroke symptom onset; (4) they were clinical evidence of a motor

deficit based on neurological examination; and (5) they were right-handed before the stroke. The exclusion criteria for both stroke patients and HC were the presence of any of the following: (1) other brain abnormalities, or clinically significant or unstable medical diseases; (2) unconsciousness, cognitive impairment, or cooperation difficulties; (3) patients with use of medications that could affect motor examination, such as antipsychotics and antiepileptics; (4) patients with cerebellar lesions; and (5) contraindications for MRI scanning. For all stroke patients, the right hemisphere corresponded to the ipsilesional hemisphere. The National Institutes of Health Stroke Scale (NIHSS) and Mini-Mental State Examination (MMSE) were used to evaluate neurological function impairment and cognitive conditions. FMA for upper and lower extremities was applied to evaluate the degree of motor deficit. These clinical behavior scores were collected on the same day as fMRI data acquisition.

Data Acquisition

All resting-state fMRI data were acquired using a Philips Achieva 3.0 T MR scanner (Philips Medical Systems, Best, Netherlands). Tight but comfortable foam pads and earplugs were used to reduce head motion and scanner noise. Resting-state fMRI was collected using an echo-planar (EPI) sequence with the following scan parameters: repetition time (TR) = 2000 ms; repetition echo time (TE) = 30 ms; flip angle (FA) = 90°; field of view (FOV) = 220 mm × 220 mm; voxel size = 3 mm × 3 mm × 3 mm; matrix = 64 × 64; slice thickness = 3 mm; gap = 1 mm; interleaved transversal slices = 38; and number of volumes = 180. High-resolution sagittal T1-weighted images were acquired using a 3D magnetization prepared rapid gradient echo (MPRAGE) sequence: TR = 8.0 ms; TE = 3.7 ms; FA = 12°; FOV = 256 mm × 256 mm; voxel size = 1 mm × 1 mm × 1 mm; matrix = 256 × 256; slice thickness = 1 mm; and slices = 180. During scanning, all participants were instructed to remain awake, keep their eyes closed, and stay motionless without thinking of anything in particular.

The lesion location of each patient was determined by an experienced neuroradiologist on T1-weighted MRI images. We manually outlined the lesion profiles on T1-weighted MRI images slice by slice using the software MRIcron[1] and generated a lesion mask for each patient. After spatial normalization to Montreal Neurological Institute (MNI) space, all the patients' lesion masks overlapped. We then averaged the individual lesion masks and overlaid them with a template to create the lesion overlap map shown in **Figure 1**.

Preprocessing of Resting-State fMRI Data

The preprocessing of resting-state fMRI data was performed using the Data Processing Assistant for Resting-State fMRI (DPARSF) version 4.0[2]. The first 10 volumes of each participant were deleted to allow the signal to reach equilibrium and the subjects to adapt to the environment. The remaining 170 volumes were corrected for acquisition time delay between slices. Realignment was conducted to correct head motion. The participants with head motion of >2.0 mm in maximum displacement or >2.0° rotation in angular motion were excluded from the study. The mean framewise displacement (FD) was computed by averaging the FD of each subject across the time points, and no significant differences were found between stroke patients and HC (p = 0.235). In addition, each subject's mean FD was included in all group-level analyses as a covariate to further control the head move effect. Subsequently, the structural image was coregistered to the mean functional image after the motion correction, and the transformed structural image was segmented into gray matter, white matter, and cerebrospinal fluid. Then, the segmented images were normalized to MNI space using Diffeomorphic Anatomical Registration Through Exponentiated Lie algebra (DARTEL) algorithm (Ashburner, 2007). Next, the motion-corrected functional volumes were normalized to the MNI space using the normalization parameters for their respective structure images and resampled into a voxel size of 3 mm × 3 mm × 3 mm. Nuisance covariates (24 head motion parameters, cerebrospinal fluid signal, white matter signal and linear trend) were regressed out. Given that it is still a controversy of removing the global signal (Murphy et al., 2009); we did not regress out the global signal. For the ReHo calculation, an additional processing step was that the regressed functional images were temporally bandpass filtered (0.01–0.08 Hz) to reduce low frequency drift and high-frequency noise.

dALFF and dReHo Analysis

Dynamic regional metrics analysis was performed using Temporal Dynamic Analysis (TDA) toolkits based on DPABI

[1]http://www.mccauslandcenter.sc.edu/mricro/mricron/

[2]http://rfmri.org/DPARSF/

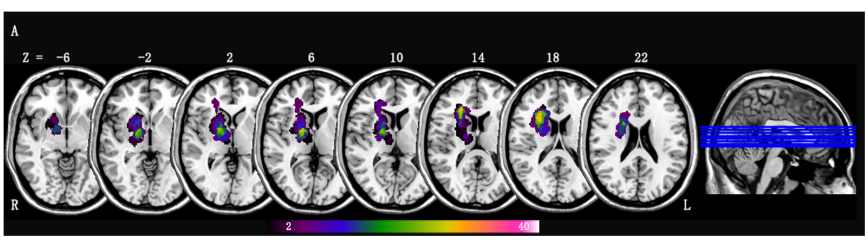

FIGURE 1 | Lesion overlap map across stroke patients with right-sided lesions (n = 42); Lesion maps were normalized to an MNI reference brain. The color bar indicates the percentage of lesion overlap.

(Yan et al., 2017). Sliding window-based analysis, which is sensitive in detecting time-dependent variations (Hindriks et al., 2016; Liu F. et al., 2017; Yip et al., 2017), was applied to examine the dALFF or dReHo variability over the whole brain. In the sliding window analysis, a temporal window of certain size and shape is chosen, and ALFF and ReHo within that window are calculated. Ideally, the window size should be small enough to detect potentially transient signals, and yet large enough to analyze the lowest frequencies of interest in the signals (Sakoglu et al., 2010). Previous work of sliding window connectivity have applied a sliding window length of as small as 10 s (Thompson et al., 2013) and as long 180 s (Gonzalez-Castillo et al., 2015). In this work, a moderate-length sliding window of 32 TR (64 s) and a shifting step size of one TR (2 s) were used to simultaneously maximize statistical power within the window and also maximize statistical power for cross-level analyses (Allen et al., 2014). The remaining 170 time points after removing the first 10 time points for each individual were segmented into 139 windows in total. In each sliding window, ALFF and ReHo were calculated. For ALFF, the time series was first converted to the frequency domain using a fast Fourier transform, and then the ALFF value of a given voxel was obtained by calculating and summing the square root of the power spectrum between 0.01 and 0.08 Hz. For ReHo, the Kendall's coefficient of concordance (KCC) of the time course of every 27 nearest neighboring voxels was calculated (Zang et al., 2004). The standard deviation (SD) of ALFF values and ReHo values at each voxel across 139 windows was calculated to assess the variability of ALFF and ReHo. To reduce the global effects of variability across subjects, the dALFF and dReHo of each voxel were divided by the global mean dALFF and dReHo values within a gray matter mask, respectively. Finally, the mean normalized dALFF and dReHo maps were spatially smoothed with an isotropic Gaussian kernel of 4 mm full-width-at-half-maximum (FWHM).

Statistical Analysis

A general linear model (GLM) was used in a voxel-wise manner to compare group differences between the stroke group and HC group in dALFF and dReHo with age, gender, educational level, MMSE and mean FD as covariates. Multiple comparisons were corrected using a voxel-level familywise error rate (FWE) method with corrected $p < 0.05$ (cluster size $\geq$50 voxels).

The Shapiro–Wilk statistic was first used to test for normality, and then group comparisons of clinical measures were performed using two-sample *t*-tests for continuous data and Pearson's chi-squared test for categorical data. Partial correlation analyses were conducted in stroke patients between the clinical measures (NIHSS scores, FMA scores and lesion volume size) and the mean dALFF/dReHo value of each cluster showing significant group differences between stroke group and HC group. The age, gender, educational level, MMSE, mean FD, illness duration and intravenous thrombolysis (IVT) were also considered as covariates. As the correlation analyses were exploratory in nature, the significance levels were set at uncorrected $p < 0.05$. Furthermore, receiver operating characteristic (ROC) curve analysis was performed to examine the potential value of altered dynamic ALFF or ReHo values in clusters showing significant correlations with clinical behaviors in stroke patients. The optimal cut-off between sensitivity and specificity was determined by maximizing the Youden's index J (J = sensitivity + specificity − 1). A two-tailed *p*-value of 0.05 was considered statistically significant for the analyses conducted with SPSS version 19.0 statistical software (IBM Corporation, Armonk, NY, United States).

RESULTS

Clinical Data

Data obtained from three stroke patients were excluded because of excessive head motion during scanning. Demographic and clinical characteristics of 42 patients with right hemisphere stroke (21 men; mean age, 57.86 ± 11.17 years) and 55 HC (29 men; mean age, 56.73 ± 10.21 years) are listed in **Table 1**. No significant differences in were found ($p > 0.05$) in gender, age, education level, high risk factors (hypertension, diabetes, hyperlipidemia and atrial fibrillation) and MMSE scores between the stroke group and HC group. The mean lesion volume of stroke patients was 6.10 ± 8.55 cc^3. Among them, four patients received IVT therapy. Of the 42 patients, 15 had corona radiate lesions, 15 had internal capsule lesions, 10 had basal ganglia lesions, and two had thalamus lesions. The lesion overlaps of stroke patients are shown in **Figure 1**.

TABLE 1 | Demographic and clinical data.

	Stroke patients (*n* = 42)	Healthy control (*n* = 55)	t/χ^2	*p*
Gender, male	21 (50.0)	29 (52.7)	0.071	0.790
Age, years	57.86 ± 11.17	56.73 ± 10.21	0.518	0.605
Educational level, years	10.74 ± 3.39	11.00 ± 3.82	−0.351	0.727
High risk factor				
Hypertension	25 (59.5)	29 (52.7)	0.446	0.504
Diabetes	11 (26.2)	12 (21.8)	0.252	0.616
Hyperlipidemia	12 (28.6)	16 (29.1)	0.003	0.955
Atrial fibrillation	2 (2.1)	1(1.8)	0.689	0.407
MMSE	28.07 ± 1.28	28.15 ± 1.27	−0.284	0.777
Illness duration, days	14.29 ± 2.14	–		
Stroke type				
Ischemia	40 (95.2)	–		
Hemorrhage	2 (4.8)	–		
Location of lesion				
Coronal radiate	15 (35.7)	–		
Internal capsule	15 (35.7)	–		
Basel ganglia	10 (23.8)	–		
Thalamus	2 (4.8)	–		
Lesion volume, cc^3	6.10 ± 8.55	–		
NIHSS	5.86 ± 4.14	–		
FMA-total	76.45 ± 14.12	–		
IVT use	4 (9.5)	–		

Data represent n (%) or mean ± SD. MMSE, the Mini-Mental State Examination; NIHSS, the National Institutes of Health Stroke Scale; FMA-total, Fugl-Meyer assessment for upper and lower extremities; IVT, intravenous thrombolysis.

Differences in Dynamic ALFF and Dynamic ReHo

The significant differences in dALFF and dReHo between the stroke group and HC group are shown in **Figures 2A,B**, respectively. Compared with HC, significantly increased dALFF variability in the contralesional cerebellum posterior lobe (CPL), ipsilesional superior parietal lobe, ipsilesional inferior temporal gyrus (ITG), ipsilesional CPL and cerebellum tonsil and decreased dALFF variability in the midline supplementary motor area (SMA), ipsilesional putamen and lentiform nucleus were detected in stroke patients (**Table 2** and **Figures 2A,C**). Relative to the dReHo variability of subjects in the HC group, these stroke patients showed a significant increase in contralesional rectal gyrus, contralesional ITG, contralesional pons and a significant decrease in ipsilesional middle frontal gyrus (MFG) (**Table 3** and **Figures 2B,D**).

Correlational Analysis

A significant positive correlation was detected between the FMA scores and dALFF variability in the SMA (r = 0.347, p = 0.035, uncorrected; **Figure 3A**), a significant negative correlation between the FMA scores and dReHo variability in the midline ipsilesional MFG was found in stroke patients (r = −0.462, p = 0.004, uncorrected; **Figure 3B**). No other significant correlations between NIHSS, size of lesion volume and dynamic regional indexes were observed in the stroke group.

ROC Analysis

As shown above, significant correlations were detected between the FMA scores and dynamic ALFF variability in SMA or dynamic ReHo variability in ipsilesional MFG, which proposed that the dynamic ALFF/ReHo in these regions might be utilized to differentiate the stroke patients from healthy persons. To verify this possibility, mean dALFF/dReHo values in the SMA or ipsilesional MFG were extracted. Then, ROC analysis was performed to investigate this possibility. The results demonstrated that the area under the curves (AUC) of SMA and ipsilesional MFG were 0.965 and 0.911, respectively (**Figure 4**), which suggested that dynamic ALFF in SMA and ReHo values in the ipsilesional MFG might have the potential to distinguish the stroke patients from healthy subjects. Further diagnostic analysis showed that the sensitivity and specificity were relatively high (**Table 4**).

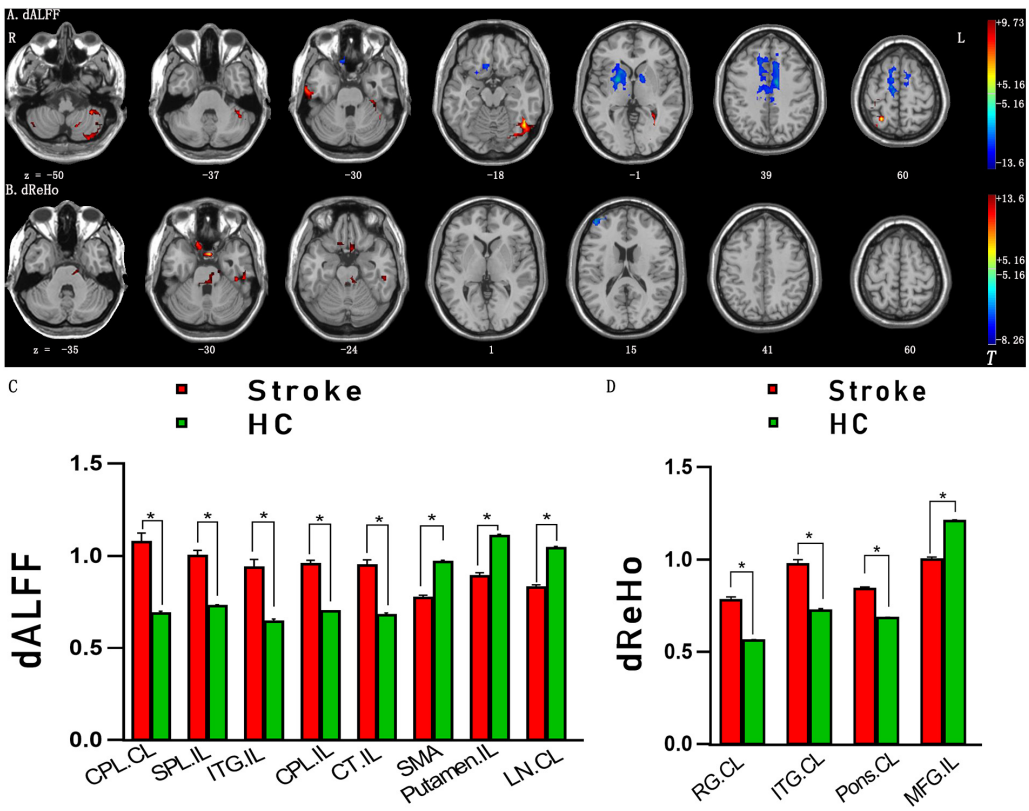

FIGURE 2 | (A) Brain regions with significant intergroup differences in dALFF between the stroke group and HC group. **(B)** Brain regions with significant intergroup differences in dReHo between the stroke group and HC group. **(C)** The histogram indicates mean values and standard error of dALFF variability between the stroke group and HC group. **(D)** The histogram indicates mean value and standard error of dReHo variability between the stroke group and HC group. Familywise error rate corrected ($p < 0.05$, cluster size ≥ 50 voxels). The color bar indicates the T value. *$p < 0.05$. HC, healthy controls; dALFF, dynamic amplitude of low-frequency fluctuation; dReHo, dynamical regional homogeneity; CPL, cerebellum posterior lobe; SPL, superior parietal lobe; ITG, inferior temporal gyrus; CT, cerebellum tonsil; SMA, supplementary motor area; LN, lentiform nucleus; RG, rectal gyrus; MFG, middle frontal gyrus; IL, ipsilesional; CL, contralesional.

TABLE 2 | Brain regions with significant differences in dynamic ALFF between groups.

Group comparisons	Brain regions/BA	Peak MNI coordinates			Cluster size (voxels)	Peak *t* values
		X	Y	Z		
Stroke patients > HC	Cerebellum posterior lobe, CL	−15	−69	−39	1175	9.73
	Superior parietal lobe, IL/4	27	−57	60	179	9.32
	Inferior temporal gyrus, IL/20	39	−57	−18	298	9.27
	Cerebellum posterior lobe, IL	39	−87	−39	53	8.33
	Cerebellum tonsil, IL	48	−63	−54	50	6.57
Stroke patients < HC	Supplementary motor area, 6	12	−12	57	1670	13.6
	Putamen, IL	24	0	0	814	12.18
	Lentiform nucleus, CL	−18	−6	18	298	11.01

ALFF, amplitude of low-frequency fluctuation; HC, healthy controls; BA, Brodmann's area; MNI, Montreal Neurological Institute; IL, ipsilesional; CL, contralesional.

TABLE 3 | Brain regions with significant differences in dynamic ReHo between groups.

Group comparisons	Brain regions/BA	Peak MNI coordinates			Cluster size (voxels)	Peak *t* values
		X	Y	Z		
Stroke patients > HC	Rectal gyrus, CL/11	−3	6	−30	105	13.16
	Inferior temporal gyrus, CL/20	−42	−30	−30	58	8.85
	Pons, CL	−12	−21	−33	95	7.86
Stroke patients < HC	Middle frontal gyrus, IL/9	45	54	18	52	7.32

ReHo, regional homogeneity; HC, healthy controls; BA, Brodmann's area; MNI, Montreal Neurological Institute; IL, ipsilesional; CL, contralesional.

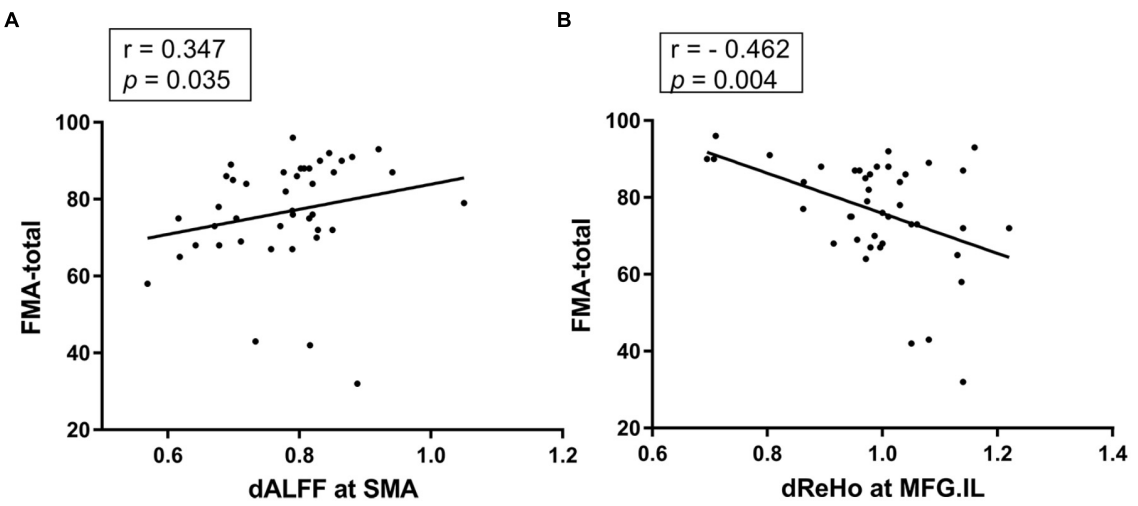

FIGURE 3 | (A) The dALFF variability in the SMA was positively correlated with the FMA scores of the stroke patients (r = 0.347, p = 0.035, uncorrected). **(B)** The dReHo variability in the ipsilesional MFG was negatively correlated with the FMA scores of the stroke patients (r = –0.462, p = 0.004, uncorrected). dALFF, dynamic amplitude of low-frequency fluctuation; dReHo, dynamic regional homogeneity; FMA-total, Fugl-Meyer assessment for upper and lower extremities; SMA, supplementary motor area; MFG, middle frontal gyrus; IL, ipsilesional.

DISCUSSION

In the present study, dynamic regional brain activity between stroke patients with motor deficits and healthy controls was examined using resting-state fMRI. To the best of our knowledge, there is no prior study using a TDA approach to detect stroke-related brain activity changes in humans. Given that young adult stroke could be different both in causes and in outcomes (Edwards et al., 2018) and the role of educational level in recovery should not be ignored (Hillis and Tippett, 2014). Therefore, we used age and educational level as covariates in intergroup difference analyses and correlation analyses. Moreover, patients were enrolled in this current study within 1–3 weeks after stroke symptom onset, during which period imaging data and behavior performance were obtained. This period is well within the recovery window for stroke (Venketasubramanian et al., 2017).

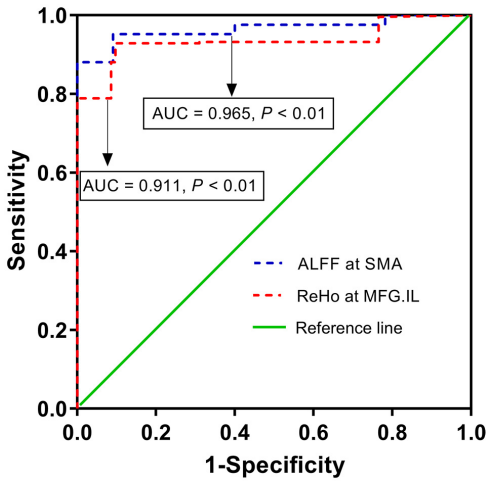

FIGURE 4 | The diagnostic performance of altered dynamic ALFF in SMA and dynamic ReHo in ipsilesional MFG in distinguishing stroke patients from healthy subjects. ALFF, amplitude of low-frequency fluctuation; ReHo, regional homogeneity; SMA, supplementary motor area; MFG, middle frontal gyrus; IL, ipsilesional; AUC, area under curve.

Additionally, medication, especially IVT therapy, can largely improve patients' functional outcomes for hyperacute ischemic stroke (Ferrigno et al., 2018). Hence, we also considered patients' illness duration and IVT use status as covariates in correlation analyses to reduce the confounding effects.

Differences in dALFF variability were observed between the stroke group and HC group in the contralesional CPL, ipsilesional superior parietal lobe, ipsilesional ITG, ipsilesional CPL, cerebellum tonsil, the midline SMA, ipsilesional putamen and lentiform nucleus, while differences of dReHo variability in contralesional rectal gyrus, contralesional ITG, contralesional pons and MFG distinguished stroke patients from HC. In addition, relationships were observed between the FMA scores and dynamic ALFF or ReHo variability in SMA or ipsilesional MFG in stroke patients. Further ROC analyses suggested that dynamic ALFF in SMA or ReHo in ipsilesional MFG had the potential to distinguish the patients of subacute stroke from healthy subjects.

Our findings were in line with previous studies that investigated stroke patients with movement disorders by functional connectivity, structural connectivity or regional metrics, such as ALFF or ReHo (Skidmore et al., 2013; Tsai et al., 2014; Zhu et al., 2015). The sensorimotor network (SMN), which is critical for voluntary movement, connects primary motor cortex function with SMA function (Damoiseaux et al., 2006; Chang et al., 2013). The SMA is a part of the primate cerebral cortex that contributes to the control of movement. Neurons in the SMA project directly to the spinal cord and may play a role in the direct control of movement (Nudo and Masterton, 1990). It has been reported that SMA plays roles in the postural stabilization of the body, the coordination of both sides of the body such as during bimanual action, the control of movements that are internally generated rather than triggered by sensory events, and the control of sequences of movements (Shima and Tanji, 1998; Cunnington et al., 2003; Zhang et al., 2012). Stroke-induced disturbance of intrinsic neural activity, which may be due to a complex cascade of events that are associated with structural reorganization and axonal sprouting as demonstrated by tract-tracing studies in animal models of stroke (Carmichael et al., 2001; Dancause et al., 2005), impedes brain network function of voluntary motion. Based on prior studies, we speculate that altered dALFF and dReHo variability in the SMN (e.g., in the superior parietal lobe and SMA) of stroke patients with motor deficits might occur as a compensatory mechanism and might be a significant factor in the reorganization and integration of resting-state functional networks at the subacute stage.

We observed decreased dReHo variability in the ipsilesional MFG, which belongs to the default mode network (DMN). This finding may indicate that stroke-related brain activity changes not only occurred in motor-related areas but also in non-motor regions. The DMN plays a pivotal role in "resting" brain activity, which is involved in sustaining attention, self-consciousness and exhibiting self-control (Andrews et al., 2011; Yuan et al., 2018). In stroke patients, alterations in brain activity of the DMN may be associated with advanced neural function of cognitive and emotional control (Liu F. et al., 2017). Evidence has shown that the DMN regulates consciousness, processes emotionally salient stimuli, and coordinates the interactions of cognitive function and emotional processing (Soddu et al., 2012; Zhang et al., 2017). In the current study, we demonstrated that the stroke group showed significantly decreased ReHo variability in the ipsilesional MFG, indicating that the synchronous neural activity was also disrupted in the ipsilesional MFG in stroke patients.

The increased regional brain activity in contralesional pons and bilateral cerebellum CPL, ipsilesional cerebellum tonsil may

TABLE 4 | ROC analysis for differentiating stroke patients from healthy person.

	MNI coordinates						
Brain regions	**X**	**Y**	**Z**	**AUC**	**Maximal Youden's index J**	**Sensitivity**	**Specificity**
dALFF at SMA	12	−12	57	0.965	0.861*	95.2% (40/42)	90.9% (50/55)
dReHo at MFG.IL	45	54	18	0.911	0.832	92.9% (39/42)	90.3% (49/55)

**By this optimal cut-off point, the dynamic ALFF value of SMA could correctly classify 40 of 42 patients and 50 of 55 healthy subjects, resulted in a sensitivity of 95.2% and a specificity of 90.9.2%. The means of other optimal cut-off point was similar. MNI, Montreal Neurological Institute; AUC, areas under the curves; dALFF, dynamic amplitude of low-frequency fluctuation; dReHo, dynamic regional homogeneity; SMA, supplementary motor area; MFG, middle frontal gyrus; IL, ipsilesional.*

result from the dysfunction of the cerebro-ponto-cerebellar circuit and act as a compensatory response (Lu et al., 2011). The excessive ReHo variability of the prefrontal cortex (the rectal gyrus) may compensate for the deficits in motor function in stroke patients. However, this concept needs to be confirmed. Moreover, rectal gyrus is considered as a part of affective network (AN). Study has reported that abnormal regional neural activity was observed mainly in component of DMN, SMN, cerebellar lobes (CPL) and AN in stroke patients with emotional abnormality (Liu T. et al., 2017). Hence, we tend to speculate that the dysfunction of the volitional system may lead to the disorder of emotional system in stroke patients.

We also found decreased dALFF variability in the ipsilesional putamen and contralesional lentiform nucleus in stroke patients. Considered the entrance to the basal ganglia, the lentiform nucleus receives the input from cerebral cortex, and there was partial stroke lesion overlap observed in the present study and shown in **Figure 1**. The primary roles of these regions are to regulate movements at various stages, such as during motor preparation and motor execution. Meanwhile, they play important roles in motor learning, which can be considered a sensory feedback of frontal mediated goal parameters and posterior-mediated motor programs; there are anatomical links that exist between these motor-execution and frontal-parietal motor control systems (Ween, 2008). Previous human and non-human studies of stroke models have shown that decreased ALFF values were found in the core of stroke lesions (Liu et al., 2007; Skidmore et al., 2013). The mechanism may involve abrupt decreases of the blood flow resulting from cytotoxic swelling, calcium overload and membrane ion pump failure in core regions of stroke lesions (Badaut et al., 2011). Based on the previous studies and this present study, we infer that deceased or vanished oxygen consumption and intrinsic brain activity may contribute to less variation and low ALFF values.

In addition, we also detected excessive intrinsic brain activity variability reflected both in dALFF in the ipsilesional ITG and in dReHo in the contralesional ITG of the stroke patients. The ITG belongs to the higher levels of the ventral stream of visual processing and is related to the representation of complex object features. A previous study found that the visual network was activated in recovery from sensorimotor stroke, and limb movement critically relies on visual guidance (Archer et al., 2016). The mechanism underlying the abnormal brain activity of contralesional ITG is presently poorly understood.

The current study has several limitations. First, although we identified significant differences between the stroke patients and the HCs, the sample size of 42 stroke patients analyzed in the current study was somewhat lacking in statistical power, and large sample size studies are needed for further demonstration. Second, it was reported that corticospinal tract lesion load was a significant predictor of motor deficit (Zhu et al., 2010; Feng et al., 2015). However, in the current study, we focused on investigating whether subcortical stroke patients would exhibit abnormal dynamic characteristics of brain activity relative to healthy controls and to investigate whether the altered dynamic regional indexes were associated with clinical behavior in stroke patients. Hence, here, we did not give much thought to the characteristics of diffusion-tensor imaging of the patients. Third, the correlation analyses cannot pass the FDR or Bonferroni correction. Larger sample size will be necessary to confirm the current results in the future studies. Fourth, physiological noise of cardiac and respiratory cycles was not monitored during the MRI scanning, which may influence brain activity alterations. It is possible that alterations in network dynamics may reflect changes in brain state, since few constraints were imposed on a participant's cognitive processes during the scanning. Finally, although the correlation analyses between dynamic regional indexes in regions showing significant group differences and size of lesion volume revealed no significant correlation, the heterogeneous clinical characteristics, such as lesion location, stroke severity and size of lesion volume, exhibited a relatively large variation across subjects and should be taken into consideration when interpreting the results.

CONCLUSION

The pattern of intrinsic brain activity variability in multiple brain networks is altered in stroke patients with motor deficits compared with healthy controls. The alterations of dynamic brain activity in the SMN and DMN were correlated with the degree of motor functional impairment. Resting-state fMRI dynamic regional indexes might be potential tools to assess stroke patients' motor function. Future studies will be needed to clarify the underlying mechanisms of alterations in the dynamic regional metrics after stroke.

AUTHOR CONTRIBUTIONS

JC contributed to the experiments, data analysis and writing of the manuscript. DS contributed to performing the experiments, and writing and revising the manuscript. YS contributed to the data collection. WJ designed the experiments and revised the manuscript. YW contributed to the data analysis and manuscript revision. QX contributed to the manuscript revision. CR is the guarantor of this study and had complete access to all data in the study. All authors are accountable for the contents of this research.

FUNDING

The study was supported by the National Natural Science Foundation of China (81571277).

ACKNOWLEDGMENTS

The authors thank all volunteers who participated in the study and the staff of the Med-X Research Institute and School of Biomedical Engineering Shanghai Jiao Tong University in Shanghai, China for their selfless and valuable assistance.

REFERENCES

Abrams, D. A., Lynch, C. J., Cheng, K. M., Phillips, J., Supekar, K., Ryali, S., et al. (2013). Underconnectivity between voice-selective cortex and reward circuitry in children with autism. *Proc. Natl. Acad. Sci. U.S.A.* 110, 12060–12065. doi: 10.1073/pnas.1302982110

Allen, E. A., Damaraju, E., Plis, S. M., Erhardt, E. B., Eichele, T., and Calhoun, V. D. (2014). Tracking whole-brain connectivity dynamics in the resting state. *Cereb. Cortex* 24, 663–676. doi: 10.1093/cercor/bhs352

Andrews, S. C., Hoy, K. E., Enticott, P. G., Daskalakis, Z. J., and Fitzgerald, P. B. (2011). Improving working memory: the effect of combining cognitive activity and anodal transcranial direct current stimulation to the left dorsolateral prefrontal cortex. *Brain Stimul.* 4, 84–89. doi: 10.1016/j.brs.2010.06.004

Archer, D. B., Misra, G., Patten, C., and Coombes, S. A. (2016). Microstructural properties of premotor pathways predict visuomotor performance in chronic stroke. *Hum. Brain Mapp.* 37, 2039–2054. doi: 10.1002/hbm.23155

Ashburner, J. (2007). A fast diffeomorphic image registration algorithm. *Neuroimage* 38, 95–113. doi: 10.1016/j.neuroimage.2007.07.007

Badaut, J., Ashwal, S., Adami, A., Tone, B., Recker, R., Spagnoli, D., et al. (2011). Brain water mobility decreases after astrocytic aquaporin-4 inhibition using RNA interference. *J. Cereb. Blood Flow Metab.* 31, 819–831. doi: 10.1038/jcbfm.2010.163

Biswal, B., Yetkin, F. Z., Haughton, V. M., and Hyde, J. S. (1995). Functional connectivity in the motor cortex of resting human brain using echo-planar MRI. *Magn. Reson. Med.* 34, 537–541. doi: 10.1002/mrm.1910340409

Calhoun, V. D., Kiehl, K. A., and Pearlson, G. D. (2008). Modulation of temporally coherent brain networks estimated using ICA at rest and during cognitive tasks. *Hum. Brain Mapp.* 29, 828–838. doi: 10.1002/hbm.20581

Carmichael, S. T., Wei, L., Rovainen, C. M., and Woolsey, T. A. (2001). New patterns of intracortical projections after focal cortical stroke. *Neurobiol. Dis.* 8, 910–922. doi: 10.1006/nbdi.2001.0425

Chang, E. F., Niziolek, C. A., Knight, R. T., Nagarajan, S. S., and Houde, J. F. (2013). Human cortical sensorimotor network underlying feedback control of vocal pitch. *Proc. Natl. Acad. Sci. U.S.A.* 110, 2653–2658. doi: 10.1073/pnas.1216827110

Cunnington, R., Windischberger, C., Deecke, L., and Moser, E. (2003). The preparation and readiness for voluntary movement: a high-field event-related fMRI study of the Bereitschafts-BOLD response. *Neuroimage* 20, 404–412. doi: 10.1016/s1053-8119(03)00291-x

Damoiseaux, J. S., Rombouts, S. A., Barkhof, F., Scheltens, P., Stam, C. J., Smith, S. M., et al. (2006). Consistent resting-state networks across healthy subjects. *Proc. Natl. Acad. Sci. U.S.A.* 103, 13848–13853. doi: 10.1073/pnas.0601417103

Dancause, N., Barbay, S., Frost, S. B., Plautz, E. J., Chen, D., Zoubina, E. V., et al. (2005). Extensive cortical rewiring after brain injury. *J. Neurosci.* 25, 10167–10179. doi: 10.1523/JNEUROSCI.3256-05.2005

Duncan, E. S., and Small, S. L. (2017). Changes in dynamic resting state network connectivity following aphasia therapy. *Brain Imaging Behav.* 12, 1141–1149. doi: 10.1007/s11682-017-9771-2

Edwards, J. D., Kapoor, A., Linkewich, E., and Swartz, R. H. (2018). Return to work after young stroke: a systematic review. *Int. J. Stroke* 13, 243–256. doi: 10.1177/1747493017743059

Feng, W., Wang, J., Chhatbar, P. Y., Doughty, C., Landsittel, D., Lioutas, V. A., et al. (2015). Corticospinal tract lesion load: an imaging biomarker for stroke motor outcomes. *Ann. Neurol.* 78, 860–870. doi: 10.1002/ana.24510

Ferrigno, M., Bricout, N., Leys, D., Estrade, L., Cordonnier, C., Personnic, T., et al. (2018). Intravenous recombinant tissue-type plasminogen activator: influence on outcome in anterior circulation ischemic stroke treated by mechanical thrombectomy. *Stroke* 49, 1377–1385. doi: 10.1161/STROKEAHA.118.020490

Fox, M. D., and Raichle, M. E. (2007). Spontaneous fluctuations in brain activity observed with functional magnetic resonance imaging. *Nat. Rev. Neurosci.* 8, 700–711. doi: 10.1038/nrn2201

Fu, Z., Tu, Y., Di, X., Du, Y., Pearlson, G. D., Turner, J. A., et al. (2017). Characterizing dynamic amplitude of low-frequency fluctuation and its relationship with dynamic functional connectivity: an application to schizophrenia. *Neuroimage* 180(Pt B), 619–631. doi: 10.1016/j.neuroimage.2017.09.035

Gonzalez-Castillo, J., Hoy, C. W., Handwerker, D. A., Robinson, M. E., Buchanan, L. C., Saad, Z. S., et al. (2015). Tracking ongoing cognition in individuals using brief, whole-brain functional connectivity patterns. *Proc. Natl. Acad. Sci. U.S.A.* 112, 8762–8767. doi: 10.1073/pnas.1501242112

Grefkes, C., and Fink, G. R. (2014). Connectivity-based approaches in stroke and recovery of function. *Lancet Neurol.* 13, 206–216. doi: 10.1016/S1474-4422(13)70264-3

Hillis, A. E., and Tippett, D. C. (2014). Stroke recovery: surprising influences and residual consequences. *Adv. Med.* 2014:378263. doi: 10.1155/2014/378263

Hindriks, R., Adhikari, M. H., Murayama, Y., Ganzetti, M., Mantini, D., Logothetis, N. K., et al. (2016). Corrigendum to "Can sliding-window correlations reveal dynamic functional connectivity in resting-state fMRI?". *Neuroimage* 132:115. doi: 10.1016/j.neuroimage.2016.02.007

Li, Z., Kadivar, A., Pluta, J., Dunlop, J., and Wang, Z. (2012). Test-retest stability analysis of resting brain activity revealed by blood oxygen level-dependent functional MRI. *J. Magn. Reson. Imaging* 36, 344–354. doi: 10.1002/jmri.23670

Liao, X., Yuan, L., Zhao, T., Dai, Z., Shu, N., Xia, M., et al. (2015). Spontaneous functional network dynamics and associated structural substrates in the human brain. *Front. Hum. Neurosci.* 9:478. doi: 10.3389/fnhum.7015.00478

Liu, F., Guo, W., Liu, L., Long, Z., Ma, C., Xue, Z., et al. (2013). Abnormal amplitude low-frequency oscillations in medication-naive, first-episode patients with major depressive disorder: a resting-state fMRI study. *J. Affect. Disord.* 146, 401–406. doi: 10.1016/j.jad.2012.10.001

Liu, F., Hu, M., Wang, S., Guo, W., Zhao, J., Li, J., et al. (2012). Abnormal regional spontaneous neural activity in first-episode, treatment-naive patients with late-life depression: a resting-state fMRI study. *Prog. Neuropsychopharmacol. Biol. Psychiatry* 39, 326–331. doi: 10.1016/j.pnpbp.2012.07.004

Liu, F., Wang, Y., Li, M., Wang, W., Li, R., Zhang, Z., et al. (2017). Dynamic functional network connectivity in idiopathic generalized epilepsy with generalized tonic-clonic seizure. *Hum. Brain Mapp.* 38, 957–973. doi: 10.1002/hbm.23430

Liu, G., Dang, C., Peng, K., Xie, C., Chen, H., Xing, S., et al. (2015). Increased spontaneous neuronal activity in structurally damaged cortex is correlated with early motor recovery in patients with subcortical infarction. *Eur. J. Neurol.* 22, 1540–1547. doi: 10.1111/ene.12780

Liu, L., Wang, D., Wong, K. S., and Wang, Y. (2011). Stroke and stroke care in China: huge burden, significant workload, and a national priority. *Stroke* 42, 3651–3654. doi: 10.1161/STROKEAHA.111.635755

Liu, T., Li, J., Huang, S., Li, C., Zhao, Z., Wen, G., et al. (2017). Altered resting-state functional activity in isolated pontine infarction patients with pathological laughing and crying. *Oncotarget* 8, 84529–84539. doi: 10.18632/oncotarget.19307

Liu, Y., D'Arceuil, H., He, J., Duggan, M., Gonzalez, G., Pryor, J., et al. (2007). MRI of spontaneous fluctuations after acute cerebral ischemia in nonhuman primates. *J. Magn. Reson. Imaging* 26, 1112–1116. doi: 10.1002/jmri.21131

Logothetis, N. K., Pauls, J., Augath, M., Trinath, T., and Oeltermann, A. (2001). Neurophysiological investigation of the basis of the fMRI signal. *Nature* 412, 150–157. doi: 10.1038/35084005

Lu, J., Liu, H., Zhang, M., Wang, D., Cao, Y., Ma, Q., et al. (2011). Focal pontine lesions provide evidence that intrinsic functional connectivity reflects polysynaptic anatomical pathways. *J. Neurosci.* 31, 15065–15071. doi: 10.1523/JNEUROSCI.2364-11.2011

Mohamed, M. A., Yousem, D. M., Tekes, A., Browner, N., and Calhoun, V. D. (2004). Correlation between the amplitude of cortical activation and reaction time: a functional MRI study. *AJR Am. J. Roentgenol.* 183, 759–765. doi: 10.2214/ajr.183.3.1830759

Murphy, K., Birn, R. M., Handwerker, D. A., Jones, T. B., and Bandettini, P. A. (2009). The impact of global signal regression on resting state correlations: are anti-correlated networks introduced? *Neuroimage* 44, 893–905. doi: 10.1016/j.neuroimage.2008.09.036

Nudo, R. J., and Masterton, R. B. (1990). Descending pathways of the spinal cord, III: sites of origin of the corticospinal tract. *J. Comp. Neurol.* 296, 559–583. doi: 10.1002/cne.902960405

Qiu, Y. W., Han, L. J., Lv, X. F., Jiang, G. H., Tian, J. Z., Zhuo, F. Z., et al. (2011). Regional homogeneity changes in heroin-dependent individuals: resting-state functional MR imaging study. *Radiology* 261, 551–559. doi: 10.1148/radiol.11102466

Raichle, M. E. (2006). Neuroscience. The brain's dark energy. *Science* 314, 1249–1250. doi: 10.1126/science.1134405

Sakoglu, U., Pearlson, G. D., Kiehl, K. A., Wang, Y. M., Michael, A. M., and Calhoun, V. D. (2010). A method for evaluating dynamic functional network connectivity and task-modulation: application to schizophrenia. *MAGMA* 23, 351–366. doi: 10.1007/s10334-010-0197-8

Shima, K., and Tanji, J. (1998). Both supplementary and presupplementary motor areas are crucial for the temporal organization of multiple movements. *J. Neurophysiol.* 80, 3247–3260. doi: 10.1152/jn.1998.80.6.3247

Skidmore, F. M., Yang, M., Baxter, L., von Deneen, K. M., Collingwood, J., He, G., et al. (2013). Reliability analysis of the resting state can sensitively and specifically identify the presence of Parkinson disease. *Neuroimage* 75, 249–261. doi: 10.1016/j.neuroimage.2011.06.056

Soddu, A., Vanhaudenhuyse, A., Bahri, M. A., Bruno, M. A., Boly, M., Demertzi, A., et al. (2012). Identifying the default-mode component in spatial IC analyses of patients with disorders of consciousness. *Hum. Brain Mapp.* 33, 778–796. doi: 10.1002/hbm.21249

Thompson, G. J., Magnuson, M. E., Merritt, M. D., Schwarb, H., Pan, W. J., McKinley, A., et al. (2013). Short-time windows of correlation between large-scale functional brain networks predict vigilance intraindividually and interindividually. *Hum. Brain Mapp.* 34, 3280–3298. doi: 10.1002/hbm.22140

Tsai, Y., Yuan, R., Huang, Y., Weng, H., Yeh, M., Lin, C., et al. (2014). Altered resting-state fMRI signals in acute stroke patients with ischemic penumbra. *PLoS One* 9:e105117. doi: 10.1371/journal.pone.0105117

Venketasubramanian, N., Lee, C. F., Young, S. H., Tay, S. S., Umapathi, T., Lao, A. Y., et al. (2017). Prognostic factors and pattern of long-term recovery with MLC601 (NeuroAiD) in the Chinese medicine neuroaid efficacy on stroke recovery - extension study. *Cerebrovasc. Dis.* 43, 36–42. doi: 10.1159/000452285

Wang, L., Yu, C., Chen, H., Qin, W., He, Y., Fan, F., et al. (2010). Dynamic functional reorganization of the motor execution network after stroke. *Brain* 133, 1224–1238. doi: 10.1093/brain/awq043

Ween, J. E. (2008). Functional imaging of stroke recovery: an ecological review from a neural network perspective with an emphasis on motor systems. *J. Neuroimaging* 18, 227–236. doi: 10.1111/j.1552-6569.2007.00180.x

Wu, J., Quinlan, E. B., Dodakian, L., McKenzie, A., Kathuria, N., Zhou, R. J., et al. (2015). Connectivity measures are robust biomarkers of cortical function and plasticity after stroke. *Brain* 138, 2359–2369. doi: 10.1093/brain/awv156

Yan, C. G., Yang, Z., Colcombe, S. J., Zuo, X. N., and Milham, M. P. (2017). Concordance among indices of intrinsic brain function: insights from inter-individual variation and temporal dynamics. *Sci. Bull.* 23, 1572–1584. doi: 10.1016/j.scib.2017.09.015

Yang, G., Wang, Y., Zeng, Y., Gao, G. F., Liang, X., Zhou, M., et al. (2013). Rapid health transition in China, 1990-2010: findings from the global burden of disease study 2010. *Lancet* 381, 1987–2015. doi: 10.1016/S0140-6736(13)61097-1

Yin, D., Luo, Y., Song, F., Xu, D., Peterson, B. S., Sun, L., et al. (2013). Functional reorganization associated with outcome in hand function after stroke revealed by regional homogeneity. *Neuroradiology* 55, 761–770. doi: 10.1007/s00234-013-1146-9

Yip, E., Yun, J., Wachowicz, K., Gabos, Z., Rathee, S., and Fallone, B. G. (2017). Sliding window prior data assisted compressed sensing for MRI tracking of lung tumors. *Med. Phys.* 44, 84–98. doi: 10.1002/mp.12027

Yuan, C., Zhu, H., Ren, Z., Yuan, M., Gao, M., Zhang, Y., et al. (2018). Precuneus-related regional and network functional deficits in social anxiety disorder: a resting-state functional MRI study. *Compr. Psychiatry* 82, 22–29. doi: 10.1016/j.comppsych.2017.12.002

Zang, Y., Jiang, T., Lu, Y., He, Y., and Tian, L. (2004). Regional homogeneity approach to fMRI data analysis. *Neuroimage* 22, 394–400. doi: 10.1016/j.neuroimage.2003.12.030

Zang, Y. F., He, Y., Zhu, C. Z., Cao, Q. J., Sui, M. Q., Liang, M., et al. (2007). Altered baseline brain activity in children with ADHD revealed by resting-state functional MRI. *Brain Dev.* 29, 83–91. doi: 10.1016/j.braindev.2006.07.002

Zhang, S., Ide, J. S., and Li, C. S. (2012). Resting-state functional connectivity of the medial superior frontal cortex. *Cereb. Cortex* 22, 99–111. doi: 10.1093/cercor/bhr088

Zhang, Y., Wang, L., Yang, J., Yan, R., Zhang, J., Sang, L., et al. (2017). Abnormal functional networks in resting-state of the sub-cortical chronic stroke patients with hemiplegia. *Brain Res.* 1663, 51–58. doi: 10.1016/j.brainres.2017.02.012

Zhu, J., Jin, Y., Wang, K., Zhou, Y., Feng, Y., Yu, M., et al. (2015). Frequency-dependent changes in the regional amplitude and synchronization of resting-state functional MRI in stroke. *PLoS One* 10:e0123850. doi: 10.1371/journal.pone.0123850

Zhu, L. L., Lindenberg, R., Alexander, M. P., and Schlaug, G. (2010). Lesion load of the corticospinal tract predicts motor impairment in chronic stroke. *Stroke* 41, 910–915. doi: 10.1161/STROKEAHA.109.577023

Conflict of Interest Statement: The authors declare that the research was conducted in the absence of any commercial or financial relationships that could be construed as a potential conflict of interest.

frontiers in Psychiatry

ORIGINAL RESEARCH
published: 04 March 2019
doi: 10.3389/fpsyt.2019.00084

Altered Brain Signal Variability in Patients With Generalized Anxiety Disorder

*Liyuan Li [1,2], YiFeng Wang [1,2], Liangkai Ye [1,2], Wang Chen [1,2], Xinju Huang [1,2], Qian Cui [1,3], Zongling He [1,2,4], Dongfeng Liu [1,2] and Huafu Chen [1,2]**

[1] The Clinical Hospital of Chengdu Brain Science Institute, MOE Key Lab for Neuroinformation, University of Electronic Science and Technology of China, Chengdu, China, [2] School of Life Science and Technology, Center for Information in BioMedicine, University of Electronic Science and Technology of China, Chengdu, China, [3] School of Public Affairs and Administration, University of Electronic Science and Technology of China, Chengdu, China, [4] Mental Health Center, The Fourth People's Hospital of Chengdu, Sichuan, China

Generalized anxiety disorder (GAD) is characterized by a chronic, continuous symptom of worry and exaggerated startle response. Although functional abnormality in GAD has been widely studied using functional magnetic resonance imaging (fMRI), the dynamic signatures of GAD are not fully understood. As a vital index of brain function, brain signal variability (BSV) reflects the capacity of state transition of neural activities. In this study, we recruited 47 patients with GAD and 38 healthy controls (HCs) to investigate whether or not BSV is altered in patients with GAD by measuring the standard deviation of fMRI signal of each voxel. We found that patients with GAD exhibited decreased BSV in widespread regions including the visual network, sensorimotor network, frontoparietal network, limbic system, and thalamus, indicating an inflexible brain state transfer pattern in these systems. Furthermore, the correlation between BSV and trait anxiety score was prone to be positive in patients with GAD but negative in HCs. The opposite relationships between BSV and anxiety level in the two groups indicate that the brain with moderate anxiety level may stay in the most stable rather than in the flexible state. As the first study of BSV in GAD, we revealed extensively decreased BSV in patients with GAD similar to that in other mental disorders but with a non-linear relationship between BSV and anxiety level indicating a novel neurodynamic mechanism of the anxious brain.

Keywords: brain signal variability, fMRI, generalized anxiety disorder, neurodynamics, non-linear relationship

OPEN ACCESS

Edited by:
Feng Liu,
Tianjin Medical University General Hospital, China

Reviewed by:
Feng Kong,
Shaanxi Normal University, China
Sufang Li,
Johns Hopkins University, United States

***Correspondence:**
Huafu Chen
chenhf@uestc.edu.cn

Specialty section:
This article was submitted to Neuroimaging and Stimulation, a section of the journal Frontiers in Psychiatry

Received: *17 October 2018*
Accepted: *06 February 2019*
Published: *04 March 2019*

Citation:
Li L, Wang Y, Ye L, Chen W, Huang X, Cui Q, He Z, Liu D and Chen H (2019) Altered Brain Signal Variability in Patients With Generalized Anxiety Disorder. Front. Psychiatry 10:84. doi: 10.3389/fpsyt.2019.00084

INTRODUCTION

Generalized anxiety disorder (GAD) is one of the most prevalent mental disorders characterized by exaggerated startle response and chronic, pervasive, and intrusive worry (1, 2). Based on static analysis methods, many functional magnetic resonance imaging (fMRI) studies have found aberrant brain activation related to cognition and emotion functions in GAD (3, 4). Inefficient intrinsic brain activity associated with integration of interoceptive and somesthetic functions has also been found in anxiety disorders (5–7). These static analysis methods for brain activity or activation have provided abundant evidence for us to understand the neural mechanism of GAD. However, clinically effective biomarker is still lacking. Recently, a mass of studies have shown that dynamic brain activity can provide novel information of neural characteristics for various neural

disorders (8–10). Whether the dynamic brain activity analysis can provide insightful information about the neural mechanism of GAD, however, is unknown.

Human brain activity is naturally variable (11). In previous years, fMRI research had regressed blood oxygen level-dependent (BOLD) signal variance as measurement-related or other confounds (12, 13). However, researchers found that the "noise" variance in data is an important feature of brain function in the recent 10 years (14, 15). In a neuroimaging time series, BSV measures the magnitude of variability from moment to moment (16). The forms of BSV include variance (17) and mean square successive differences (18), especially standard deviation (SD) (14, 15). As the next frontier in brain mapping, the brain signal variability (BSV) reflects the capacity of state transition of neural activities and dynamic range of brain functional systems (16). BSV has been suggested to be an excellent proxy of the characteristics of neural dynamics, cognitive performance, and brain disorders (14, 19–21). Great BSV has been suggested to be associated with increased ability to transfer between brain states (22) and to process varying and unexpected external stimuli (16, 23). Measured with the SD of brain signal, the BSV is more powerful than mean brain signal in predicting neural aging (14). Recently, the quadratic change in lifespan BSV trajectory has been further uncovered (24). Furthermore, a number of studies have demonstrated abnormal BSV in schizophrenia, attention deficit hyperactivity disorder, autism, and patients with disorders of consciousness, reflecting the dynamical dysfunction of neural activities in mental disorders (25, 26). Specifically, the non-linear dynamics of brain signal over a range of temporal scales are mainly decreased compared with those in healthy controls (HCs) (27). The hypothesis of "unhealthy brain is less variable than healthy brain" has been demonstrated in various clinical populations, such as dementia, untreated patients with schizophrenia, autism, and mesial temporal lobe epilepsy (16, 27, 28). In other words, many findings support Pool's opinion that "healthy brain is a chaotic brain" (11).

The anxious brain was viewed as an inflexible system, grounded in poor inhibition (29). In patients with GAD, a reduced capacity to inhibit cognitive (worry), behavioral (avoidance), and accompanying physiological manifestations was associated with cognitive rigidity and inflexibility (30). By using the mean-based methods, the core symptom, worry, which predominantly reflected a stimulus-independent mental processing also leads to the inflexible functional brain configurations in the prefrontal cortex, cingulate gyrus, and amygdala (31). However, the respective spatial patterns profiled by the SD-based method (like BSV) and mean-based method were highly different (14). To profile the flexibility of brain, BSV is a brand new effective index. Therefore, we hypothesized that patients with GAD may show decreased BSV compared with HCs in more related core regions.

In this study, we investigated the altered BSV in patients with GAD and healthy participants. To perform comprehensive comparisons, the relationship between BSV and anxiety level was also observed. Notably, this work is the first study of altered BSV in patients with GAD. Therefore, the BSV may be able to provide new insights into understanding the neural dynamics of GAD.

METHODS AND MATERIALS

Participants

Forty-seven patients with GAD were recruited from the mental health center of Chengdu, Sichuan, China. All patients were determined by consensus of two experienced psychiatrists by using the Structured Clinical Interview for DSM-IV (patient edition) (32). Clinical states of the patients were evaluated using the Hamilton anxiety scale (HAMA). Data from one patient was deleted because the BSV is extremely lower than the others ($<$ mean-5 SD). The exclusion criteria included schizophrenia, mental retardation, or personality disorder, history of loss of consciousness, substance abuse, and serious medical or neurological illness. The HC group was composed of 38 age-, gender-, education-, mean frame-wise displacement (FD) (33)-matched healthy participants. The Structured Clinical Interview for DSM-IV non-patient version was employed to ensure the absence of psychiatric illnesses in the HCs. The HCs did not finish the HAMA scale test because the test was only obtained in hospital by two well-trained psychiatrists. None of the HCs had a history of serious medical or neuropsychiatric illness or a family history of major psychiatric or neurological illness in their first-degree relatives. All participants (including GADs and HCs) finished the Chinese vision of Trait Anxiety Inventory (TAI) questionnaire (34), which is often used in clinical application in the diagnostic work-up of mental disorders and has good validity and reliability (35, 36).

Ultimately, 47 patients with GAD and 38 HC were included in the study (**Table 1**). Written informed consent, approved by the research ethical committee of the School of Life Science and Technology at University of Electronic Science and Technology of China, was obtained from each participant.

Data Acquisition

MRI data were acquired using a 3.0T GE 750 scanner (General Electric, Fairfield, Connecticut, USA) equipped with high-speed gradients. An 8-channel prototype quadrature birdcage head coil fitted with foam padding was applied to minimize the head motion. Ear plugs were used to minimize the scanner noise. Participants were instructed to simply rest with their eyes closed, minds relaxed, awake, and motionless. Functional images were acquired using a gradient-recalled echo-planar imaging (EPI) sequence. The parameters were as follows: repetition time/echo time = 2,000 ms/30 ms, 90° flip angle, bandwidth = 250 Hz/pixel, 43 axial slices (3.2 mm slice thickness without gap), 64 × 64 matrix, and 22 cm field of view. For each participant, 255 volumes were obtained.

Data Preprocessing

Functional images were preprocessed using the Data Processing Assistant for resting-state fMRI (DPARSF 2.2, http://www.restfmri.net/forum/DPARSF). The first five volumes were discarded to ensure signal equilibrium and for the participants to familiarize themselves with the scanning environment. The

TABLE 1 | Demographic information and characteristics of patients with GAD and HCs.

Variables (Mean ± SD)	GAD	HC	*P*-value
Gender (Male/Female)	47 (17/30)	38 (19/19)	0.200a
Age (years)	38.38 ± 9.08	35.24 ± 10.34	0.139b
Education (years)	11.30 ± 3.64	12.37 ± 3.89	0.195b
mean FD (mm)	0.0923 ± 0.0470	0.1049 ± 0.0555	0.261b
Course of illness (months)	61.96 ± 73.98	-	-
HAMA score	24.28 ± 6.583	-	-
TAI	55.04 ± 8.698	41.28 ± 5.43	<0.0001 b
Medication load index	1.40 ± 0.85	-	-
ANTIANXIETY MEDICATIONS, NO. OF PATIENTS			
Fluoxetine	1	-	-
Sertraline	5	-	-
Paroxetine	13	-	-
Citalopram	1	-	-
Escitalopram	9	-	-
Fluvoxamine	1	-	-
Venlafaxine	5	-	-
Duloxetine	1	-	-
Mirtazapine	8	-	-

SD, standard deviation; GAD, generalized anxiety disorder; HCs, healthy controls; HAMA, Hamilton Anxiety Rating Scale; TAI, Spielberger Trait Anxiety Inventory. a Chi-square test; b Independent-sample t-test.

remaining 250 images were slice-time corrected, spatially aligned, and spatially normalized to the Montreal Neurological Institute (MNI) EPI template and resampled to $3 \times 3 \times 3$ mm^3 voxels. After signal detrending, the images were spatially smoothed (8 mm full width at half maximum Gaussian kernel). Afterwards, Friston 24 head motion parameters, white matter signal, and cerebrospinal fluid signal were further regressed out. Finally, signal was filtered at 0.04–0.07 Hz because of the less noise contamination within this frequency range (37). The frame-wise displacement (FD) was used to represent instantaneous head motion. The mean FD of each participant was <0.5 mm.

Brain Signal Variability

Firstly, before calculating the BSV, we performed the temporal normalization for each voxel during the entire time of 500 s. The purpose of this step is to eliminate the contamination of the mean signal (14). Secondly, the SD which is simply the square root transformation of variance, was calculated in each voxel cross time series by using a custom-built function in MATLAB (The MathWorks, Inc.). According to Garrett's study, the SD of BOLD signal is temporal variability called BSV (14). The Anatomical Automatic Labeling 90 template was transformed to a binary mask and used to constrain the calculation in the gray matter (21).

Statistical Analysis

Two-sample *t*-test was used to assess the difference of BSV between the GAD and HC groups. Multiple-comparison correction was performed on the contrast brain map via the false discovery rate approach ($p < 0.05$). Pearson correlations were calculated between the BSV and TAI score in the two groups, correspondingly, with age, sex, education, and mean FD as control variables. The correlation analysis was performed under the regions with significantly different BSVs between the two groups. We adopted the cross-voxel correlation (21, 38) to evaluate the spatial correlation between the correlation maps of the GAD and HC groups. As suggested by Liang et al., the two 3D maps of correlation coefficient were first transformed into columns and then transformed into z-score by minus mean then divided by SD. Pearson correlation was finally computed between these two columns of data. Then, we built a linear mixed-effects model with State-Trait Anxiety Inventory (STAI) score as a factor to show the differences in these correlations between BSV and STAI score in the two groups.

RESULTS

Decreased BSV in Patients With GAD

Compared with the HC group, patients with GAD show decreased BSV across the widespread brain regions (**Figure 1A**). Significantly low BSV is primarily located in the visual network, sensorimotor network, frontoparietal network, limbic system, and thalamus (**Figure 1B** and **Table 2**).

Correlations Between BSV and Anxiety Severity in GAD and HC

As shown in **Figure 2A**, the correlation between BSV and TAI score in the HC group is mainly negative, whereas that in the GAD group is mainly positive. **Figures 2B,C** show the correlation map for the HC and GAD groups, respectively. The correlation coefficients in the HC group and GAD group are negatively related to each other ($r = -0.285$, $p = 4.12e{-}274$). In other words, if the correlation between BSV and TAI score in the HC group is negative in one voxel, that correlation in the GAD group is positive in that voxel. The differences of correlations between BSV and STAI score in the two groups are also mainly located in the visual network, sensorimotor network, and frontoparietal network (**Figure 3**).

DISCUSSION

To the best of our knowledge, this work is the first study on the abnormal BSV in patients with GAD. In accordance with other studies in mental disorders, we observed widely decreased BSV in patients with GAD compared with HCs, suggesting multiple deficits in neural systems of GAD. Interestingly, we observed opposite distributions of linear relationship between TAI score and BSV in the GAD and HC groups, indicating a non-linear relationship between anxiety level and BSV. In other words, the chaotic brain might be not always the healthy one.

Decreased Temporal Variability in Patients With GAD

In line with reduced BSV in other mental disorders, the current study revealed widely decreased BSV in patients with GAD, arguing that reduced BSV is a general characteristic of mental

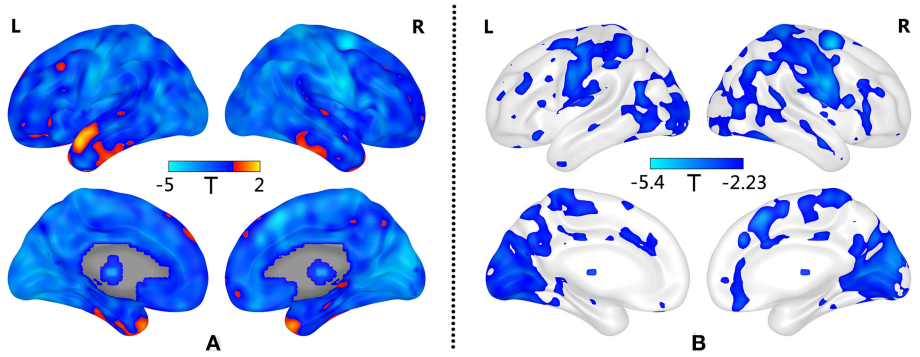

FIGURE 1 | Decreased BSV in widespread brain regions of GAD patients. **(A)** Decreased BSV across the brain in GAD; **(B)** Significantly decreased BSV in patients with GAD is primarily located in the visual network, sensorimotor network, frontoparietal network, limbic system and thalamus (FDR correction, $p < 0.05$). L: left; R: right.

TABLE 2 | Decreased BSV in patients with GAD compared with HC group.

	Brain regions	BA	Cluster size	T value	MNI coordinates		
					X	Y	Z
Cluster 1	Right superior frontal gyrus	5\6\17\18\32	13576	−5.4	21	0	57
	Bilateral postcentral gyrus						
	Bilateral supplementary motor area						
	Bilateral precentral gyrus						
	Bilateral occipital cortex						
	Dorsal anterior cingulate cortex						
Cluster 2	Right medial frontal gyrus	10	57	−4.10	9	66	27
Cluster 3	Left thalamus		194	−3.65	−3	−9	9
	Right caudate						
Cluster 4	Right inferior temporal gyrus	20\21	83	−3.61	60	−6	21
	Right middle temporal gyrus						
Cluster 5	Medial frontal gyrus	24	251	−3.45	6	39	−18
	Bilateral anterior cingulate						
Cluster 6	Left middle frontal gyrus	46	144	−3.42	−33	39	15

BA, Brodmann's area; MNI, Montreal Neurological Institute; X, Y, Z, coordinates of primary peak locations in the MNI space; T statistical value of peak voxel showing BSV decreased. All the clusters survived $p < 0.05$, FDR corrected, and a minimum cluster size of 50 voxels. Degree of freedom= 78.

disorders. Recent studies have shown that low amplitude of low-frequency fluctuation (ALFF) in the left supplementary motor area, right middle occipital gyrus, cerebellum, prefrontal-limbic system, and thalamus is associated with high-trait anxiety (32, 39, 40). Because ALFF is the square root of power (41) and power is equivalent to BSV (21). The BSV may reflect similar neural mechanisms to ALFF but in a non-linear way (21). Specifically, decreased BSV is associated with small potential kinetic energy to handle external environmental demands (16, 22) and low ability to transfer between different brain states (i.e., rest state and task state) (42). In patients with anxiety disorder, the functional deficit of environmental detection and the inflexible functional brain configurations has been found (31, 43). Therefore, the widely decreased BSV in patients with GAD may be associated with limited ability to adapt different external conditions and inflexible pattern of information transfer.

Low BSV in GAD is mainly located in the visual cortex, somatosensory cortex, anterior cingulate cortex (ACC), and thalamus. Multiple studies have documented deficits in the visual cortex in different anxiety disorders (44–46). Visual cortex plays a core role in the social brain network during visual and emotion processing (47). Visual cortex is also involved in the processing of fear generalization (48), which may greatly contribute to the GAD psychopathology (49, 50). The postcentral gyrus, as a critical substrate of interoceptive processing (51), is responsible for receiving, integrating, and interpreting most of the sensory information transmitted by the thalamus (52, 53). As shown by many studies, the thalamus is also strongly involved in interoceptive awareness (54–57). Abnormal connectivity between the postcentral gyrus and thalamus has been found in panic disorder, which may be associated with the typical symptoms (e.g., the extreme feeling of heartbeat) of panic disorder

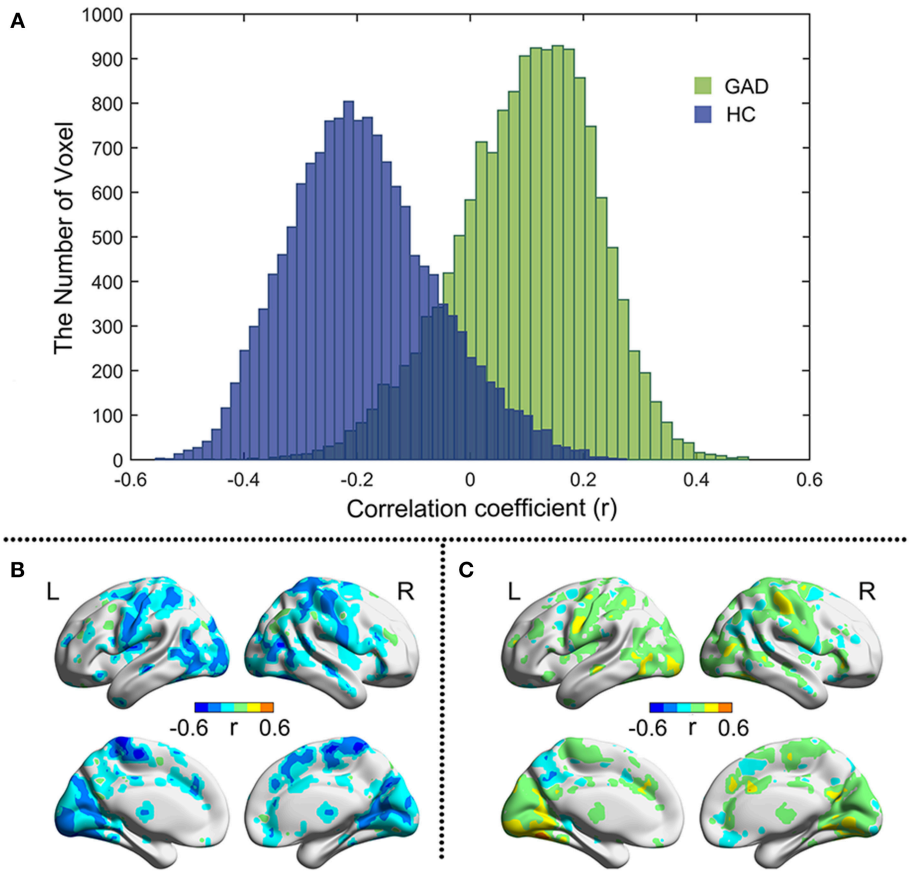

FIGURE 2 | Pearson correlation between BSV and TAI score in two groups. **(A)** Histogram illustrates voxel-wise correlations for GAD (green) and HC (blue) groups, respectively; **(B)** The r map of HC group; **(C)** The r map of GAD group. L: left; R: right.

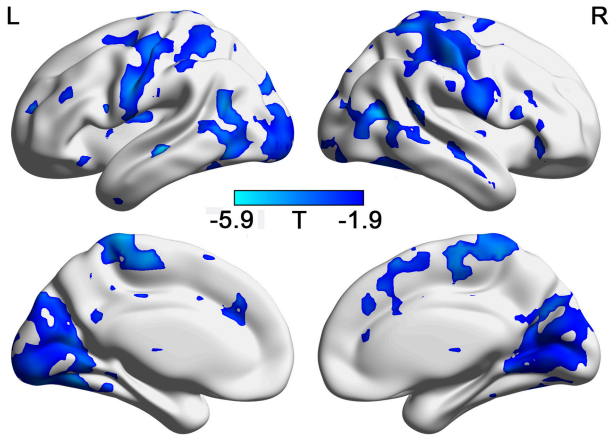

FIGURE 3 | The different relationship with STAI in GADs and in HCs. (FDR correction, $p < 0.05$). L: left; R: right.

(6). In general, as a hub of the interoceptive network, the ACC participates in mediating visceromotor activity and has projections into motor systems (56). Decreased functional connections between the ACC and thalamus was negatively correlated with HAMA in GAD, which may cause some somatic disturbed symptoms, such as rapid heart rate, low skin conductance, and difficulty breathing (58). Above all, the reduction of variability in these brain areas may be related to biased perception in processing exogenous and endogenous information (6, 59), which is implicated in the GAD pathological mechanism.

Reduced BSV in patients with GAD is also found in the dorsolateral prefrontal cortex and inferior parietal lobe, which are the key brain regions of the frontoparietal network (FPN). The deficiencies in FPN have been found in individuals with high-trait anxiety who have poor cognitive control and are easily distracted by emotional distractors from external environment (60, 61). Individuals with high anxiety generally require additional attentional control even in the absence of threat-related stimuli (62). The FPN is also a flexible hub during brain state transition (63). Low variability in the FPN may be associated with low ability to transfer between different brain states (42). Therefore, low BSV in the FPN may be associated with inflexible information to transform patterns facing the external world in patients with GAD.

Opposite Relationships Between BSV and Anxiety in the GAD and HC Groups

The opposite correlations between the BSV and TAI score in the HC group and in the GAD group has been found in the present study, indicating that the moderate anxious brain has small BSV. Moderate anxiety is associated with the best performance (64–66), and BSV has been demonstrated to be closely related to behavior performance (19, 24). In certain brain regions, maintaining great signal stability is also a critical marker of good task performance (22). In other words, the direction of correlation between BSV and behavioral performance depends on both cognition and brain region (21, 24, 67). Therefore, the opposite relationships between BSV and anxiety level may indicate that (1) moderate anxiety is associated with the most stable brain state and the best performance, and (2) increased BSV in subjects with high anxiety and low anxiety may be related to distinctive brain states, leading to different performances. Considering that (1) the dopaminergic system is closely associated with both anxiety and BSV (68, 69), (2) the non-linear relationship between dopaminergic system and behavioral performance (70), and (3) the quadratic relationship between anxiety and behavioral performance (66), the opposite BSV-anxiety relationship may reflect different neural dynamical configurations mediated by the dopaminergic system in patients with GAD and healthy people. Furthermore, the negative correlation between the HC group and GAD group suggests that the neuropsychological association in HC and patients with GAD may be driven by the same mechanism rather than independent from each other. This hypothesis deserves further investigations.

Although increased anxious levels in GADs showed increased BSV which indicated the great capacity of detection, the mechanism of this seemingly increasing ability can be totally different from healthy participants. In patients with GAD, the excessive activation is an apparent clinical symptom (1, 2), which might be associated with the high detection. In addition, this conclusion still needs further research. Meanwhile, the great BSV in some regions can be a compensation mechanism of an inefficient brain (14).

Overall, the opposite correlations between the BSV and TAI score in two groups indicate close relationships among dopaminergic system, behavioral performance, anxiety level, and BSV. These relationships can be described by the U law. Therefore, BSV is not always linearly related to brain health (24). These results provide valuable insights into understanding the relationship between BSV and health.

LIMITATIONS

Some limitations remain in this study. First, the sample is relatively small (n=85), impeding the uncovering of a strong correlation between BSV and anxiety level. Second, the HAMA score is lacking in the HC group because these participants were tested at the university rather than at the hospital, hindering the full investigation of clinical relevance of BSV. Third, some undiagnosed comorbid psychological disorders may exist in this sample, which may mix the true relationship between BSV and anxiety. A large sample with accurate diagnosis and complete scale collection is needed in future studies.

CONCLUSION

In summary, the decreased BSV in patients with GAD and different neuropsychological relationships in patients with GAD and HCs may reveal a novel neurodynamic mechanism, suggesting that the chaotic brain is not always the healthy one.

DATA AVAILABILITY

The datasets generated for this study are available on request to the corresponding author.

ETHICS STATEMENT

All procedures followed were in accordance with the ethical standards of the responsible committee on human experimentation (institutional and national) and with the Helsinki Declaration of 1975 and the applicable revisions at the time of investigation. Informed consent was obtained from all patients included in the study.

AUTHOR CONTRIBUTIONS

LL, YW, and HC designed the study. LY, WC, DL, and HX wrote the computing scripts. QC and ZH interviewed all patients by using the DSM-IV. LL managed the literature searches and analyses, acquired, and analyzed the data, and wrote the first manuscript draft. All authors contributed and have approved the final manuscript. The authors thank all subjects participating in this study.

FUNDING

This work was supported by the National Natural Science Foundation of China (31600930, 81771919, and 61533006), the Fundamental Research Funds for the Central Universities (ZYGX2016KYQD120), the Sichuan Science and Technology Program (2018TJPT0016), the Science Foundation of Ministry of Education of China (14XJC190003), the Scientific Research Project of Sichuan Medical Association (S15012), and the Youth Innovation Project of Sichuan Provincial Medical Association (Q14014).

ACKNOWLEDGMENTS

The authors also thank the two reviewers for their suggestions and comments.

REFERENCES

1. Shin LM, Liberzon I. The neurocircuitry of fear, stress and anxiety disorders. *Neuropsychopharmacology*. (2010) 35:169–91. doi: 10.1038/npp.2009.83
2. American Psychiatric Association. *Diagnostic and Statistical Manual of Mental Disorders*. 5th ed. Washington, DC: American Psychiatric Association (2013). p. 280.
3. Makovac E, Meeten F, Watson DR, Herman A, Garfinkel SN D, et al. Alterations in amygdala-prefrontal functional connectivity account for excessive worry and autonomic dysregulation in generalized anxiety disorder. *Biol Psychiatry*. (2016) 80:786–95. doi: 10.1016/j.biopsych.2015.10.013
4. Cui Q, Vanman EJ, Long Z, Pang Y, Chen Y, Wang Y, et al. Social anxiety disorder exhibit impaired networks involved in self and theory of mind processing. *Soc Cogn Affect Neurosci.* (2017) 12:1284–95. doi: 10.1093/scan/nsx050
5. Liu F, Guo W, Fouche J-P, Wang Y, Wang W, Ding J, et al. Multivariate classification of social anxiety disorder using whole brain functional connectivity. *Brain Struct Func.* (2015) 220:101–15. doi: 10.1007/s00429-013-0641-4
6. Cui H, Zhang J, Liu Y, Li Q, Li H, Zhang L, et al. Differential alterations of resting-state functional connectivity in generalized anxiety disorder and panic disorder. *Hum Brain Mapp.* (2016) 37:1459–73. doi: 10.1002/hbm.23113
7. Xia L, Li S, Wang T, Guo Y, Meng L, Feng Y, et al. Spontaneous alterations of regional brain activity in patients with adult generalized anxiety disorder. *Neuropsychiatr Dis Treat.* (2017) 13:1957–65. doi: 10.2147/NDT.S133853
8. Liu F, Wang Y, Li M, Wang W, Li R, Zhang Z, et al. Dynamic functional network connectivity in idiopathic generalized epilepsy with generalized tonic-clonic seizure. *Hum Brain Mapp.* (2016) 38:957–73. doi: 10.1002/hbm.23430
9. Nelson B, McGorry PD, Wichers M, Wigman JTW, Hartmann JA. Moving from static to dynamic models of the onset of mental disorder. *JAMA Psychiatry*. (2017) 74:528. doi: 10.1001/jamapsychiatry.2017.0001
10. Barber AD, Lindquist MA, DeRosse P, Karlsgodt KH. Dynamic functional connectivity states reflecting psychotic-like experiences. *Biol Psychiatry Cogn Neurosci Neuroimaging*. (2018) 3:443–53. doi: 10.1016/j.bpsc.2017.09.008
11. Pool R. Is it healthy to be chaotic? *Science*. (1989) 243:604–7. doi: 10.1126/science.2916117
12. Biswal B, Zerrin Yetkin F, Haughton VM, Hyde JS. Functional connectivity in the motor cortex of resting human brain using echo-planar MRI. *Magn Resonance Med.* (1995) 34:537–41. doi: 10.1002/mrm.1910340409
13. Stein T. Bacillus subtilis antibiotics: structures, syntheses and specific functions. *Mol Microbiol.* (2005) 56:845–57. doi: 10.1111/j.1365-2958.2005.04587.x
14. Garrett DD, Kovacevic N, McIntosh AR, Grady CL. Blood oxygen level-dependent signal variability is more than just noise. *J Neurosci.* (2010) 30:4914–21. doi: 10.1523/JNEUROSCI.5166-09.2010
15. Wutte MG, Smith MT, Flanagin VL, Wolbers T. Physiological signal variability in hMT+ reflects performance on a direction discrimination task. *Front Psychol.* (2011) 2:185. doi: 10.3389/fpsyg.2011.00185
16. Garrett DD, Samanez-Larkin GR, MacDonald SWS, Lindenberger U, McIntosh AR, Grady CL. Moment-to-moment brain signal variability: a next frontier in human brain mapping? *Neurosci Biobehav Rev.* (2013) 37:610–24. doi: 10.1016/j.neubiorev.2013.02.015
17. He BJ. Scale-free properties of the functional magnetic resonance imaging signal during rest and task. *J Neurosci.* (2011) 31:13786–95. doi: 10.1523/JNEUROSCI.2111-11.2011
18. Leo A, Bernardi G, Handjaras G, Bonino D, Ricciardi E, Pietrini P. Increased BOLD variability in the parietal cortex and enhanced parieto-occipital connectivity during tactile perception in congenitally blind individuals. *Neural Plast.* (2012) 2012:720278. doi: 10.1155/2012/720278
19. Wang Y-F, Dai G-S, Liu F, Long Z-L, Yan JH, Chen H-F. Steady-state BOLD response to higher-order cognition modulates low-frequency neural oscillations. *J Cogn Neurosci.* (2015) 27:2406–15. doi: 10.1162/jocn_a_00864
20. Wang Y-F, Liu F, Long Z-L, Duan X-J, Cui Q, Yan JH, et al. Steady-state BOLD response modulates low frequency neural oscillations. *Sci Rep.* (2015) 4:7376. doi: 10.1038/srep07376
21. Wang Y, Chen W, Ye L, Biswal BB, Yang X, Zou Q, et al. Multiscale energy reallocation during low-frequency steady-state brain response. *Hum Brain Mapp.* (2018) 39:2121–32. doi: 10.1002/hbm.23992
22. Garrett DD, Kovacevic N, McIntosh AR, Grady CL. The importance of being variable. *J Neurosci.* (2011) 31:4496–503. doi: 10.1523/JNEUROSCI.5641-10.2011
23. Garrett DD, McIntosh AR, Grady CL. Brain signal variability is parametrically modifiable. *Cereb Cortex*. (2014) 24:2931–40. doi: 10.1093/cercor/bht150
24. Nomi JS, Bolt TS, Ezie CEC, Uddin LQ, Heller AS. Moment-to-moment BOLD signal variability reflects regional changes in neural flexibility across the lifespan. *J Neurosci.* (2017) 37:5539–48. doi: 10.1523/JNEUROSCI.3408-16.2017
25. Huang Z, Zhang J, Wu J, Qin P, Wu X, Wang Z, et al. Decoupled temporal variability and signal synchronization of spontaneous brain activity in loss of consciousness: an fMRI study in anesthesia. *Neuroimage*. (2016) 124:693–703. doi: 10.1016/j.neuroimage.2015.08.062
26. Zhang J, Cheng W, Liu Z, Zhang K, Lei X, Yao Y, et al. Neural, electrophysiological and anatomical basis of brain- network variability and its characteristic changes in mental disorders. *Brain*. (2016) 139:2307–21. doi: 10.1093/brain/aww143
27. Takahashi T. Complexity of spontaneous brain activity in mental disorders. *Prog Neuro-Psychopharmacol Biol Psychiatry*. (2013) 45:258–66. doi: 10.1016/j.pnpbp.2012.05.001
28. Protzner AB, Valiante T, Kovacevic N, McCormick C, McAndrews MP. Hippocampal signal complexity in mesial temporal lobe epilepsy: a noisy brain is a healthy brain. *Arch Ital Biol.* (2010) 148:289–97.
29. Friedman BH, Thayer JF. Autonomic balance revisited: panic anxiety and heart rate variability. *J Psychosom Res.* (1998) 44:133–51. doi: 10.1016/S0022-3999(97)00202-X
30. Ottaviani C, Watson DR, Meeten F, Makovac E, Garfinkel SN, Critchley HD. Neurobiological substrates of cognitive rigidity and autonomic inflexibility in generalized anxiety disorder. *Biol Psychol.* (2016) 119:31–41. doi: 10.1016/j.biopsycho.2016.06.009
31. Fonzo GA, Etkin A. Affective neuroimaging in generalized anxiety disorder: an integrated review. *Dialogues Clin Neurosci.* (2017) 19:169–79.
32. Yuan C, Zhu H, Ren Z, Yuan M, Gao M, Zhang Y, et al. Precuneus-related regional and network functional deficits in social anxiety disorder: a resting-state functional MRI study. *Compr Psychiatry*. (2018) 82:22–9. doi: 10.1016/j.comppsych.2017.12.002
33. Power JD, Barnes KA, Snyder AZ, Schlaggar BL, Petersen SE. Spurious but systematic correlations in functional connectivity MRI networks arise from subject motion. *Neuroimage*. (2012) 59:2142–54. doi: 10.1016/j.neuroimage.2011.10.018
34. Speilberger CD, Gorsuch RL, Lushene R, Vagg PR. *Manual for the State-Trait Anxiety Inventory (Form Y1 - Y2).* Palo Alto, CA: Consulting Psychologists (1983).
35. Shek DTL. The Chinese version of the state-trait anxiety inventory: its relationship to different measures of psychological well-being. *J Clin Psychol.* (1993) 49:349–58.
36. Kvaal K, Ulstein I, Nordhus IH, Engedal K. The Spielberger state-trait anxiety inventory (STAI): the state scale in detecting mental disorders in geriatric patients. *Int J Geriatr Psychiatry*. (2005) 20:629–34. doi: 10.1002/gps.1330
37. Glerean E, Salmi J, Lahnakoski JM, Jääskeläinen IP, Sams M. Functional magnetic resonance imaging phase synchronization as a measure of dynamic functional connectivity. *Brain Connect.* (2012) 2:91–101. doi: 10.1089/brain.2011.0068
38. Liang X, Zou Q, He Y, Yang Y. Coupling of functional connectivity and regional cerebral blood flow reveals a physiological basis for network hubs of the human brain. *Proc Nat Acad Sci.* (2013) 110:1929–34. doi: 10.1073/pnas.1214900110
39. Wang W, Hou J, Qian S, Liu K, Li B, Li M, et al. Aberrant regional neural fluctuations and functional connectivity in generalized anxiety disorder revealed by resting-state functional magnetic resonance imaging. *Neurosci Lett.* (2016) 624:78–84. doi: 10.1016/j.neulet.2016.05.005
40. Yin P, Zhang M, Hou X, Tan Y, Fu Y, Qiu J. The brain structure and spontaneous activity baseline of the behavioral bias in trait anxiety. *Behav Brain Res.* (2016) 312:355–61. doi: 10.1016/j.bbr.2016.06.036

41. Yang H, Long X-Y, Yang Y, Yan H, Zhu C-Z, Zhou X-P, et al. Amplitude of low frequency fluctuation within visual areas revealed by resting-state functional MRI. *Neuroimage*. (2007) 36:144–52. doi: 10.1016/j.neuroimage.2007.01.054
42. Garrett DD, Kovacevic N, McIntosh AR, Grady CL. The modulation of BOLD variability between cognitive states varies by age and processing speed. *Cerebral Cortex*. (2013) 23:684–93. doi: 10.1093/cercor/bhs055
43. de Rooij SR, Schene AH, Phillips DI, Roseboom TJ. Depression and anxiety: associations with biological and perceived stress reactivity to a psychological stress protocol in a middle-aged population. *Psychoneuroendocrinology*. (2010) 35:866–77. doi: 10.1016/j.psyneuen.2009.11.011
44. Etkin A, Wager TD. Functional neuroimaging of anxiety: a meta-analysis of emotional processing in PTSD, social anxiety disorder, and specific phobia. *Am J Psychiatry*. (2007) 164:1476–88. doi: 10.1176/appi.ajp.2007.07030504
45. Gentili C, Gobbini MI, Ricciardi E, Vanello N, Pietrini P, Haxby JV, et al. Differential modulation of neural activity throughout the distributed neural system for face perception in patients with Social Phobia and healthy subjects. *Brain Res Bull.* (2008) 77:286–92. doi: 10.1016/j.brainresbull.2008.08.003
46. Syal S, Hattingh CJ, Fouché, J-P, Spottiswoode B, Carey PD, Lochner C, et al. Grey matter abnormalities in social anxiety disorder: a pilot study. *Metab Brain Dis.* (2012) 27:299–309. doi: 10.1007/s11011-012-9299-5
47. Sabatinelli D, Bradley MM, Fitzsimmons JR, Lang PJ. Parallel amygdala and inferotemporal activation reflect emotional intensity and fear relevance. *Neuroimage*. (2005) 24:1265–70. doi: 10.1016/j.neuroimage.2004.12.015
48. Lissek S, Bradford DE, Alvarez RP, Burton P, Espensen-Sturges T, Reynolds RC, et al. Neural substrates of classically conditioned fear-generalization in humans: a parametric fMRI study. *Soc Cogn Affect Neurosci.* (2014) 9:1134–42. doi: 10.1093/scan/nst096
49. Lissek S. Toward an account of clinical anxiety predicated on basic, neurally-mapped mechanisms of pavlovian fear-learning: the case for conditioned overgeneralization. *Depress Anxiety*. (2012) 29:257–63. doi: 10.1002/da.21922
50. Lissek S, Kaczkurkin AN, Rabin S, Geraci M, Pine DS, Grillon C. Generalized anxiety disorder is associated with overgeneralization of classically conditioned-fear. *Biol Psychiatry*. (2014) 75:909–15. doi: 10.1016/j.biopsych.2013.07.025
51. Critchley HD, Wiens S, Rotshtein P, Öhman A, Dolan RJ. Neural systems supporting interoceptive awareness. *Nat Neurosci.* (2004) 7:189–95. doi: 10.1038/nn1176
52. Nelson AJ, Chen R. Digit somatotopy within cortical areas of the postcentral gyrus in humans. *Cereb Cortex*. (2008) 18:2341–51. doi: 10.1093/cercor/bhm257
53. Northoff G. *Unlocking the Brain, Volume 2: Consciousness*. New York, NY: Oxford University Press (2013).
54. Rieck RW, Ansari MS, Whetsell WO, Deutch AY, Kessler RM. Distribution of dopamine d2-like receptors in the human thalamus: autoradiographic and PET studies. *Neuropsychopharmacology*. (2004) 29:362–72. doi: 10.1038/sj.npp.1300336
55. Pollatos O, Schandry R, Auer DP, Kaufmann C. Brain structures mediating cardiovascular arousal and interoceptive awareness. *Brain Res.* (2007) 1141:178–87. doi: 10.1016/j.brainres.2007.01.026
56. Khalsa SS, Rudrauf D, Feinstein JS, Tranel D. The pathways of interoceptive awareness. *Nat Neurosci.* (2009) 12:1494–6. doi: 10.1038/nn.2411
57. Cho YT, Fromm S, Guyer AE, Detloff A, Pine DS, Fudge JL, et al. Nucleus accumbens, thalamus and insula connectivity during incentive anticipation in typical adults and adolescents. *Neuroimage*. (2013) 66:508–21. doi: 10.1016/j.neuroimage.2012.10.013
58. Hoehn-Saric R, McLeod DR, Funderburk F, Kowalski P. Somatic symptoms and physiologic responses in generalized anxiety disorderand panic disorder. *Arch Gen Psychiatry*. (2004) 61:913. doi: 10.1001/archpsyc.61.9.913
59. Wang Y, Zhu L, Zou Q, Cui Q, Liao W, Duan X, et al. Frequency dependent hub role of the dorsal and ventral right anterior insula. *Neuroimage*. (2018) 165:112–7. doi: 10.1016/j.neuroimage.2017.10.004
60. Pacheco-Unguetti AP, Acosta A, Callejas A, Lupiáñez J. Attention and anxiety: different attentional functioning under state and trait anxiety. *Psychol Sci.* (2010) 21:298–304. doi: 10.1177/0956797609359624
61. Hofmann SG, Ellard KK, Siegle GJ. Neurobiological correlates of cognitions in fear and anxiety: a cognitive-neurobiological information-processing model. *Cognit Emot*. (2012) 26:282–99. doi: 10.1080/02699931.2011.579414
62. Basten U, Stelzel C, Fiebach CJ. Trait anxiety modulates the neural efficiency of inhibitory control. *J Cogn Neurosci.* (2011) 23:3132–45. doi: 10.1162/jocn_a_00003
63. Cole MW, Reynolds JR, Power JD, Repovs G, Anticevic A, Braver TS. Multi-task connectivity reveals flexible hubs for adaptive task control. *Nat Neurosci.* (2013) 16:1348–55. doi: 10.1038/nn.3470
64. Sonstroem RJ, Bernardo P. Intraindividual pregame state anxiety and basketball performance: a re-examination of the inverted-U curve. *J Sport Psychol.* (1982) 4:235–45. doi: 10.1123/jsp.4.3.235
65. Gould D, Petlichkoff L, Simons J, Vevera M. Relationship between competitive state anxiety—inventory-2 subscale scores and pistol shooting performance. *J Sport Psychol.* (1987) 9:33–42. doi: 10.1123/jsp.9.1.33
66. Raglin JS, Turner PE. Anxiety and performance in track and field athletes: a comparison of the inverted-U hypothesis with zone of optimal function theory. *Pers Individ Dif.* (1993) 14:163–71. doi: 10.1016/0191-8869(93)90186-7
67. Armbruster-Genc DJN, Ueltzhoffer K, Fiebach CJ. Brain signal variability differentially affects cognitive flexibility and cognitive stability. *J Neurosci.* (2016) 36:3978–87. doi: 10.1523/JNEUROSCI.2517-14.2016
68. Guitart-Masip M, Salami A, Garrett D, Rieckmann A, Lindenberger U, Bäckman L. BOLD variability is related to dopaminergic neurotransmission and cognitive aging. *Cereb Cortex*. (2016) 26:2074–83. doi: 10.1093/cercor/bhv029
69. Kim S, Shou J, Abera S, Ziff EB. Sucrose withdrawal induces depression and anxiety-like behavior by Kir2. 1 upregulation in the nucleus accumbens. *Neuropharmacology*. (2018) 130:10–7. doi: 10.1016/j.neuropharm.2017.11.041
70. Cools R, D'Esposito M. Inverted-U shaped dopamine actions on human working memory and cognitive control. *Biol. Psychiatry*. (2011) 69:e113–25. doi: 10.1016/j.biopsych.2011.03.028

Conflict of Interest Statement: The authors declare that the research was conducted in the absence of any commercial or financial relationships that could be construed as a potential conflict of interest.

frontiers in Neuroscience

ORIGINAL RESEARCH
published: 22 March 2019
doi: 10.3389/fnins.2019.00268

Reduced Dynamic Interactions Within Intrinsic Functional Brain Networks in Early Blind Patients

Xianglin Li[1,2], Ailing Wang[3], Junhai Xu[4], Zhenbo Sun[2], Jikai Xia[5], Peiyuan Wang[5], Bin Wang[2], Ming Zhang[1]* and Jie Tian[1,6]**

[1] Department of Medical Imaging, The First Affiliated Hospital of Xi'an Jiaotong University, Xi'an, China, [2] Medical Imaging Research Institute, Binzhou Medical University, Yantai, China, [3] Department of Clinical Laboratory, Yantai Affiliated Hospital of Binzhou Medical University, Yantai, China, [4] Tianjin Key Laboratory of Cognitive Computing and Application, School of Artificial Intelligence, College of Intelligence and Computing, Tianjin University, Tianjin, China, [5] Department of Radiology, Yantai Affiliated Hospital of Binzhou Medical University, Yantai, China, [6] School of Life Sciences and Technology, Xidian University, Xi'an, China

OPEN ACCESS

Edited by:
Feng Liu,
Tianjin Medical University General Hospital, China

Reviewed by:
Yifeng Wang,
University of Electronic Science and Technology of China, China
Mengting Liu,
University of Southern California, United States

***Correspondence:**
Bin Wang
binwang001@aliyun.com
Ming Zhang
zhangming01@mail.xjtu.edu.cn
Jie Tian
jie.tian@ia.ac.cn

Specialty section:
This article was submitted to Brain Imaging Methods, a section of the journal Frontiers in Neuroscience

Received: 28 December 2018
Accepted: 07 March 2019
Published: 22 March 2019

Citation:
Li X, Wang A, Xu J, Sun Z, Xia J, Wang P, Wang B, Zhang M and Tian J (2019) Reduced Dynamic Interactions Within Intrinsic Functional Brain Networks in Early Blind Patients. Front. Neurosci. 13:268. doi: 10.3389/fnins.2019.00268

Neuroimaging studies in early blind (EB) patients have shown altered connections or brain networks. However, it remains unclear how the causal relationships are disrupted within intrinsic brain networks. In our study, we used spectral dynamic causal modeling (DCM) to estimate the causal interactions using resting-state data in a group of 20 EB patients and 20 healthy controls (HC). Coupling parameters in specific regions were estimated, including the medial prefrontal cortex (mPFC), posterior cingulate cortex (PCC), and inferior parietal lobule (IPC) in the default mode network (DMN); dorsal anterior cingulate cortex (dACC) and bilateral anterior insulae (AI) in the salience network (SN), and bilateral frontal eye fields (FEF) and superior parietal lobes (SPL) within the dorsal attention network (DAN). Statistical analyses found that all endogenous connections and the connections from the mPFC to bilateral IPCs in EB patients were significantly reduced within the DMN, and the effective connectivity from the PCC and lIPC to the mPFC, and from the mPFC to the PCC were enhanced. For the SN, all significant connections in EB patients were significantly decreased, except the intrinsic right AI connections. Within the DAN, more significant effective connections were observed to be reduced between the EB and HC groups, while only the connections from the right SPL to the left SPL and the intrinsic connection in the left SPL were significantly enhanced. Furthermore, discovery of more decreased effective connections in the EB subjects suggested that the disrupted causal interactions between specific regions are responsive to the compensatory brain plasticity in early deprivation.

Keywords: early blindness, effective connectivity, spectral dynamic causal modeling, intrinsic brain networks, brain plasticity

INTRODUCTION

The recognition of objects could be manipulated through the coordinated cross-modal interactions of different modalities, such as vision, touch and audition (Amedi et al., 2005; Dormal et al., 2018). Deprivation of one sensory modality could give us a chance to explore the plasticity changes of the cognitive functions (Jiang et al., 2015). Two hypotheses have been raised to explain the plasticity in early blindness. The first hypothesis indicated a kind of maladjustment caused by the

early blindness. When the sensory information is manipulated, there is a decrease in processing capacities by the early visual deprivation (Jiang et al., 2015). The other hypothesis is based on the compensatory explanation, in which the blind patients exhibit a superior ability in retained sensory modalities (Pascual-Leone et al., 2005). The early visual deprivation has been demonstrated to cause the structural and functional remodeling or reorganization in both intact and deprived sensory cortices (Bauer et al., 2017, 2018; Hou et al., 2017). Furthermore, impaired cognitive performances have been discovery in specific brain regions or networks (Dormal et al., 2018; Manescu et al., 2018; Vercillo et al., 2018). The baseline metabolism and blood flow in specific cortices have been suggested to show a significant increase in early blind (EB) patients (Viski et al., 2016). Functional correlations were observed between the subregions of the visual cortex in the retinotopic pattern in EB subjects at rest (Bock et al., 2015). Furthermore, EB patients also exhibit disrupted functional connections and stronger parietal and auditory networks compared with sighted subjects (Boldt et al., 2014; Hou et al., 2017; Abboud and Cohen, 2019). Therefore, EB patients showed a compensatory pattern in the primary sensory networks, while the other brain networks related to cognition might be disrupted due to the early deprivation.

The resting-state technique on functional magnetic resonance imaging (fMRI) has been proved to be powerful in revealing the abnormalities of intrinsic functional connections. The default mode network (DMN) is the most prominent system in the resting state (Mccormick and Telzer, 2018; Prestel et al., 2018), which consists of the medial prefrontal cortex (mPFC), posterior cingulate cortex (PCC), and bilateral inferior parietal lobule (IPL), and some brain areas in the temporal lobe (Sharaev et al., 2016). By applying advanced brain network analyses to the resting-state data, abnormalities of the functional integration in EB patients have been examined in many studies, reflecting the statistical dependencies between distant brain regions (Heine et al., 2015; Sabbah et al., 2016). However, correlation parameters can only calculate the statistical dependency between two regions, while the causal interactions cannot be estimated. Moreover, DMN regions have been observed to be hyperactivated in many cognitive tasks, like autobiographical information retrieval, mind-wandering, emotional processing, and spontaneous cognition (Turkheimer et al., 2015; Hu et al., 2017).

In addition to the DMN, two other distinct brain networks (ventral and dorsal) play a vital role in EB subjects in the allocation of attention (Jimenez et al., 2016). The ventral network consists of the temporoparietal junction, anterior cingulate cortex (ACC), and anterior insulae (AI), which has been suggested to be responsible for stimulus-driven attention (Jimenez et al., 2016; Liu et al., 2017; Wang et al., 2018). The other dorsal network, constituted of the lateral frontal eye field (FEF) as well as the bilateral superior parietal lobes (SPL), is correlated with the voluntary, sustained orienting of attention (Corbetta and Shulman, 2011; Tsvetanov et al., 2016). Recent studies have highlighted the dysfunction in the ventral network in subjects with disorders, but not in the dorsal network (White et al., 2013; Wynn et al., 2015). The ventral attention network can also be called the "salience network" (SN). Pathophysiological studies have demonstrated that EB subjects with dysfunctions could result in the incorrect assigning of salience (Palaniyappan and Liddle, 2012). Therefore, the application of the resting-state fMRI approach can be potentially powerful in the assessment of attentional deficits in EB patients when we intend to examine the relative contributions of these two networks.

Dynamic causal modeling (DCM) is an appropriate approach to examine the causal influence, which is designed to calculate the effective connectivity changes underlying human responses based on Bayesian analysis. When one specific model is constructed (including specific brain regions, directed connections, and modulations), the parameters are estimated based on the observed data and model structures. Dynamic causal modeling is model-based, and shows great advantages compared to the functional connectivity or data-driven effective connectivity like the Granger causality, as DCM allows different hypotheses to be tested, which could capture the functional brain architectures corresponding to a specific hypothesis (Friston et al., 2017). Many studies have been reported by applying DCM to fMRI data and Magnetoencephalography/electroencephalography (MEG/EEG) (Chahine et al., 2017; Yang et al., 2017; He and Johnson, 2018; Van De Steen et al., 2019). Recently, a new version of DCM-spectral DCM was developed to estimate the intrinsic effective connections from resting-state data using the cross spectra of the signals through a deterministic model (Friston et al., 2014). The cross-spectra can be considered as a more complete measure of functional connections (Park et al., 2018). Spectral DCM renders the model essentially in a deterministic way to get rid of the heavy load in estimating the random fluctuations in neural states. Therefore, spectral DCM makes DCM in resting-state fMRI slightly simpler and does not require a bilinear term accounting for condition-specific effects (Razi et al., 2015). Furthermore, spectral DCM is intended to simply compare the endogenous coupling between different groups (healthy controls vs. patients), so it only estimates the time-invariant parameters of the cross spectra. As the frequency domain is used in estimating the effective connectivity, the high computational efficiency and stable estimation make spectral DCM significantly powerful to compare the couplings and directionality in the intrinsic brain networks between groups of subjects, like patients and healthy cohorts (Li et al., 2017). Therefore, this is the reason for choosing the spectral DCM approach in this study.

Previous studies have suggested that the EB subjects showed a disruption of functional connectivity both in the visual cortex and other brain regions located in other cognitive brain networks (Liu et al., 2017; Dormal et al., 2018; Abboud and Cohen, 2019). Early deprivation could trigger the functional preference for the selective auditory recruitment in the cognitive brain networks (Dormal et al., 2018) and a reduction of the interhemispheric functional connectivity in the cognitive regions (Hou et al., 2017). Although the disruption of the functional interactions among the regions from the visual cortex and the cognitive brain networks, like the DMN and SN, it remains unclear how the directed interactions between these regions changed in the EB subjects. The purpose of our study is to examine the changes in the

effective connectivity within three high-order cognitive networks between EB patients and healthy controls (HC) by estimating the corresponding parameters with a newly developed spectral DCM. In this study, we had one hypothesis: early deprivation could affect the dynamic interactions between regions within three brain networks. Furthermore, the strength of the effective connectivity between regions in all three networks might be decreased due to the early deprivation. The spectral DCM was used to explore the causal neuronal influences within the intrinsic functional networks (DMN, SN and DAN) in a sample of 20 EB patients and 20 matched HC. Firstly, an independent component analysis was made to the resting-state functional images to generate the DMN, SN and DAN components. Then, the spectral DCM was employed to compute the effective connectivity within DMN, SN, and DAN of EB patients and HC. A Bayesian model selection procedure was adopted to determine the optimal DCM model at the group level. Statistical analyses were further conducted to compare the differences in the effective connectivity parameters within DMN, SN, and DAN between EB and HC subjects.

MATERIALS AND METHODS

Participants

Twenty EB subjects and 20 sighted subjects participated in this study. The mean age was 22.3 ± 1.4 years for the blind group, and 20.7 ± 1.2 years for the sighted group; there was no significant difference between both groups. The blindness of these subjects was evaluated and diagnosed by two professional ophthalmologists from Yantai Affiliated Hospital of Binzhou Medical University based on the retinal pathology. All the EB subjects had the same categories of blindness, mainly caused by cataracts and retinal pigment degeneration (Cataract: 8; Retinal pigment degeneration: 12). **Table 1** shows the detailed information for all EB subjects. All subjects were right-handed, and no subject had neurological problems except for the visual deprivation. After hearing a detailed explanation on the study, all subjects gave written informed consent. This study was carried out in accordance with the recommendations of Institutional Review Board of Binzhou Medical University. The protocol was approved by the Institutional Review Board of Binzhou Medical University. All subjects gave written informed consent in accordance with the Declaration of Helsinki after hearing detailed explanation about the study.

TABLE 1 | Demographic information for the early blind (EB) groups.

Onset of visual deprivation	Number of subjects	Age (Year)	Education level (Year)
At birth	15	22.14 ± 1.43	13.27 ± 1.16
4 years old	1	24.3	11
5 years old	3	22.27 ± 0.83	13.67 ± 0.58
6 years old	1	22.9	12

Onset of visual deprivation means the age of the EB subject sight loss.

Data Acquisition

The functional images were scanned using a 3.0 T Siemens Skyra scanner with a 32-channel head coil at Yantai Affiliated Hospital of Binzhou Medical University. Participants were instructed to relax and keep their eyes closed without thinking about anything in particular. A high-resolution structural image was collected using a T1 weighted 3D MPRAGE sequence (repetition time (TR) = 1900 ms, echo time (TE) = 2.52 ms, inversion time (TI) = 1100 ms, voxel size = 1 × 1 × 1 mm^3, matrix size = 256 × 256, flip angle (FA) = 90°). A gradient-echo planar imaging (EPI) sequence (TR = 2000 ms, TE = 30 ms, voxel size = 3.1 × 3.1 × 4.0 mm^3, matrix size = 64 × 64, slices = 33, slices thickness = 4 mm, slices gap = 0.6 mm, FA = 9°) was used for functional data collection. Earplugs and foam pads were used to reduce the scanner noise and head motion.

Data Preprocessing

SPM12 was used for the data preprocessing[1]. For each participant, the first 10 functional images were first removed to allow for participants' adaptation to the environment and equilibration effects. The remaining data were processed by a slice timing correction and head motion correction by a realign analysis. No participant was excluded, as all participants' head movements were not larger than 1.5 mm and 1 degree. The high-resolution structural image was coregistered with the functional images and subsequently segmented into the gray matter, white matter and cerebrospinal fluid (CSF). The generated spatial parameters from the segmentation procedure were then applied to spatially normalize the realigned images to 3 × 3 × 3 mm^3 in the Montreal Neurological Institute (MNI) space. Finally, the functional images were smoothed with a full-width at half-maximum Gaussian filter (FWHM = 4 mm) to attenuate spatial noise. Several variances were regressed out with the temporal derivatives with the linear regression, including six head motion parameters and averaged signals from the CSF and white matter. Specifically, the global signal regression was not performed in this study, as global signals are thought to be irrelevant to non-neural noise and should not be regressed out (Chen et al., 2012).

Group Independent Component Analysis (Group ICA)

To extract the regions for the subsequent DCM analysis, the DMN, SN, and DAN components were first identified for each subject. Group ICA was performed to decompose the resting state functional images into spatially independent components (ICs) using the GIFT software[2] after data preprocessing. First, the number of the optimal components were estimated using the minimum description length criteria (MDL) (Li et al., 2007). The number of components in our experiment were 41. Therefore 41 independent spatial components were produced using the infomax algorithm. For each participant, the corresponding spatial maps were generated through a back-reconstruction step.

The DMN, SN, and DAN templates were generated by the WFU PickAtlas Tool 3.0 to identify the DMN, SN, and DAN

[1]http://www.fil.ion.ucl.ac.uk/spm/

[2]http://icatb.sourceforge.net/

components (Calhoun et al., 2008). In our study, we generated the DMN template by including the posterior cingulate cortex, bilateral precuneus, superior medial frontal cortex, and inferior parietal lobe. A multiple spatial regression analysis between the template and ICs was then conducted to sort all the spatial components. By comparing the regression coefficients, the component that fit best with the template with the greatest one was identified as the DMN component. The one-sample *t*-test was used to generate a group-mean pattern ($p < 0.001$, uncorrected, cluster size = 10 voxels). For the SN and DAN components, the same procedure was performed by creating the SN and DAN templates. To keep the consistency of the locations of each ROI between two groups, the Euclidean distance was also calculated between the individual ROI and group-mean ROI.

Definition of Region of Interest (ROI)

For each subject, all the specific ROIs were selected based on the spatial map of the individual component representing three brain networks. Based on the regions identified above, four ROIs were defined for DMN: the mPFC, PCC, and bilateral parietal cortex (lIPC and rIPC). We defined three regions: dorsal cingulate cortex (dACC), left anterior (lAI), and right anterior insulae (rAI) for the salience network. Additionally, the DAN included the bilateral frontal eye fields (lFEF, rFEF) and bilateral superior parietal lobes (lSPL, rSPL). The detailed information of ROIs is shown in **Table 2**.

All the subject-specific ROIs were defined as spheres with a radius of 8 mm centered at the local maximum from the identified DMN, DAN, and SN components for each subject. We also included a white matter mask to remove the influence of the white matter. This procedure would ensure the further DCM analysis was conducted on the consistent regions identified as one functionally connected network for each subject. Finally, time series were extracted from all ROIs as the residuals of the general linear model, which was constructed by the following regressors: the head motion parameters, cosine basis functions to model the aliased respiratory and cardiac signals, one constant regressor to model the baseline and a high-pass filter of 1/128 Hz to regress the ultraslow fluctuations.

TABLE 2 | Coordinates of the regions of interest used in spectral dynamic causal modeling (DCM) analysis.

Region	Brain network	MNI coordinates		
		x	*y*	*z*
mPFC	DMN	3	54	−2
lIPC	DMN	−49	−62	32
rIPC	DMN	47	−68	35
PCC	DMN	0	−52	26
dACC	SN	0	−10	40
lAI	SN	−43	−11	−1
rAI	SN	43	−11	−1
lFEF	DAN	−24	−15	66
rFEF	DAN	28	−10	58
lSPL	DAN	−24	−55	72
rSPL	DAN	24	−55	72

mPFC, medial prefrontal cortex; IPC, inferior parietal lobule; PCC, posterior cingulate cortex; dACC, dorsal cingulate cortex; AI, anterior insulae; FEF, frontal eye field; SPL, superior parietal lobe; DMN, default mode network; SN, salience network; DAN, dorsal attention network; l, left; r, right.

Spectral Dynamic Causal Modeling

To estimate the effective connectivity parameters in specific regions, the spectral DCM analysis was conducted for the defined nodes of all three networks using DCM12 in SPM12. The spectral DCM is designed to estimate the intrinsic effective connectivity from resting state fMRI images with the cross-spectra of the signals. The cross spectral in the frequency domain could be considered as a more complete measure of functional connectivity (Park et al., 2018). In theory, the spectral DCM is distinct from stochastic DCM, which can estimate the coupling parameters among coupled populations of neurons in the frequency domain. It calculates the spectral measure by using a neuronally plausible power-law model among measured responses, and the time-invariant parameters. It models the observed functional connectivity between nodes with their second-order statistics instead of the neural signals under a deterministic assumption. In other words, spectral DCM could estimate the covariance of the random fluctuations from previous experiences to create the complex cross spectra among measured responses (Razi et al., 2015).

The expected cross spectra can be generated by the following model:

$$g_y(\omega, \theta) = |K(\omega)|^2 g_v(\omega, \theta) + g_e(\omega, \theta)$$

Here, $g_y(\omega, \theta)$ represents the predicted cross spectra that can be estimated. $K(\omega)$ is a function of the effective connection, which is the Fourier transform of the system's Volterra kernel.

For each participant, a fully connected model was constructed with reciprocal connectivity between any pair of all ROIs by a Bayesian network discovery analysis (Friston et al., 2011). For resting-state fMRI data, no exogenous input was added to the model construction, then we made a parameter estimation for all models. Unlike the stochastic DCM, the convolution kernel representation in the spectral DCM was transformed to a spectral representation in the frequency domain. An estimation procedure was applied to characterize the spectral densities over frequencies for all estimated parameters within the DMN, SN, and DAN. Bayesian model selection (BMS) was finally performed with a *post hoc* optimization method to estimate the optimal model with the best balance between complexity and accuracy. The BMS was conducted on both groups separately, as we assumed both groups did not share the same model structure. The corresponding parameters for the best model were also estimated.

Statistical Analysis

After the parameter estimation was completed for the optimal model, one-sample *t*-tests were conducted to examine whether the effective connectivity between regions was significant for both EB and HC groups. Multiple comparison corrections were made on the results of one-sample *t*-tests at $p < 0.05$ by

applying the false discovery rate (FDR) procedure. To examine the abnormalities of the effective connectivity within all three networks between EB and HC cohorts, the coupling parameters from both groups were tested using the two-sample *t*-tests. A correction for FDR was used to determine the results of two-sample *t*-test at $p < 0.05$.

RESULTS

Independent Component Analysis

We first decomposed the separated spatial patterns by conducting the group ICA on the resting-state functional images. Forty-one independent components were generated according to the MDL criterion, and the generated components were sorted by their correlations with the DMN, SN, and DAN templates. The independent components that showed a best fit with all three templates were identified as the DMN, SN, and DAN components. Subject-specific nodes were defined as 8-mm spheres centered at the peak values of all ROIs for each subject. **Figure 1** shows the profiles of the DMN, SN, and DAN components. Based on the group ICA analysis, four ROIs were defined for DMN, including the mPFC, PCC, bilateral IPC; three ROIs for SN: dACC, lAI, and rAI, and four bilateral ROIs for DAN: lEFF, rFEF, lSPL, and rSPL. The coordinates of all selected ROIs are shown in **Table 2**. The statistical analysis on the Euclidean distance suggested there was no significant difference in the Euclidean distance between two groups, indicating the consistency of the locations of the subject-specific ROI.

DCM Analysis and Effective Connectivity of DMN, SN, and DAN

The time series of all ROIs were first extracted for each subject. For illustration, we extracted the principal eigenvariates from the corresponding time series of the selected regions within the DMN, as shown in **Figure 2**. The generalized fitting procedure

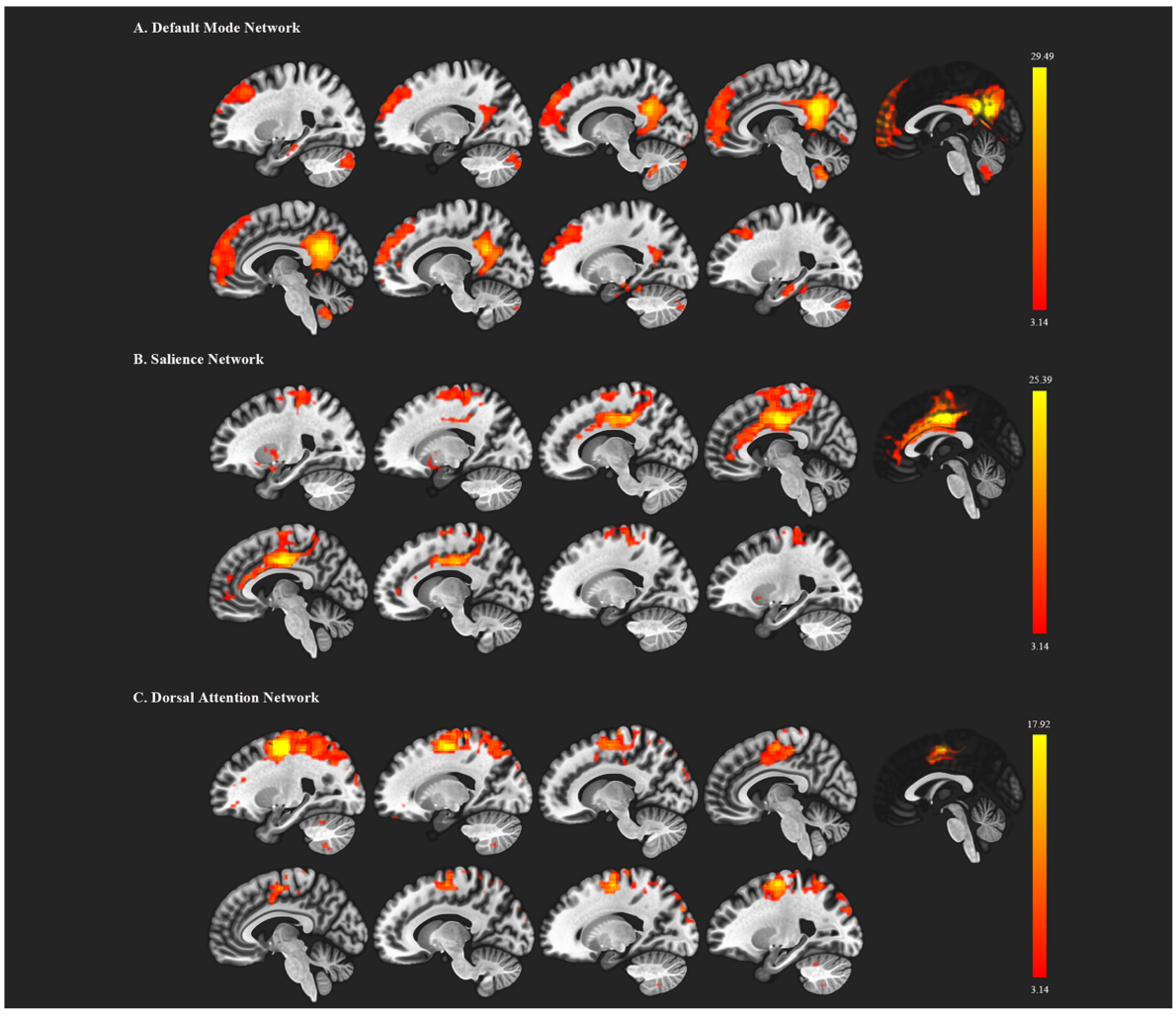

FIGURE 1 | Functional brain networks chosen from the independent component analysis. **(A)** represents the default mode network (DMN); **(B)** represents the salience network; **(C)** represents the dorsal attention network. The red color regions correspond to the threshold *z*-value.

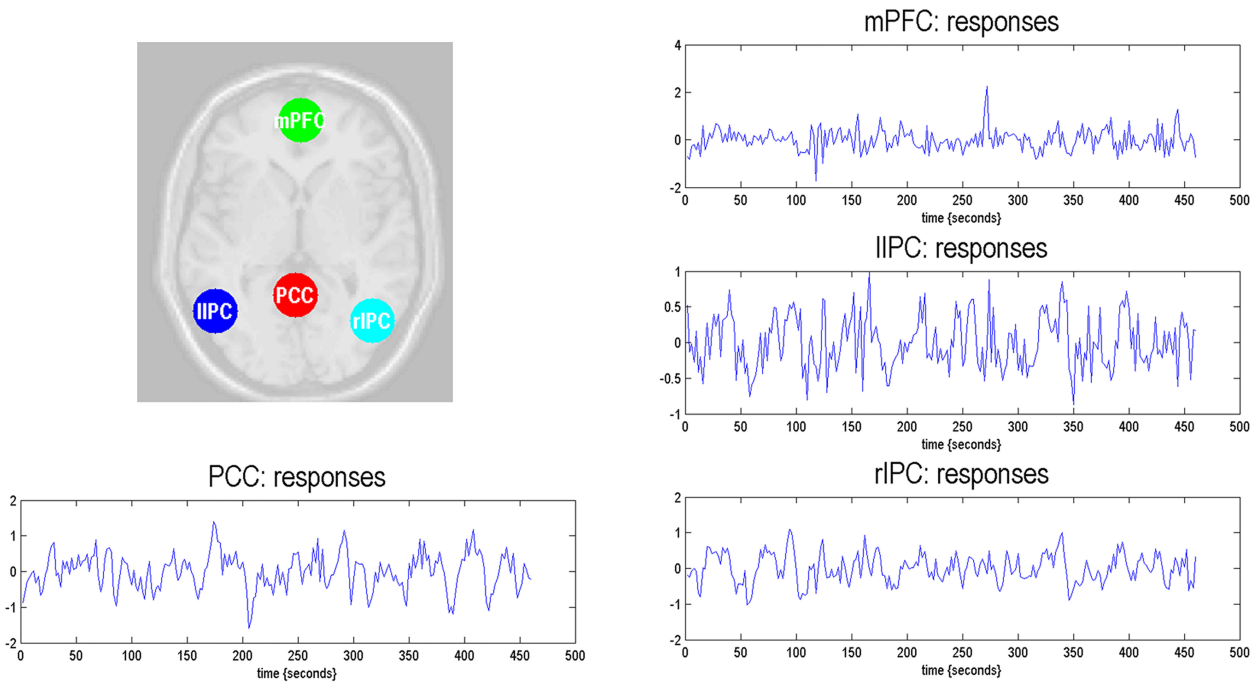

FIGURE 2 | Locations of the representative regions within the DMN. The DMN regions are identified from the independent component analysis. The principal eigenvariates are extracted from the corresponding time series of regions.

suggested that the observed spontaneous fMRI signals can be modeled by the conditional expectations in the neuronal activations. For each participant, a Bayesian model reduction procedure was used to search for the optimal model from the model space. The detailed results of the estimation are shown in **Figure 3**. Finally, 6536 models were constructed with all possible combinations using four ROIs. The log-evidence of all models for DMN is shown in **Figure 3A**, suggesting a model with more connections shared larger evidence. In this study, we found that the fully connected model was optimal with the most significant efficiency. The meant that our resting-state fMRI data could be stimulated by the fully connected model. There was a deduction of the log-evidence when any connection was removed.

The same DCM analyses were conducted for SN and DAN. As expected for DMN, the best models were the fully connected models for SN and DAN. In the EB and HC groups, the coupling parameters of the optimal model for each network were calculated by the Bayes model average analysis. **Figures 3B–D** shows the estimated fixed effects and the posterior probabilities for DMN, SN, and DAN in one typical subject. The Bayes model average parameters were then estimated for all subjects, as shown in **Figure 4**. Most of the coupling parameters within the DMN for EB and HC groups were observed to be significant ($p < 0.05$, df = 19), except the connections from PCC and mPFC to the right IPC and from bilateral IPC to PCC in the HC group; the connection from the left IPC to the other three regions and from the mPFC to the left IPC in the EB subjects, as shown in **Table 3**. All the effective connections within the SN were found to be significant in both the EB and NC groups ($p < 0.05$, df = 19). For the DAN, no significance was found except in one effective connection (left SPL→ left FEF) in the HC group, and in two connections (left SPL→ left FEF and left FEF→ right FEF). **Tables 4**, **5** showed the details of the average parameters of SN and DAN.

Alteration of the Effective Connectivity Within DMN, SN, and DAN

After the parameters within the DMN, SN, and DAN were estimated, the two-sample *t*-tests analysis between the EB and HC groups showed that EB subjects showed significantly enhanced effective connectivity from PCC and lIPC to mPFC, and from mPFC to PCC ($p < 0.05$, df = 18). Besides all endogenous connections, the effective connectivity from the mPFC to bilateral IPC were significantly decreased (**Figure 5A**). For the SN, almost all the significant effective connections between the EB and NC groups were reduced, except the intrinsic connection in the right AI including the connections from the dACC to bilateral AI, right AI to dACC, and effective connections from the left AI to right AI ($p < 0.05$, df = 18; **Figure 5B**). As shown in **Figure 5C**, more significant effective connections were found to be reduced within the DAN between EB and HC groups, which included the connections from the left FEF to right FEF, and left SPL, the connections from the right FEF to all the other three nodes, and the intrinsic connections in the rSPL ($p < 0.05$, df = 18) Only the connections from the right SPL and itself to the left SPL were observed to be enhanced. **Figure 5** shows the significantly enhanced and reduced effective connections within the DMN, SN, and DAN between EB and HC subjects.

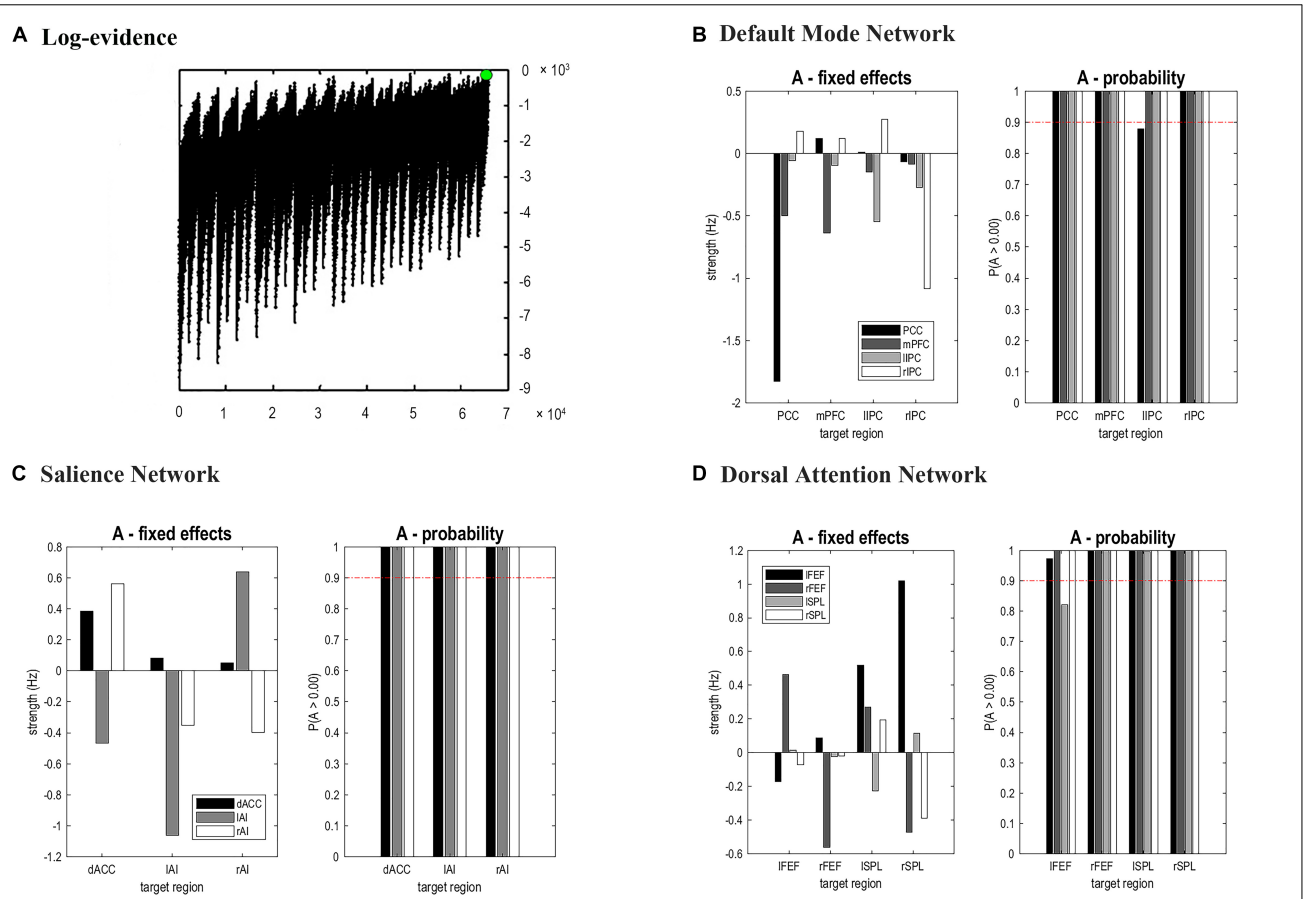

FIGURE 3 | Results of Bayesian Model Selection analysis and estimations of the fixed effects. For DMN, the fully connected model showed the highest evidence **(A)**, which suggests that the full model was the best explanation for our data. **(B–D)** showed the estimated fixed effects and posterior probabilities of these effective connectivity parameters for DMN, SN, and DAN. The red dashed line depicted the 95% threshold. mPFC, medial prefrontal cortex; IPC, inferior parietal lobule; PCC, posterior cingulate cortex; dACC, dorsal cingulate cortex; AI, anterior insulae; FEF, frontal eye field; SPL, superior parietal lobe; l, left; r, right.

DISCUSSION

In this study, the spectral DCM was used to compute the effective connections within the DMN, SN and DAN with resting-state fMRI data. The intrinsic brain networks were identified using the group ICA, and several nodes were defined for further DCM analyses. The fully connected model was found to be the optimal explanation for all three networks for our functional data. The one-sample *t*-test analysis suggested that most effective connections within all three networks were significant in both the EB and HC groups. Two-sample *t*-test analyses found that reduced coupling parameters of the effective connectivity for each network were observed by comparing the EB patients to the HC subjects, suggesting that there was a disruption of the effective integration within the resting-state brain networks in EB subjects.

Effective Connectivity Analysis Within DMN

Increasing attention has been paid to the functional interactions within the DMN in normal and disordered people (Fang et al., 2016; Van Den Heuvel and Thomason, 2016; Khalili-Mahani et al., 2017). Directed functional interactions within the DMN regions have been explored using a series of approaches, such as the partial coherence analysis (Silfverhuth et al., 2011), Granger causality analysis (GCA) (Zhou et al., 2011) and Bayesian networks (Wu et al., 2011). One latest study found a reduction of interhemispheric functional connectivity in early blindness using the resting-state fMRI (Hou et al., 2017), suggesting the disruption of the functional connections by early deprivation. However, the DCM method was distinct from the above approaches in theory, because the DCM was model-based by constructing a hemodynamic model to estimate the hidden neuronal states (Li et al., 2012). In our study, the model evidence suggests that the optimal models for all three networks were the whole-connected model. For the EB subjects, there were bidirectional connections between the bilateral IPC and PCC, mPFC and left IPC, as well as the mPFC and right IPC, which was consistent with previous causal studies on the effective connectivity within the DMN (Zhou et al., 2011; Xu et al., 2017). We also discovered directed connections between the PCC and mPFC, which are both functionally and anatomically connected, and play a crucial role in the DMN.

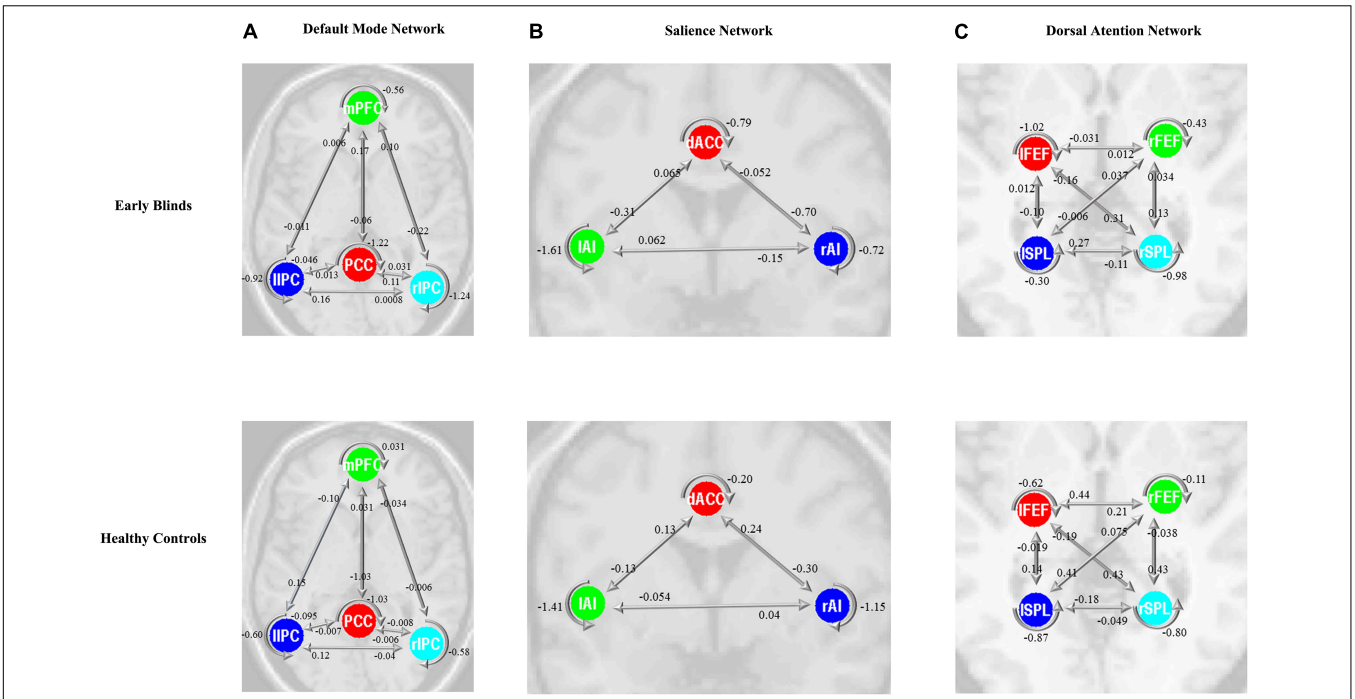

FIGURE 4 | Bayes model average parameters of intrinsic brain networks (**A**, default mode network; **B**, salience network; and **C**, dorsal attention network) for early blinds and healthy controls (HCs). The number behind the colored lines represents the parameters of the effective connectivity between ROIs. mPFC, medial prefrontal cortex; IPC, inferior parietal lobule; PCC, posterior cingulate cortex; dACC, dorsal cingulate cortex; AI, anterior insulae; FEF, frontal eye field; SPL, superior parietal lobe; l, left; r, right. Double arrow means reciprocal connections.

Inconsistent findings on the coupling between regions within the DMN have been reported in many studies. Using the stochastic DCM, our recent study found an influence from the PCC on the mPFC (Xu et al., 2017). Some other studies using GCA showed an mPFC to PCC effective connection. Inconsistent with our findings, bilateral IPC were observed to be capable of modulating mPFC and PCC (Di and Biswal, 2014). Furthermore, reciprocal connections between bilateral IPC were observed in the present study, as suggested in another fMRI study (Li et al., 2012). In our study, bilateral IPC showed a slight functional asymmetry and exerted causal influences on the PCC and mPFC, but not vice versa. Therefore we can assume that bilateral IPCs possess a modulating or driving role, as confirmed by a previous study (Di and Biswal, 2014). However, some inconsistent results were reported. Using GCA, the directed connection from the left IPC to mPFC was observed for EB subjects, whereas there were symmetrical connections from the bilateral IPC to PCC, as well as the connectivity from the mPFC to bilateral IPCs (Jiao et al., 2011). This discrepancy may be caused by the smaller sample

TABLE 3 | Bayes model average parameters of the DMN for healthy controls (HCs) and EBs.

Groups		From PCC	From mPFC	From rIPC	From lIPC
HCs	To PCC	−1.03**	−1.03**	−0.0085	−0.0074
	To mPFC	0.031*	0.031*	−0.034*	−0.10**
	To rIPC	−0.0059	−0.0059	−0.58**	−0.040*
	To lIPC	−0.095*	0.15**	0.12*	−0.60**
EBs	To PCC	−1.22**	−0.061*	0.031*	0.013
	To mPFC	0.17**	−0.56**	0.10*	0.0064
	To rIPC	0.11*	−0.22**	−1.24**	0.00078
	To lIPC	−0.046*	−0.011	0.16**	−0.92**

*The averaged parameters represented the effective connectivity between regions within the DMN. The positive value between from node A to node B showed a positive modulation, suggesting that node A caused an increase in the rate of change of node B's signal and vice versa. mPFC, medial prefrontal cortex; IPC, inferior parietal lobule; PCC, posterior cingulate cortex; DMN, default mode network; l, left; r, right. *means $p < 0.05$; **means $p < 0.001$.*

TABLE 4 | Bayes model average of the salience network for HCs and EBs.

Groups		From dACC	From lAI	From rAI
HCs	To dACC	−0.20**	0.13**	0.24**
	To lAI	−0.13**	−1.41**	−0.054*
	To rAI	−0.30**	0.04*	−1.15**
EBs	To dACC	−0.79**	0.065*	−0.052*
	To lAI	−0.31**	−1.61**	0.062*
	To rAI	−0.70**	−0.15**	−0.72**

*The averaged parameters represented the effective connectivity between regions within the salience network. The positive value between from node A to node B showed a positive modulation, suggesting that node A caused an increase in the rate of change of node B's signal and vice versa. dACC, dorsal cingulate cortex; AI, anterior insulae; SN, salience network; l, left; r, right. *means $p < 0.05$; **means $p < 0.001$.*

TABLE 5 | Bayes model average parameters of the dorsal attention network for HCs and EBs.

Groups		From lFEF	From rFEF	From lSPL	From rSPL
HCs	To lFEF	−0.62**	0.44**	−0.019	−0.19**
	To rFEF	0.21**	−0.11*	0.075*	−0.038*
	To lSPL	0.14**	0.41**	−0.87**	−0.18**
	To rSPL	0.43**	0.43**	−0.049*	−0.80**
EBs	To lFEF	−1.02**	−0.031*	0.012	−0.16**
	To rFEF	0.012	−0.43**	0.037*	0.034*
	To lSPL	−0.10*	−0.0062	−0.30**	0.27**
	To rSPL	0.31**	0.13**	−0.11*	−0.98**

*The averaged parameters represented the effective connectivity between regions within the dorsal attention network. The positive value between from node A to node B showed a positive modulation, suggesting that node A caused an increase in the rate of change of node B's signal and vice versa. FEF, frontal eye field; SPL, superior parietal lobe; DAN, dorsal attention network; l, left; r, right. *means $p < 0.05$; **means $p < 0.001$.*

sizes in previous studies, which lead to several connections not being significant.

In addition, the approach of the spectral DCM in this study is crucial, as it can elucidate the neuronal connectivity abnormalities underlying the functional correlations of fMRI signals and provide more insight into the organization of the functional networks (Birnbaum and Weinberger, 2013). Our DCM analysis suggested that the mPFC appeared to be a zonal area, as there were separate efferent and afferent connections between the mPFC and other regions, which was of particular interest given its role in personal evaluation, choice behavior and reality monitoring (Rushworth et al., 2004; Metzak et al., 2015). The function of the mPFC has been proposed to manipulate the correlations between learning associations between different actions, context and adaptive responses (Euston et al., 2012). Moreover, one functional connectivity study has further demonstrated that signals in the mPFC may be responsible for the signal integration between mPFC and other brain regions, such as the posterior superior temporal cortex and AI (Hare et al., 2010). Using a multimodal MR-imaging technique, decreased functional connectivity were observed between the parietal and frontal areas (Bauer et al., 2017), while this reduced effective connectivity were also discovered in the DMN in the EB subjects.

Effective Connectivity Analysis Within Other Functional Brain Networks

The left AI has played a critical role not only in the semantic and language network (Binder and Desai, 2011), but has also been considered as a "supramodal convergence zone" (Binder et al., 2009; Binder and Desai, 2011), which is involved in the association network and information integration from several sensory modalities. Decreased effective connection between right AI and other regions were observed in our study, as shown in **Figure 5**. The right AI has been confirmed to be a functional hub in coordinating brain networks to produce adaptive behavior, especially the modulation in the DMN and DAN (Wang et al., 2018), as suggested in our study. A weakened functional connection in the early deprivation subject was discovered between the subregions of AI (Nomi et al., 2016; Liu et al., 2017), as the reduced connection from left AI to right AI in our study. Abnormalities within the IPL have been associated with working memory dysfunction as well as impairments in cognitive insight and reality perception (Guo et al., 2014; Lee et al., 2015; Chahine et al., 2017). A recent research based on connectivity-based parcellation of the left inferior parietal lobule suggested that this region was functionally connected to areas more strongly involved in the higher level of social cognitive and language processes, as opposed to more rostro-ventral areas of the IPL that appeared to be associated with the lower functionality level (Bzdok et al., 2016). Our findings suggest that the specific abnormalities of the AI and general alterations within the IPL may be mediated by inhibitory interactions from other regions of the left dorsal attention network. A recent study in EB subjects also suggested that early visual deprivation can selectively reshape the functional architecture of the salience network (Liu et al., 2017). Our study found that most of the effective connections were decreased in the EB subjects, suggesting a corresponding reorganization of the human brain due to the early deprivation.

There are several limitations to our study. First, our analysis does not allow us to conclusively determine the functional

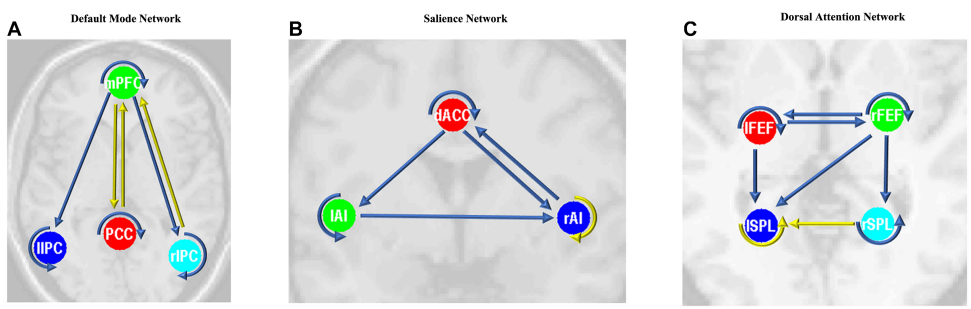

FIGURE 5 | Significant effective connections within the default mode network **(A)**, salience network **(B)**, and dorsal attention network **(C)** between the early blind (EB) and healthy control (HC) subjects. The yellow line indicates the coupling parameter of the effective connectivity is enhanced by comparing the EB group to the HC group, while the blue line indicates reduced strength. The arrow represents the direction of the effective connectivity. mPFC, medial prefrontal cortex; IPC, inferior parietal lobule; PCC, posterior cingulate cortex; dACC, dorsal cingulate cortex; AI, anterior insulae; FEF, frontal eye field; SPL, superior parietal lobe; l, left; r, right.

significance of these correlations. This study displayed low average positive symptomatology which possibly precluded us from finding additional correlations and, more importantly, our resting-state experiments were not accompanied by the working memory, executive functioning or language-related behavioral paradigms, so that we could obtain more functionally specific correlations. Second, the sample size of both the EB patients and normal control groups was relatively small and moderate. More qualified subjects should be recruited in future studies to increase the reliability of our observations and the effect of the causal interactions in the DMN, SN, and DAN. This study showed preliminary findings and further studies are needed to retest our discoveries in other blind cohorts. Finally, we did not examine the changes of the effective connectivity within all the brain networks, especially the primary sensory networks like the visual network. The purpose of this study is to see if there were disruptions in the high-order cognitive networks that are associated with the cognitive behaviors in the EB subjects. And the Group ICA could not separate the visual cortex into small parcellations. In future studies, we could examine the dynamic changes of EB subjects using other techniques that could parcellate the visual cortex. In this study, we tested the hypothesis that there was a disruption of the effective connectivity in the cognitive networks. The cognitive networks may functionally connected as a whole, thus the future direction will focus on the causal interactions between the cognitive networks besides the directed connections between regions.

CONCLUSION

In this study, fully connected models were identified to be the optimal model for the effective connections within the intrinsic functional brain networks in EB subjects. Statistical analyses suggested significant differences in the effective connectivity within the DMN, SN, and DAN between EB and HC groups. More reduced effective connections within three networks by comparing the EB to HC groups indicated that the interactions within the high-order brain networks got greatly suppressed due to the early deprivation. Our analysis additionally revealed the neural connective abnormalities that may underlie alterations of the intrinsic brain network in EB subjects.

DATA AVAILABILITY

The datasets generated for this study are available on request to the corresponding author.

AUTHOR CONTRIBUTIONS

MZ and JT designed the experiments. XL, AW, JiX, and PW performed the experiments. XL, JuX, and ZS analyzed the data. XL, JuX, and ZS wrote the manuscript. BW, MZ, and JT revised the manuscript.

FUNDING

This work was supported by National Natural Science Foundation of China (No. 61703302), Shandong Provincial Natural Science Foundation of China (No. ZR2015HM081), Project of Shandong Province Higher Educational Science and Technology Program (J15LL01), and Shandong Provincial Key Research and Development Project (No. 2018GSF118156).

REFERENCES

Abboud, S., and Cohen, L. (2019). Distinctive interaction between cognitive networks and the visual cortex in early blind individuals. *Cereb Cortex* doi: 10.1093/cercor/bhz006 [Epub ahead of print].

Amedi, A., Von Kriegstein, K., Van Atteveldt, N. M., Beauchamp, M. S., and Naumer, M. J. (2005). Functional imaging of human crossmodal identification and object recognition. *Exp. Brain Res.* 166, 559–571. doi: 10.1007/s00221-005-2396-5

Bauer, C. M., Cattaneo, Z., and Merabet, L. B. (2018). Early blindness is associated with increased volume of the uncinate fasciculus. *Eur. J. Neurosci.* 47, 427–432. doi: 10.1111/ejn.13848

Bauer, C. M., Hirsch, G. V., Zajac, L., Koo, B. B., Collignon, O., and Merabet, L. B. (2017). Multimodal MR-imaging reveals large-scale structural and functional connectivity changes in profound early blindness. *PLoS One* 12:e0173064. doi: 10.1371/journal.pone.0173064

Binder, J. R., and Desai, R. H. (2011). The neurobiology of semantic memory. *Trends Cogn. Sci.* 15, 527–536. doi: 10.1016/j.tics.2011.10.001

Binder, J. R., Desai, R. H., Graves, W. W., and Conant, L. L. (2009). Where is the semantic system? A critical review and meta-analysis of 120 functional neuroimaging studies. *Cereb Cortex* 19, 2767–2796. doi: 10.1093/cercor/bhp055

Birnbaum, R., and Weinberger, D. R. (2013). Functional neuroimaging and schizophrenia: a view towards effective connectivity modeling and polygenic risk. *Dialogues Clin. Neurosci.* 15, 279–289.

Bock, A. S., Binda, P., Benson, N. C., Bridge, H., Watkins, K. E., and Fine, I. (2015). Resting-state retinotopic organization in the absence of retinal input and visual experience. *J. Neurosci.* 35, 12366–12382. doi: 10.1523/JNEUROSCI.4715-14.2015

Boldt, R., Seppa, M., Malinen, S., Tikka, P., Hari, R., and Carlson, S. (2014). Spatial variability of functional brain networks in early-blind and sighted subjects. *Neuroimage* 95, 208–216. doi: 10.1016/j.neuroimage.2014.03.058

Bzdok, D., Hartwigsen, G., Reid, A., Laird, A. R., Fox, P. T., and Eickhoff, S. B. (2016). Left inferior parietal lobe engagement in social cognition and language. *Neurosci. Biobehav. Rev.* 68, 319–334. doi: 10.1016/j.neubiorev.2016.02.024

Calhoun, V. D., Maciejewski, P. K., Pearlson, G. D., and Kiehl, K. A. (2008). Temporal lobe and "default" hemodynamic brain modes discriminate between schizophrenia and bipolar disorder. *Hum. Brain Mapp.* 29, 1265–1275. doi: 10.1002/hbm.20463

Chahine, G., Richter, A., Wolter, S., Goya-Maldonado, R., and Gruber, O. (2017). Disruptions in the left frontoparietal network underlie resting state endophenotypic markers in schizophrenia. *Hum. Brain Mapp.* 38, 1741–1750. doi: 10.1002/hbm.23477

Chen, G., Xie, C., Ward, B. D., Li, W., Antuono, P., and Li, S. J. (2012). A method to determine the necessity for global signal regression in resting-state fMRI studies. *Magn. Reson. Med.* 68, 1828–1835. doi: 10.1002/mrm.24201

Corbetta, M., and Shulman, G. L. (2011). Spatial neglect and attention networks. *Annu. Rev. Neurosci.* 34, 569–599. doi: 10.1146/annurev-neuro-061010-113731

Di, X., and Biswal, B. B. (2014). Identifying the default mode network structure using dynamic causal modeling on resting-state functional magnetic resonance imaging. *Neuroimage* 86, 53–59. doi: 10.1016/j.neuroimage.2013.07.071

Dormal, G., Pelland, M., Rezk, M., Yakobov, E., Lepore, F., and Collignon, O. (2018). Functional preference for object sounds and voices in the brain of early

blind and sighted individuals. *J. Cogn. Neurosci.* 30, 86–106. doi: 10.1162/jocn_a_01186

Euston, D. R., Gruber, A. J., and Mcnaughton, B. L. (2012). The role of medial prefrontal cortex in memory and decision making. *Neuron* 76, 1057–1070. doi: 10.1016/j.neuron.2012.12.002

Fang, X., Zhang, Y., Wang, Y., Zhang, Y., Hu, J., Wang, J., et al. (2016). Disrupted effective connectivity of the sensorimotor network in amyotrophic lateral sclerosis. *J. Neurol.* 263, 508–516. doi: 10.1007/s00415-015-8013-z

Friston, K. J., Kahan, J., Biswal, B., and Razi, A. (2014). A DCM for resting state fMRI. *Neuroimage* 94, 396–407. doi: 10.1016/j.neuroimage.2013.12.009

Friston, K. J., Li, B., Daunizeau, J., and Stephan, K. E. (2011). Network discovery with DCM. *Neuroimage* 56, 1202–1221. doi: 10.1016/j.neuroimage.2010.12.039

Friston, K. J., Preller, K. H., Mathys, C., Cagnan, H., Heinzle, J., Razi, A., et al. (2017). Dynamic causal modelling revisited. *Neuroimage* doi: 10.1016/j.neuroimage.2017.02.045 [Epub ahead of print].

Guo, S., Kendrick, K. M., Yu, R., Wang, H. L., and Feng, J. (2014). Key functional circuitry altered in schizophrenia involves parietal regions associated with sense of self. *Hum. Brain Mapp.* 35, 123–139. doi: 10.1002/hbm.22162

Hare, T. A., Camerer, C. F., Knoepfle, D. T., and Rangel, A. (2010). Value computations in ventral medial prefrontal cortex during charitable decision making incorporate input from regions involved in social cognition. *J. Neurosci.* 30, 583–590. doi: 10.1523/JNEUROSCI.4089-09.2010

He, W., and Johnson, B. W. (2018). Development of face recognition: dynamic causal modelling of MEG data. *Dev. Cogn. Neurosci.* 30, 13–22. doi: 10.1016/j.dcn.2017.11.010

Heine, L., Bahri, M. A., Cavaliere, C., Soddu, A., Laureys, S., Ptito, M., et al. (2015). Prevalence of increases in functional connectivity in visual, somatosensory and language areas in congenital blindness. *Front. Neuroanat.* 9:86. doi: 10.3389/fnana.2015.00086

Hou, F., Liu, X., Zhou, Z., Zhou, J., and Li, H. (2017). Reduction of interhemispheric functional brain connectivity in early blindness: a resting-state fMRI study. *Biomed Res. Int.* 2017:6756927. doi: 10.1155/2017/6756927

Hu, M. L., Zong, X. F., Mann, J. J., Zheng, J. J., Liao, Y. H., Li, Z. C., et al. (2017). A review of the functional and anatomical default mode network in schizophrenia. *Neurosci. Bull.* 33, 73–84. doi: 10.1007/s12264-016-0090-1

Jiang, A., Tian, J., Li, R., Liu, Y., Jiang, T., Qin, W., et al. (2015). Alterations of regional spontaneous brain activity and gray matter volume in the blind. *Neural Plast* 2015:141950. doi: 10.1155/2015/141950

Jiao, Q., Lu, G., Zhang, Z., Zhong, Y., Wang, Z., Guo, Y., et al. (2011). Granger causal influence predicts BOLD activity levels in the default mode network. *Hum. Brain Mapp.* 32, 154–161. doi: 10.1002/hbm.21065

Jimenez, A. M., Lee, J., Wynn, J. K., Cohen, M. S., Engel, S. A., Glahn, D. C., et al. (2016). Abnormal ventral and dorsal attention network activity during single and dual target detection in schizophrenia. *Front. Psychol.* 7:323. doi: 10.3389/fpsyg.2016.00323

Khalili-Mahani, N., Rombouts, S. A., Van Osch, M. J., Duff, E. P., Carbonell, F., Nickerson, L. D., et al. (2017). Biomarkers, designs, and interpretations of resting-state fMRI in translational pharmacological research: a review of state-of-the-Art, challenges, and opportunities for studying brain chemistry. *Hum. Brain Mapp.* 38, 2276–2325. doi: 10.1002/hbm.23516

Lee, J. S., Chun, J. W., Lee, S. H., Kim, E., Lee, S. K., and Kim, J. J. (2015). Altered neural basis of the reality processing and its relation to cognitive insight in schizophrenia. *PLoS One* 10:e0120478. doi: 10.1371/journal.pone.0120478

Li, B., Wang, X., Yao, S., Hu, D., and Friston, K. (2012). Task-dependent modulation of effective connectivity within the default mode network. *Front. Psychol.* 3:206. doi: 10.3389/fpsyg.2012.00206

Li, L., Li, B., Bai, Y., Liu, W., Wang, H., Leung, H. C., et al. (2017). Abnormal resting state effective connectivity within the default mode network in major depressive disorder: a spectral dynamic causal modeling study. *Brain Behav.* 7:e00732. doi: 10.1002/brb3.732

Li, Y. O., Adali, T., and Calhoun, V. D. (2007). Estimating the number of independent components for functional magnetic resonance imaging data. *Hum. Brain Mapp.* 28, 1251–1266. doi: 10.1002/hbm.20359

Liu, L., Yuan, C., Ding, H., Xu, Y., Long, M., Li, Y., et al. (2017). Visual deprivation selectively reshapes the intrinsic functional architecture of the anterior insula subregions. *Sci. Rep.* 7:45675. doi: 10.1038/srep45675

Manescu, S., Poupon, D., Ballester, J., Abdi, H., Valentin, D., Lepore, F., et al. (2018). Early-blind individuals show impaired performance in wine odor categorization. *Neuroscience* 390, 79–87. doi: 10.1016/j.neuroscience.2018.08.012

Mccormick, E. M., and Telzer, E. H. (2018). Contributions of default mode network stability and deactivation to adolescent task engagement. *Sci. Rep.* 8:18049. doi: 10.1038/s41598-018-36269-4

Metzak, P. D., Lavigne, K. M., and Woodward, T. S. (2015). Functional brain networks involved in reality monitoring. *Neuropsychologia* 75, 50–60. doi: 10.1016/j.neuropsychologia.2015.05.014

Nomi, J. S., Farrant, K., Damaraju, E., Rachakonda, S., Calhoun, V. D., and Uddin, L. Q. (2016). Dynamic functional network connectivity reveals unique and overlapping profiles of insula subdivisions. *Hum. Brain Mapp.* 37, 1770–1787. doi: 10.1002/hbm.23135

Palaniyappan, L., and Liddle, P. F. (2012). Does the salience network play a cardinal role in psychosis? An emerging hypothesis of insular dysfunction. *J. Psychiatry Neurosci.* 37, 17–27. doi: 10.1503/jpn.100176

Park, H. J., Friston, K. J., Pae, C., Park, B., and Razi, A. (2018). Dynamic effective connectivity in resting state fMRI. *Neuroimage* 180, 594–608. doi: 10.1016/j.neuroimage.2017.11.033

Pascual-Leone, A., Amedi, A., Fregni, F., and Merabet, L. B. (2005). The plastic human brain cortex. *Annu. Rev. Neurosci.* 28, 377–401. doi: 10.1146/annurev.neuro.27.070203.144216

Prestel, M., Steinfath, T. P., Tremmel, M., Stark, R., and Ott, U. (2018). fMRI BOLD correlates of EEG independent components: spatial correspondence with the default mode network. *Front. Hum. Neurosci.* 12:478. doi: 10.3389/fnhum.2018.00478

Razi, A., Kahan, J., Rees, G., and Friston, K. J. (2015). Construct validation of a DCM for resting state fMRI. *Neuroimage* 106, 1–14. doi: 10.1016/j.neuroimage.2014.11.027

Rushworth, M. F., Walton, M. E., Kennerley, S. W., and Bannerman, D. M. (2004). Action sets and decisions in the medial frontal cortex. *Trends Cogn. Sci.* 8, 410–417. doi: 10.1016/j.tics.2004.07.009

Sabbah, N., Authie, C. N., Sanda, N., Mohand-Said, S., Sahel, J. A., Safran, A. B., et al. (2016). Increased functional connectivity between language and visually deprived areas in late and partial blindness. *Neuroimage* 136, 162–173. doi: 10.1016/j.neuroimage.2016.04.056

Sharaev, M. G., Zavyalova, V. V., Ushakov, V. L., Kartashov, S. I., and Velichkovsky, B. M. (2016). Effective connectivity within the default mode network: dynamic causal modeling of resting-state fMRI data. *Front. Hum. Neurosci.* 10:14. doi: 10.3389/fnhum.2016.00014

Silfverhuth, M. J., Remes, J., Starck, T., Nikkinen, J., Veijola, J., Tervonen, O., et al. (2011). Directional connectivity of resting state human fMRI data using cascaded ICA-PDC analysis. *Acta Radiol.* 52, 1037–1042. doi: 10.1258/ar.2011.110262

Tsvetanov, K. A., Henson, R. N., Tyler, L. K., Razi, A., Geerligs, L., Ham, T. E., et al. (2016). Extrinsic and intrinsic brain network connectivity maintains cognition across the lifespan despite accelerated decay of regional brain activation. *J. Neurosci.* 36, 3115–3126. doi: 10.1523/JNEUROSCI.2733-15.2016

Turkheimer, F. E., Leech, R., Expert, P., Lord, L. D., and Vernon, A. C. (2015). The brain's code and its canonical computational motifs. From sensory cortex to the default mode network: a multi-scale model of brain function in health and disease. *Neurosci. Biobehav. Rev.* 55, 211–222. doi: 10.1016/j.neubiorev.2015.04.014

Van De Steen, F., Almgren, H., Razi, A., Friston, K., and Marinazzo, D. (2019). Dynamic causal modelling of fluctuating connectivity in resting-state EEG. *Neuroimage* 189, 476–484. doi: 10.1016/j.neuroimage.2019.01.055

Van Den Heuvel, M. I., and Thomason, M. E. (2016). Functional Connectivity of the Human Brain in Utero. *Trends Cogn. Sci.* 20, 931–939. doi: 10.1016/j.tics.2016.10.001

Vercillo, T., Tonelli, A., and Gori, M. (2018). Early visual deprivation prompts the use of body-centered frames of reference for auditory localization. *Cognition* 170, 263–269. doi: 10.1016/j.cognition.2017.10.013

Viski, S., Orgovan, D., Szabo, K., Rosengarten, B., Csiba, L., and Olah, L. (2016). Effect of reading on blood flow changes in the posterior cerebral artery in early blind and sighted people–A transcranial doppler study. *J. Neurol. Sci.* 363, 132–139. doi: 10.1016/j.jns.2016.02.050

Wang, Y., Zhu, L., Zou, Q., Cui, Q., Liao, W., Duan, X., et al. (2018). Frequency dependent hub role of the dorsal and ventral right anterior insula. *Neuroimage* 165, 112–117. doi: 10.1016/j.neuroimage.2017.10.004

White, T. P., Gilleen, J., and Shergill, S. S. (2013). Dysregulated but not decreased salience network activity in schizophrenia. *Front. Hum. Neurosci.* 7:65. doi: 10.3389/fnhum.2013.00065

Wu, X., Li, R., Fleisher, A. S., Reiman, E. M., Guan, X., Zhang, Y., et al. (2011). Altered default mode network connectivity in Alzheimer's disease–a resting functional MRI and Bayesian network study. *Hum. Brain Mapp.* 32, 1868–1881. doi: 10.1002/hbm.21153

Wynn, J. K., Jimenez, A. M., Roach, B. J., Korb, A., Lee, J., Horan, W. P., et al. (2015). Impaired target detection in schizophrenia and the ventral attentional network: findings from a joint event-related potential-functional MRI analysis. *Neuroimage Clin.* 9, 95–102. doi: 10.1016/j.nicl.2015.07.004

Xu, J., Yin, X., Ge, H., Han, Y., Pang, Z., Liu, B., et al. (2017). Heritability of the effective connectivity in the resting-state default mode network. *Cereb Cortex* 27, 5626–5634. doi: 10.1093/cercor/bhw332

Yang, Y., Zhong, N., Friston, K., Imamura, K., Lu, S., Li, M., et al. (2017). The functional architectures of addition and subtraction: network discovery using fMRI and DCM. *Hum. Brain Mapp.* 38, 3210–3225. doi: 10.1002/hbm.23585

Zhou, Z., Wang, X., Klahr, N. J., Liu, W., Arias, D., Liu, H., et al. (2011). A conditional Granger causality model approach for group analysis in functional magnetic resonance imaging. *Magn. Reson. Imaging* 29, 418–433. doi: 10.1016/j.mri.2010.10.008

Conflict of Interest Statement: The authors declare that the research was conducted in the absence of any commercial or financial relationships that could be construed as a potential conflict of interest.

frontiers in Psychiatry

ORIGINAL RESEARCH
published: 12 April 2019
doi: 10.3389/fpsyt.2019.00234

Altered Local and Large-Scale Dynamic Functional Connectivity Variability in Posttraumatic Stress Disorder: A Resting-State fMRI Study

*Shishun Fu[1,2], Xiaofen Ma[2], Yunfan Wu[2], Zhigang Bai[3], Yin Yi[1,2], Mengchen Liu[1,2], Zhihong Lan[1,2], Kelei Hua[1,2], Shumei Huang[2,4], Meng Li[2] and Guihua Jiang[2,1]**

[1] The Second School of Clinical Medicine, Southern Medical University, Guangzhou, China, [2] The Department of Medical Imaging of Guangdong Second Provincial General Hospital, Guangzhou, China, [3] The Department of Medical Imaging of Affiliated Hospital, Inner Mongolia University for Nationalities, Hohhot, China, [4] Guangdong Medical University, Dongguan, China

Posttraumatic stress disorder (PTSD) is a psychiatric condition that can emerge after exposure to an exceedingly traumatic event. Previous neuroimaging studies have indicated that PTSD is characterized by aberrant resting-state functional connectivity (FC). However, few existing studies on PTSD have examined dynamic changes in resting-state FC related to network formation, interaction, and dissolution over time. In this study, we compared the dynamic resting-state local and large-scale FC between PTSD patients (n = 22) and healthy controls (HC; n = 22; conducted as standard deviation in resting-state local and large-scale FC over a series of sliding windows). Local dynamic FC was examined by calculating the dynamic regional homogeneity (dReHo), and large-scale dynamic FC (dFC) was investigated between regions with significant dReHo group differences. For the PTSD patients, we also investigated the relationship between symptom severity and dFC/dReHo. Our results showed that PTSD patients were characterized by I) increased dynamic (more variable) dReHo in left precuneus (PCu); II) increased dynamic (more variable) dFC between the left PCu and left insula; and III) decreased dFC between left PCu and left inferior parietal lobe (IPL), and decreased dFC between left PCu and right PCu. However, there is no significant correlation between the clinical indicators and dReHo/dFC after the family-wise-error (FWE) correction. These findings provided the initial evidence that PTSD is characterized by aberrant patterns of fluctuating communication within brain system such as the default mode network (DMN) and among different brain systems such as the salience network and the DMN.

Keywords: posttraumatic stress disorder, resting-state functional magnetic resonance imaging, dynamic functional connectivity, regional homogeneity, default mode network

OPEN ACCESS

Edited by:
Feng Liu,
Tianjin Medical University General Hospital, China

Reviewed by:
Meiling Li,
Harvard Medical School, United States
Xin Di,
New Jersey Institute of Technology, United States

***Correspondence:**
Guihua Jiang
jianggh@gd2h.org.cn

Specialty section:
This article was submitted to Neuroimaging and Stimulation, a section of the journal Frontiers in Psychiatry

Received: *23 October 2018*
Accepted: *28 March 2019*
Published: *12 April 2019*

Citation:
Fu S, Ma X, Wu Y, Bai Z, Yi Y, Liu M, Lan Z, Hua K, Huang S, Li M and Jiang G (2019) Altered Local and Large-Scale Dynamic Functional Connectivity Variability in Posttraumatic Stress Disorder: A Resting-State fMRI Study. Front. Psychiatry 10:234. doi: 10.3389/fpsyt.2019.00234

INTRODUCTION

Posttraumatic stress disorder (PTSD) is a psychiatric condition that can emerge after exposure to an exceedingly traumatic event (1). In the general population, PTSD occurs most commonly after traffic accidents and affects 10%–32% of those involved within 12 months after the event (2). Symptoms of PTSD include intrusive memories, hypervigilance, insomnia, and emotional

numbing (3). Previous studies have indicated that PTSD patients exhibited abnormal interactions among the brain systems (4, 5). For example, Zhang et al. found that the dorsolateral prefrontal cortex showed increased resting-state functional connectivity (FC) with the visual cortex, suggesting that the disrupted frontal-occipital system may be associated with the dysfunction of visual information processing (5). One of robustly identifiable networks is the default mode network (DMN) (6), which is involved in processing self-relevant stimuli (7, 8). The dysfunction of the DMN in PTSD patients may indicate impaired self-generated thoughts and autobiographical memory during rest (9).

One effective approach for exploring brain communication is through the analysis of resting-state fMRI studies (10). Recent resting-state studies in both animals and humans have revealed the dynamic nature of the spatiotemporal organization of blood oxygen level-dependent (BOLD) signals (11–13). Due to unconstrained mental activity, the resting state even shows more dynamic features than in task-stimuli studies (14). A recent study of dynamic FC network indicated that the static FC represented average connectivity across different dynamic states during the whole scanning period; it may not be sensitive enough to detect the alteration of neurofluctuations (15). In order to investigate the dynamic features of inter-regional BOLD signal fluctuations over temporal scales, the sliding window analysis of dynamic FC (dFC) was developed. This approach measured the variety correlations among discrete (large-scale) brain regions (16) using a short, sliding temporal window. Kaiser et al. found that the resting-state dFC revealed the interactions among networks or subnetworks over time (17). Early studies suggested that the dFC can be associated with the changes in arousal (18) and vigilance (19) since hypervigilance and hyper-arousal are two typical symptoms of PTSD. We proposed to use dFC to investigate the characteristic features of PTSD in the resting state. Moreover, since changes in brain network topology are associated with those in local brain activity (20), it was reasonable for us to measure both the large-scale and local dynamic FC in our study.

Regional homogeneity (ReHo) is one of the commonly used algorithms in measuring local FC (21–23). ReHo is a reliable measurement technique and robust against noise in the fast imaging sequence data (24). A prior animal study has suggested an association between ReHo variability and different states of neural activity (25). A recent study of dReHo using the sliding-window approach also indicated that brain regions with high dReHo fluctuation tended to be functional hubs in brain systems (26). A resting-state study has shown that the gene variants affected dReHo in attention-deficit/hyperactivity disorder (27). These findings introduced the clinical potential of dReHo analysis.

The investigation of dFC and dReHo in the resting state may provide new insight into the aberrant brain connectivity in PTSD. Previous studies investigating major depression (28), schizophrenia (29, 30), and bipolar disorder (31) showed abnormal dFC and dReHo under the resting state of these patients, and all of these psychiatry researches found aberrant dFC or aberrant dynamic local activities in the DMN. A possible explanation for these abnormalities is the dynamic nature of the DMN, which exhibits dynamic interactions with a number of other brain systems in the resting state (32). Kaiser et al. (17) indicated that the investigation of altered dynamic activity in areas of the DMN may be important in understanding the pathophysiology of psychiatric disorders.

Although there are few studies available that have focused on the dynamic brain activity in PTSD, prior static studies have suggested that the symptoms of PTSD are associated with the DMN. Mounting evidence has indicated that PTSD is associated with aberrant DMN connectivity (33–35). A static FC (sFC) study suggested that the aberrant activities in the DMN can be a predictor of the symptom severity of PTSD (8). A previous study also approved that the static fMRI data can be used to discriminate the PTSD from HC by using the multilevel parametric classification approach (36). A recent study compared the accuracy of sFC to the accuracy of dFC in classifying PTSD patients and HC (37). The results showed that the peak classification accuracy of dFC reached 94.2%, while the peak classification accuracy of sFC was 86.7%; this research indicated that the temporal dFC is a better predictor than sFC of the diagnostic features of PTSD. Additionally, this study indicated that, in comparison with the HC, the PTSD patients were characterized by decreased temporal variability of brain connectivity. Preti et al. also indicated that PTSD patients often stay trapped in one state and exhibited a decreased dFC in comparison with HC subjects (38). All of these studies indicated that the aberrant connectivity variability of brain networks is vital in the investigation of the neurophysiological mechanism of PTSD.

In order to explore the characteristic resting-state temporal variability of PTSD, we decided to measure both large-scale and local dynamic FC. Based on previous findings, we hypothesized that PTSD patients would exhibit altered dReHo in regions within the DMN. We also expected regions with dReHo alterations to show aberrant dFC and the connectivity measures to be associated with subjects' symptomatology.

METHOD

Subjects

Permission to undertake this study was granted by the ethics committee of Guangdong Second Provincial General Hospital. In January and February 2017, we recruited 30 trauma-exposed subjects from a serious highway traffic accident in Guangdong province. Prior to the examination, none of the patients had undergone any psychotherapy. The inclusion criteria for the PTSD patients were as follows: I) age >18 years; II) right-hand dominance; III) no preexisting psychiatric disorders or physical conditions as determined by a structural clinical interview using the *Diagnostic and Statistical Manual of Mental Disorders*, 4th edition (DSM-IV); IV) no psychiatric medications or substance abuse; V) no MR imaging contraindications; VI) no head trauma or neurologic disorders; VII) fulfills the criteria of DSM-IV and has a Clinical-Administered PTSD Scale (CAPS) score >40; and VIII) not pregnant or nursing. After considering the strict requirements, eight subjects were excluded, five of them for failing to obtain the

CAPS score >40. Twenty-two demographically matched healthy controls (HCs) were recruited for this study. The inclusion criteria for HCs were as follows: I) age >18 years; II) right-hand dominance; III) no preexisting psychiatric disorders or physical conditions as determined by a structural clinical interview using the DSM-IV; IV) no psychiatric medications or substance abuse; V) no MR imaging contraindications; and VI) not pregnant or nursing. Each participant provided written informed consent, which was obtained prior to the MRI scanning.

Assessment of Mental Status

PTSD diagnosis was determined following the DSM-IV diagnostic criteria. Before undergoing resting-state MRI, all PTSD patients were screened with CAPS (39) in order to estimate the intensity and frequency of the symptoms. In addition, emotion assessments were conducted of all participants, including the Self-rating Anxiety Scale (SAS) (40) and the Self-rating Depression (SDS) (41), in order to evaluate the emotional status. A further Structured Clinical Interview for DSM-IV was also performed to evaluate psychiatric disorder comorbidities.

Magnetic Resonance Imaging Data Acquisition

Each of the participants underwent a resting-state MRI in a 3.0-T MR imager (Ingenia; Philips, Best, The Netherlands) equipped with a 32-channel head coil at the Department of Medical Imaging in Guangdong Second Provincial General Hospital. A diagnostic T1-weighted image and a T2 fluid attenuated inversion recovery (T2-FLAIR) image were taken to exclude participants with brain lesions. The resting-state fMRI data were acquired using gradient echo-planar imaging (EPI) with the following parameters: repetition time (TR)/echo time (TE) = 2,000 ms/30 ms; matrix = 64 × 64; field-of-view = 230 mm × 230 mm; flip angle = 90; slice thickness = 3.6 mm, 0.6-mm gap; interleaved scanning; 38 transverse slices covering the whole brain at all 240 volumes were acquired for each participant within 480 s; each volume was aligned along the anterior–posterior commissure. Each participant was instructed to lie still and to avoid falling asleep or thinking of anything in particular during MR scanning.

Resting-State Functional Magnetic Resonance Imaging Data Preprocess

Standard preprocessing of the functional images was performed with the DPARSF 4.3 Advanced Edition (http://rfmri.org/DPARSF) and the SPM12 package (www.fil.ion.ucl.ac.uk/spm) based on MATLAB (Mathworks, Inc., Natick, MA, USA). The first 10 volumes of each dataset were discarded for signal equilibration. The remaining data were performed using slice timing correction and realignment and co-registered with the anatomical scan. The co-registered T1-weighted images were segmented into gray matter, white matter, and cerebrospinal fluid. And then the functional images were normalized into the Montreal Neurological Institute (MNI) space with a voxel size of $3 \times 3 \times 3$ mm^3. The head movement parameters were obtained from the realignment steps in the DPARSF. We took the mean FD Jenkinson (42) as the head motion reference standard. We eliminated the subjects with motion (mean FD Jenkinson) greater than 2 × standard deviation (SD) above the group mean motion as recommended in a previous study (43). No subject was eliminated in this step. There was no significant difference in head motion between the PTSD patients and the HC (see **Table 1**). Linear detrending processing was conducted to remove the linear signal drift. Individual-level regression analysis was conducted to minimize the influence of head motion (Friston 24 model), white matter signal noise, and cerebrospinal fluid signal noise. A temporal band-pass filter (0.0167–0.10 Hz) was applied to the data to remove the physical noise and any frequencies for which the period was shorter than that of a single sliding window (44). We performed spatial smoothing with a 6-mm full-width at half-maximum (FWHM) kernel before performing the dReHo group analysis. As for the dFC, we performed the spatial smoothing with a 6-mm FWHM kernel before the linear detrending and nuisance signals regression, and band-pass filtering. Considering the size of FWHM Gaussian kernel might affect the results of dReHo/dFC analysis (45, 46), we used 4- and 8-mm FWHM Gaussian kernel to test the consistency of our results (45, 46) (see **Supplementary Figures 1** and **2**).

TABLE 1 | Demographic and clinical data.

Characteristic	PTSD (n = 22)	HC (n = 22)	t value	P value
Age (years)	37.36 ± 8.95	40.32 ± 10.34	−1.014	0.317
Gender (M/F)	8/14	8/14		
Head motion	0.169 ± 0.443	0.159 ± 0.441	0.073	0.942
Education (years)	11.82 ± 3.22	10.45 ± 4.25	1.200	0.237
CAPS	51.45 ± 6.93			
SAS	36.09 ± 8.11	38.18 ± 6.02	−0.971	0.337
SDS	38.05 ± 9.49	39.09 ± 8.08	−0.393	0.696

Demographic data are presented as mean ± SD. PTSD, posttraumatic stress disorder; HC, healthy control; CAPS, Clinical-Administrated PTSD Scale; SAS, Self-rating Anxiety Scale; SDS, Self-rating Depression Scale. The P-value was obtained by the two-sample t test.

Computation of dReHo and dFC

ReHo calculation: The ReHo algorithm measures voxel-wise short-distance FC with Kendall's coefficient of concordance (23) using the following formula:

$$W = \frac{\sum_{i=1}^{N} R_i^2 - N\overline{R}^2}{\frac{1}{12}K^2(N^3 - N)}$$

where W is the Kendall's coefficient of concordance among the given voxels, N denotes the length of the time series, K = 27 is the size of the voxel cluster containing 3 × 3 × 3 adjacent voxels, R_i denotes the summation of the rankings of the BOLD signal amplitude of all K voxels at the ith time point, and R is the mean of R_i.

To compute the dReHo for these data, the time course was segmented into 60-s Hamming windows (30 dynamics). By sliding the onset of each window by 2 dynamics (4 s), for a total of 101 overlapping windows in the first level analysis, the dReHo was estimated by using the calculated SD of the ReHo

through the windows at each voxel, yielding a set of ReHo maps for each participant.

Two-sample *t*-test with head motion parameters (mean FD Jenkinson values), age, and sex as covariates was performed to test the difference in dReHo maps between the PTSD patients and HC at each voxel. Multiple comparisons correction was performed with Gaussian random field (GRF) theory at the cluster level (minimum $z > 3.54$; cluster significance: $p < 0.05$, two-tailed GRF corrected).

To determine whether the dReHo metrics were associated with clinical indicators, we performed general linear models with the clinical indicators (CAPS, SAS, SDS) and mean dReHo values from clusters with significant group differences as independent variables, and head motion parameters, age, and sex as covariates. The correlation analysis was accomplished with the SPSS software with a significance threshold of $p < 0.05$ (uncorrected).

Voxel-wise seed-based FC analyses were performed using the DPARSF 4.3. We employed the aberrant dReHo region, which we calculated above, as a seed region. Then we used the sliding-window approach as we have used in the dReHo calculation; the time course was segmented into 60-s Hamming windows by sliding the onset of each window by 2 dynamics, for a total of 101 overlapping windows in the first level analysis. Within each sliding window, the whole brain FC maps for the seed region were computed as the Fisher *z* transformed Pearson correlation coefficient between the averaged time course of all voxels in the seed and the time course of all other voxels in the whole brain, yielding a set of sliding window *z*FC maps for each participant. The dFC was estimated by calculating the standard deviation in *z*FC values through windows at each voxel.

Two-sample *t*-test with head motion parameters (mean FD Jenkinson values), age, and sex as covariates was performed to investigate the difference of dFC values between the PTSD group and the HC group at each voxel. Multiple comparisons were performed with GRF correction at the cluster level (minimum $z > 3.29$; cluster significance: $p < 0.05$, two-tailed GRF corrected).

To explore the relationship between dFC metrics and clinical indicators, we performed general linear models with the clinical indicators and mean dFC values from clusters with significant group differences as independent variables, and head motion parameters, age, and sex as covariates. The correlation analysis was accomplished with SPSS software with significance threshold of $p < 0.05$ (uncorrected).

RESULTS

The demographic and clinical data are summarized in **Table 1**. Inconsistent with our prediction, compared with the HC, the PTSD patients exhibited an increased dReHo (more variability) in the left posterior cingulate cortex (PCC)/precuneus (PCu) (**Figure 1**). We also found a decreased dFC (less variability) between the left and right PCu, and the left inferior parietal lobe (IPL)/angular gyrus (AG), but increased dFC between the PCC and the left insula (**Table 2** and **Figure 2**).

Next, we conducted analyses to test the association between the clinical indicators (CAPS, SAS, SDS) of PTSD and dReHo within the PTSD group. There is no significant correlation between the clinical indicators and dReHo/dFC after FWE correction (see **Supplementary Figure 4**).

DISCUSSION

In this study, by using resting-state dReHo analysis, we determined the local aberrant variability in the left PCu. The PCu is a key hub in the DMN of human brain (47). Aberrant resting-state temporal dynamic brain activities were found in the dReHo and large-scale dFC of specific brain regions, which were mainly located in the posterior DMN (pDMN) and the primary region of the salience network (SN). These observations provide new insights into the aberrant brain activities in PTSD.

This study revealed a significantly increased dReHo (more variability) in left PCu, suggesting that the neurofluctuation of the left PCu is unstable in the PTSD patients in the resting state. The PCu is a key hub of the pDMN (47–49) and is considered to

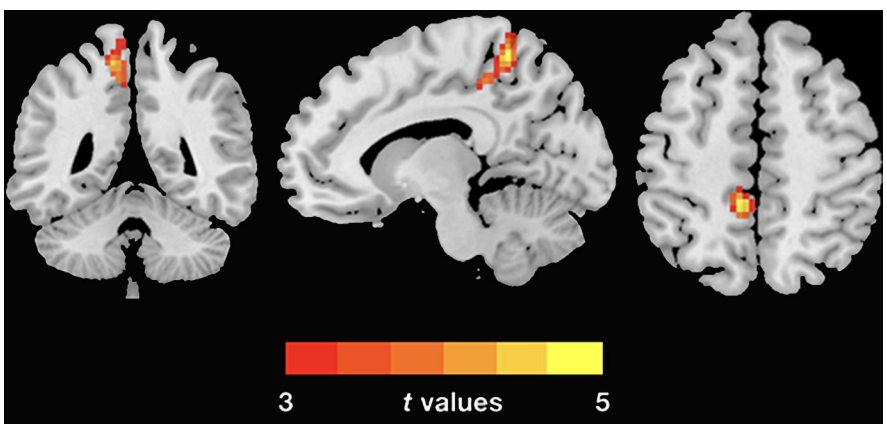

FIGURE 1 | Group differences of dReHo variability were revealed by two-sample *t*-test. The PTSD group shows increased (warm color) dReHo variability in the left PCu (cluster size: 104; AAL: Precuneus_L; Brodmann area 7; MNI coordinates: X: −12 Y: −48 Z: 60; peak *t*-value = 5.1868) relative to the HC. The Gaussian random theory was used for cluster-level multiple comparison correction (minimum $z > 3.54$; cluster significance $p < 0.05$, GRF corrected). dReHo, dynamic regional homogeneity; PTSD, posttraumatic stress disorder; AAL, anatomical automatic labeling; PCu, precuneus; MNI, Montreal Neurological Institute.

TABLE 2 | Comparison of dFC between PTSD and HC.

Brain region	Cluster size	MNI coordinates			AAL	Brodmann's area	Peak *t* value
		X	Y	Z			
R PCu	44	3	−48	45	Precuneus_R	7	−4.0992
L IPL	62	−38	−78	42	Parietal_Inf_L	19	−4.1411
L Insula	33	−36	−12	21	Insula_L	13	4.6200

L, left; R, right; MNI, Montreal Neurological Institute; dFC, dynamic functional connectivity; AAL, anatomical automatic labeling; PCu, precuneus; IPL, inferior parietal lobe.

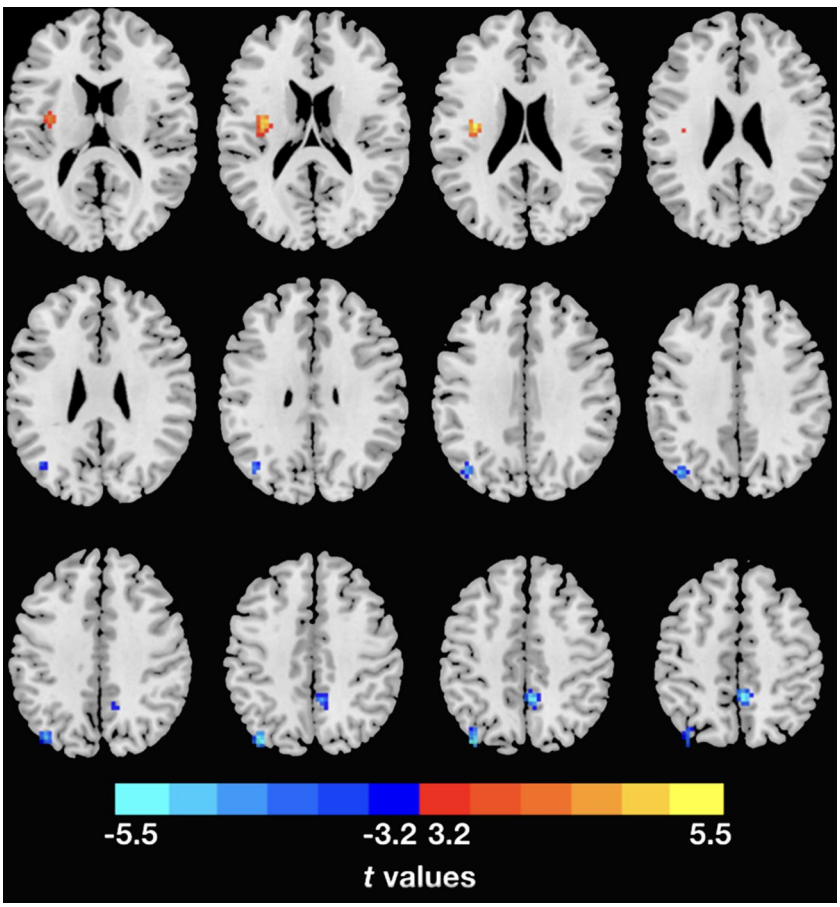

FIGURE 2 | Inter-regional dFC differences with regions showing significant dReHo differences between groups. The PTSD group shows increased dFC variability in left insula, but decreased dFC variability in right PCu and left IPL relative to the HC. Gaussian random theory was used for cluster-level multiple comparison correction (minimum $z > 3.29$; cluster significance $p < 0.05$, GRF corrected). dFC, dynamic functional connectivity; dReHo, dynamic regional homogeneity; PTSD, posttraumatic stress disorder; PCu, precuneus; IPL, inferior parietal lobe.

be involved in self-referential processing (7) and autobiographic memory (50). In the resting state, the DMN exhibits dynamic interaction with a number of brain systems, such as the frontal–parietal control network and the dorsal attention network (32). Although we found an aberrant local connectivity variety in the PCu, the evidence of aberrant DMN connectivity in PTSD patients is not entirely persuasive. In order to explore the dynamic interactions among the DMN and other brain networks, we employed the left PCu as the seed region and carried out the dFC of the whole brain.

Several studies have identified aberrant activities in the DMN of PTSD patients (6, 34, 35). In the present study, using seed-based dFC, we identified lower-variability regions located in the right PCu and the left IPL. These results suggest that compared with the normal controls, the PTSD group exhibits decreased dFC (less variability) within the pDMN. We suspected that this restrained neurofluctuation within the pDMN represents decreased regulation of the self-referential processing. Previous studies using the independent component analysis identified the aberrant pDMN in PTSD patients (4, 51). Furthermore,

Zhang et al. found a decreased intranetwork connectivity within the pDMN by measuring resting-state sFC. These researches suggested that the decreased FC in pDMN was associated with the dysfunction of evaluation of the self-related events in PTSD. The interaction between DMN and the executive control systems, which includes dorsal lateral middle frontal cortex and the IPL (52), is essential in regulating the self-generated thought (32). In the present study, a deceased dFC was found between the left PCu and the left IPL. Therefore, we inferred that the deceased dFC suggested a discrete FC state between the DMN and the executive control system, which may induce the dysregulation of self-referential processing. Previous studies indicated that the IPL is engaged in mediating visuospatial processing (53), which is critical when dealing with life-threatening events (54). Additionally, previous study indicated that the IPL is a vulnerable brain region to the neurotoxic effects of stress (55). Therefore, we suspected that the aberrant dFC between the PCu and the IPL might be a potential biomarker of PTSD.

In the present study, the left insula was the only region in the brain that exhibited significant positive dynamic correlation with the left PCu in the PTSD group. The insula is a key hub in the SN and is thought to be involved in the detection of personally salient internal and external stimuli that guide behaviors in order to maintain equilibrium (56). In addition, the insula is thought to be involved in mediation of the "switching" between activation of the DMN and the central executive network (CEN) to direct appropriate behavioral responses to the salience stimuli (57). Therefore, we suspected that the positive dynamic correlation between the left PCu and left insula might suggest an excessive interaction between the SN and the DMN. Previous studies using the graph theory approach identified dysregulation in three intrinsic brain networks (1, 58). Lei et al. found a disequilibrium among the CEN, DMN, and SN and suggested that the SN was crucial to the PTSD symptoms (58). Previous resting-state sFC study also revealed an increased correlation between the DMN seed region [PCC and ventromedial prefrontal cortex (vmPFC)] and SN (insula and precentral sulcus) (59). They found a positive correlation between the PTSD symptom severity and the vmPFC-precentral sulcus FC values. Our results provided an additional piece of evidence that, compared with the HC, the PTSD patients exhibited more variable connectivity between the DMN and the SN.

There are some limitations in the present study that should be highlighted. Firstly, little information is available on the meaning of the resting-state dFC in neurocognitive functioning. For example, it remains unknown whether the abnormal dynamic activities in the resting state are intrinsic properties or are affected by the present-moment cognitive activities (17, 60). As the number of resting-state dFC studies grows, we may gain a better understanding of these properties and their relation to the psychopathology. Secondly, since the dFC based on the sliding-window approach is composed of a few time points, the dynamic analysis is particularly sensitive to the physiological noise (61). Although, we did not denoised the physiological noise individually, we denoised the physiological noise in the preprocessing steps and group-level test and we also chose a relatively large window size in order to diminish the adverse effects of physiological noise. Thirdly, we only examined significant differences in regions exhibiting abnormal dynamic activity to focusing on the dynamic pattern related to PTSD; further exploration of static results is needed in our future works. Fourthly, the correlation results did not survive the FWE correction, so further exploration of the abnormal dynamic patterns and CAPS subscales is needed in our future large sample research to evaluate the relations between the dynamic patterns and specific clinical symptoms severity, such as intrusive memory and flash back.

In conclusion, this resting-state dFC (combine the dReHo and dFC) study provided evidence that the PTSD patients exhibited aberrant dReHo and dFC in comparison with the HC. Decreased variability within the DMN may suggest dysfunction of self-referential processing in PTSD patients, while increased variability between the insula and PCu may suggest dysregulation between the DMN and the SN.

ETHICS STATEMENT

Permission to undertake this study was granted by the ethics committee of Guangdong Second Provincial General Hospital.

AUTHOR CONTRIBUTIONS

SF designed the experiment. SF and XM carried out the experiment. ZB collected and sorted out the data. YW, MLiu, YY, ZL, SH, MLi, and KH helped on data management and processing. SF and GJ wrote the manuscript.

SUPPLEMENTARY MATERIAL

The Supplementary Material for this article can be found online at: https://www.frontiersin.org/articles/10.3389/fpsyt.2019.00234/full#supplementary-material

REFERENCES

1. Yehuda R, Hoge CW, McFarlane AC, Vermetten E, Lanius RA, Nievergelt CM, et al. Post-traumatic stress disorder. *Nat Rev Dis Primers* (2015) 1:15057. doi: 10.1038/nrdp.2015.57
2. Yaşan A, Güzel A, Tamam Y, Ozkan M. Predictive factors for acute stress disorder and posttraumatic stress disorder after motor vehicle accidents. *Psychopathology* (2009) 42:236–41. doi: 10.1159/000218521
3. American Psychiatric Publishing, Inc. *DSM-IV-TR: Diagnostic and statistical manual of mental disorders, text revision.* Washington (2000).
4. Ke J, Zhang L, Qi R, Xu Q, Zhong Y, Liu T, et al. Typhoon-related post-traumatic stress disorder and trauma might lead to functional integration abnormalities in intra- and inter-resting state networks: a resting-state fMRI

independent component analysis. *Cell Physiol Biochem* (2018) 48:99–110. doi: 10.1159/000491666
5. Zhang Y, Xie B, Chen H, Li M, Liu F, Chen H. Abnormal functional connectivity density in post-traumatic stress disorder. *Brain Topogr* (2016) 29:1–7. doi: 10.1007/s10548-016-0472-8
6. Akiki TJ, Averill CL, Wrocklage KM, Scott JC, Averill LA, Schweinsburg B, et al. Default mode network abnormalities in posttraumatic stress disorder: a novel network-restricted topology approach. *NeuroImage* (2018) 176:1–27. doi: 10.1016/j.neuroimage.2018.05.005
7. Bluhm RL, Williamson PC, Osuch EA, Frewen PA, Stevens TK, Boksman K, et al. Alterations in default network connectivity in posttraumatic stress disorder related to early-life trauma. *J Psychiatry Neurosci* (2009) 34:187–94. http://jpn.ca/vol34-issue3/34-3-187/
8. Lanius RA, Bluhm RL, Coupland NJ, Hegadoren KM, Rowe B, Théberge J, et al. Default mode network connectivity as a predictor of post-traumatic stress disorder symptom severity in acutely traumatized subjects. *Acta Psychiatr Scand* (2009) 121:33–40. doi: 10.1111/j.1600-0447.2009.01391.x
9. Koch SBJ, van Zuiden M, Nawijn L, Frijling JL, Veltman DJ, Olff M. Aberrant resting-state brain activity in posttraumatic stress disorder: a meta-analysis and systematic review. *Depress Anxiety* (2016) 33:592–605. doi: 10.1002/da.22478
10. Biswal BB. Resting state fMRI: a personal history. *NeuroImage* (2012) 62:938–44. doi: 10.1016/j.neuroimage.2012.01.090
11. Chang C, Glover GH. Time–frequency dynamics of resting-state brain connectivity measured with fMRI. *NeuroImage* (2010) 50:81–98. doi: 10.1016/j.neuroimage.2009.12.011
12. Hutchison RM, Womelsdorf T, Gati JS, Everling S, Menon RS. Resting-state networks show dynamic functional connectivity in awake humans and anesthetized macaques. *Hum Brain Mapp* (2012) 34:2154–77. doi: 10.1002/hbm.22058
13. Keilholz SD, Magnuson ME, Pan W-J, Willis M, Thompson GJ. Dynamic properties of functional connectivity in the rodent. *Brain Connect* (2013) 3:31–40. doi: 10.1089/brain.2012.0115
14. Deco G, Ponce-Alvarez A, Mantini D, Romani GL, Hagmann P, Corbetta M. Resting-state functional connectivity emerges from structurally and dynamically shaped slow linear fluctuations. *J Neurosci* (2013) 33:11239–52. doi: 10.1523/JNEUROSCI.1091-13.2013
15. Liu F, Wang Y, Li M, Wang W, Li R, Zhang Z, et al. Dynamic functional network connectivity in idiopathic generalized epilepsy with generalized tonic-clonic seizure. *Hum Brain Mapp* (2017) 38:957–73. doi: 10.1002/hbm.23430
16. Handwerker DA, Roopchansingh V, Gonzalez-Castillo J, Bandettini PA. Periodic changes in fMRI connectivity. *NeuroImage* (2012) 63:1712–9. doi: 10.1016/j.neuroimage.2012.06.078
17. Kaiser RH, Whitfield-Gabrieli S, Dillon DG, Goer F, Beltzer M, Minkel J, et al. Dynamic resting-state functional connectivity in major depression. *Neuropsychopharmacology* (2016) 41:1822–30. doi: 10.1038/npp.2015.352
18. Chang C, Metzger CD, Glover GH, Duyn JH, Heinze H-J, Walter M. Association between heart rate variability and fluctuations in resting-state functional connectivity. *NeuroImage* (2013) 68:93–104. doi: 10.1016/j.neuroimage.2012.11.038
19. Thompson GJ, Magnuson ME, Merritt MD, Schwarb H, Pan W-J, McKinley A, et al. Short-time windows of correlation between large-scale functional brain networks predict vigilance intraindividually and interindividually. *Hum Brain Mapp* (2012) 34:3280–98. doi: 10.1002/hbm.22140
20. Gross T, Blasius B. Adaptive coevolutionary networks: a review. *J R Soc Interface* (2008) 5:259–71. doi: 10.1098/rsif.2007.1229
21. Guo W-B, Liu F, Xue Z-M, Yu Y, Ma C-Q, Tan C-L, et al. Abnormal neural activities in first-episode, treatment-naïve, short-illness-duration, and treatment-response patients with major depressive disorder: a resting-state fMRI study. *J Affect Disord* (2011) 135:326–31. doi: 10.1016/j.jad.2011.06.048
22. Liu F, Hu M, Wang S, Guo W, Zhao J, Li J, et al. Abnormal regional spontaneous neural activity in first-episode, treatment-naive patients with late-life depression: a resting-state fMRI study. *Prog Neuropsychopharmacol Biol Psychiatry* (2012) 39:326–31. doi: 10.1016/j.pnpbp.2012.07.004
23. Zang Y, Jiang T, Lu Y, He Y, Tian L. Regional homogeneity approach to fMRI data analysis. *NeuroImage* (2004) 22:394–400. doi: 10.1016/j.neuroimage.2003.12.030
24. Zuo X-N, Xu T, Jiang L, Yang Z, Cao X-Y, He Y, et al. Toward reliable characterization of functional homogeneity in the human brain: preprocessing, scan duration, imaging resolution and computational space. *NeuroImage* (2013) 65:374–86. doi: 10.1016/j.neuroimage.2012.10.017
25. Hudetz AG, Liu X, Pillay S. Dynamic repertoire of intrinsic brain states is reduced in propofol-induced unconsciousness. *Brain Connect* (2015) 5:10–22. doi: 10.1089/brain.2014.0230
26. Deng L, Sun J, Cheng L, Tong S. Characterizing dynamic local functional connectivity in the human brain. *Sci Rep* (2016) 6:26976. doi: 10.1038/srep26976
27. Kim JI, Yoo JH, Kim D, Jeong B, Kim B-N. The effects of GRIN2B and DRD4 gene variants on local functional connectivity in attention-deficit/hyperactivity disorder. *Brain Imaging Behav* (2017) 12:247–57. doi: 10.1007/s11682-017-9690-2
28. Qiu L, Xia M, Cheng B, Yuan L, Kuang W, Bi F, et al. Abnormal dynamic functional connectivity of amygdalar subregions in untreated patients with first-episode major depressive disorder. *JPN* (2018) 43:262–72. doi: 10.1503/jpn.170112
29. Damaraju E, Allen EA, Belger A, Ford JM, McEwen S, Mathalon DH, et al. Dynamic functional connectivity analysis reveals transient states of dysconnectivity in schizophrenia. *Neuroimage Clin* (2014) 5:298–308. doi: 10.1016/j.nicl.2014.07.003
30. Fu Z, Tu Y, Di X, Du Y, Pearlson GD, Turner JA, et al. Characterizing dynamic amplitude of low-frequency fluctuation and its relationship with dynamic functional connectivity: an application to schizophrenia. *NeuroImage* (2017) 180:1–13. doi: 10.1016/j.neuroimage.2017.09.035
31. Calhoun VD. Dynamic connectivity states estimated from resting fMRI identify differences among schizophrenia, bipolar disorder, and healthy control subjects. *Front Hum Neurosci* (2014) 8:897–13. doi: 10.3389/fnhum.2014.00897
32. Andrews-Hanna JR, Smallwood J, Spreng RN. The default network and self-generated thought: component processes, dynamic control, and clinical relevance. *Ann N Y Acad Sci* (2014) 1316:29–52. doi: 10.1111/nyas.12360
33. Kennis M, van Rooij SJH, van den Heuvel MP, Kahn RS, Geuze E. Functional network topology associated with posttraumatic stress disorder in veterans. *Neuroimage Clin* (2016) 10:302–9. doi: 10.1016/j.nicl.2015.12.008
34. Miller DR, Logue MW, Wolf EJ, Maniates H, Robinson ME, Hayes JP, et al. Posttraumatic stress disorder symptom severity is associated with reduced default mode network connectivity in individuals with elevated genetic risk for psychopathology. *Depress Anxiety* (2017) 34:632–40. doi: 10.1002/da.22633
35. Patriat R, Birn RM, Keding TJ, Herringa RJ. Default-mode network abnormalities in pediatric posttraumatic stress disorder. *J Am Acad Child Adolesc Psychiatry* (2016) 55:319–27. doi: 10.1016/j.jaac.2016.01.010
36. Liu F, Xie B, Wang Y, Guo W, Fouche J-P, Long Z, et al. Characterization of post-traumatic stress disorder using resting-state fMRI with a multi-level parametric classification approach. *Brain Topogr* (2014) 28:221–37. doi: 10.1007/s10548-014-0386-2
37. Jin C, Jia H, Lanka P, Rangaprakash D, Li L, Liu T, et al. Dynamic brain connectivity is a better predictor of PTSD than static connectivity. *Hum Brain Mapp* (2017) 38:4479–96. doi: 10.1002/hbm.23676
38. Preti MG, Bolton TA, Van De Ville D. The dynamic functional connectome–state-of-the-art and perspectives. *NeuroImage* (2016) 160:1–33. doi: 10.1016/j.neuroimage.2016.12.061
39. Blake DD, Weathers FW, Nagy LM, Kaloupek DG, Gusman FD, Charney DS, Keane TM. The development of a Clinician-Administered PTSD Scale. *J Trauma Stress* (1995) 8:75–90. doi: 10.1007/bf02105408
40. Zung WW. A rating instrument for anxiety disorders. *Psychosomatics* (1971) 12:371–9. doi: 10.1016/S0033-3182(71)71479-0
41. Zung WW. A Self-Rating Depression Scale. *Arch Gen Psychiatry* (1965) 12:63–70. doi: 10.1001/archpsyc.1965.01720310065008
42. Jenkinson M, Bannister P, Brady M, Smith S. Improved optimization for the robust and accurate linear registration and motion correction of brain images. *NeuroImage* (2002) 17:825–41. doi: 10.1006/nimg.2002.1132
43. Yan C-G, Craddock RC, Zuo X-N, Zang Y-F, Milham MP. Standardizing the intrinsic brain: towards robust measurement of inter-individual variation in 1000 functional connectomes. *NeuroImage* (2013) 88:1–17. doi: 10.1016/j.neuroimage.2013.04.081
44. Leonardi N, Van De Ville D. On spurious and real fluctuations of dynamic functional connectivity during rest. *NeuroImage* (2015) 104:430–6. doi: 10.1016/j.neuroimage.2014.09.007

45. Ball T, Breckel TPK, Mutschler I, Aertsen A, Schulze-Bonhage A, Hennig J, et al. Variability of fMRI-response patterns at different spatial observation scales. *Hum Brain Mapp* (2011) 33:1155–71. doi: 10.1002/hbm.21274
46. Pajula J, Tohka J. Effects of spatial smoothing on inter-subject correlation based analysis of FMRI. *Magn Reson Imaging* (2014) 32:1114–24. doi: 10.1016/j.mri.2014.06.001
47. Leech R, Sharp DJ. The role of the posterior cingulate cortex in cognition and disease. *Brain* (2013) 137:12–32. doi: 10.1093/brain/awt162
48. Guo W, Liu F, Yao D, Jiang J, Su Q, Zhang Z, et al. Decreased default-mode network homogeneity in unaffected siblings of schizophrenia patients at rest. *Psychiatry Res Neuroimaging* (2014) 224:218–24. doi: 10.1016/j.pscychresns.2014.08.014
49. Liu F, Guo W, Fouche J-P, Wang Y, Wang W, Ding J, et al. Multivariate classification of social anxiety disorder using whole brain functional connectivity. *Brain Struct Funct* (2013) 220:101–15. doi: 10.1007/s00429-013-0641-4
50. Buckner RL, Andrews-Hanna JR, Schacter DL. The brain's default network: anatomy, function, and relevance to disease. *Ann N Y Acad Sci* (2008) 1124:1–38. doi: 10.1196/annals.1440.011
51. Zhang Y, Liu F, Chen H, Li M, Duan X, Xie B, et al. Intranetwork and internetwork functional connectivity alterations in post-traumatic stress disorder. *J Affect Disord* (2015) 187:114–21. doi: 10.1016/j.jad.2015.08.043
52. Cole MW, Repovš G, Anticevic A. The frontoparietal control system. *Neuroscientist* (2014) 20:652–64. doi: 10.1177/1073858414525995
53. Petersen SE, Fox PT, Posner MI, Mintun M, Raichle ME. Positron emission tomographic studies of the cortical anatomy of single-word processing. *Nature* (1988) 331:585–9. doi: 10.1038/331585a0
54. Yin Y, Li L, Jin C, Hu X, Duan L, Eyler LT, et al. Abnormal baseline brain activity in posttraumatic stress disorder: a resting-state functional magnetic resonance imaging study. *Neurosci Lett* (2011) 498:185–9. doi: 10.1016/j.neulet.2011.02.069
55. Patel NV, Finch CE. The glucocorticoid paradox of caloric restriction in slowing brain aging. *Neurobiol Aging* (2002) 23:707–17. doi: 10.1016/S0197-4580(02)00017-9
56. Uddin LQ. Salience processing and insular cortical function and dysfunction. *Nat Rev Neurosci* (2015) 16:55–61. doi: 10.1038/nrn3857
57. Menon V, Uddin LQ. Saliency, switching, attention and control: a network model of insula function. *Brain Struct Funct* (2010) 214:655–67. doi: 10.1007/s00429-010-0262-0
58. Lei D, Li K, Li L, Chen F, Huang X, Lui S, et al. Disrupted functional brain connectome in patients with posttraumatic stress disorder. *Radiology* (2015) 276:818–27. doi: 10.1148/radiol.15141700
59. Sripada RK, King AP, Welsh RC, Garfinkel SN, Wang X, Sripada CS, et al. Neural dysregulation in posttraumatic stress disorder. *Psychosom Med* (2012) 74:904–11. doi: 10.1097/PSY.0b013e318273bf33
60. Buckner RL, Krienen FM, Yeo BTT. Opportunities and limitations of intrinsic functional connectivity MRI. *Nat Neurosci* (2013) 16:832–7. doi: 10.1038/nn.3423
61. Hutchison RM, Womelsdorf T, Allen EA, Bandettini PA, Calhoun VD, Corbetta M, et al. Dynamic functional connectivity: promise, issues, and interpretations. *NeuroImage* (2013) 80:360–78. doi: 10.1016/j.neuroimage.2013.05.079

Conflict of Interest Statement: The authors declare that the research was conducted in the absence of any commercial or financial relationships that could be construed as a potential conflict of interest.

frontiers in Neurology

ORIGINAL RESEARCH
published: 02 July 2019
doi: 10.3389/fneur.2019.00668

Predicting the Post-therapy Severity Level (UPDRS-III) of Patients With Parkinson's Disease After Drug Therapy by Using the Dynamic Connectivity Efficiency of fMRI

Xuesong Li[1], Yuhui Xiong[2], Simin Liu[2], Rongsong Zhou[3], Zhangxuan Hu[2], Yan Tong[4], Le He[2], Zhendong Niu[1], Yu Ma[3] and Hua Guo[2]*

[1] School of Computer Science and Technology, Beijing Institute of Technology, Beijing, China, [2] Department of Biomedical Engineering, Center for Biomedical Imaging Research, School of Medicine, Tsinghua University, Beijing, China, [3] Department of Neurosurgery, Tsinghua University Yuquan Hospital, Beijing, China, [4] Nuffield Department of Clinical Neurosciences, Wellcome Centre for Integrative Neuroimaging, FMRIB, University of Oxford, Oxford, United Kingdom

OPEN ACCESS

Edited by:
Feng Liu,
Tianjin Medical University General Hospital, China

Reviewed by:
Bing Zhang,
Nanjing Drum Tower Hospital, China
Hui-Jie Li,
Chinese Academy of Sciences, China
Heng Chen,
Guizhou University, China

***Correspondence:**
Yu Ma
mayu@tsinghua.edu.cn

Specialty section:
This article was submitted to Applied Neuroimaging, a section of the journal Frontiers in Neurology

Received: *01 February 2019*
Accepted: *06 June 2019*
Published: *02 July 2019*

Citation:
Li X, Xiong Y, Liu S, Zhou R, Hu Z, Tong Y, He L, Niu Z, Ma Y and Guo H (2019) Predicting the Post-therapy Severity Level (UPDRS-III) of Patients With Parkinson's Disease After Drug Therapy by Using the Dynamic Connectivity Efficiency of fMRI. Front. Neurol. 10:668. doi: 10.3389/fneur.2019.00668

Parkinson's disease (PD) is a multi-systemic disease in the brain arising from the dysfunction of several neural networks. The diagnosis and treatment of PD have gained more attention for clinical researchers. While there have been many fMRI studies about functional topological changes of PD patients, whether the dynamic changes of functional connectivity can predict the drug therapy effect is still unclear. The primary objective of this study was to assess whether large-scale functional efficiency changes of topological network are detectable in PD patients, and to explore whether the severity level (UPDRS-III) after drug treatment can be predicted by the pre-treatment resting-state fMRI (rs-fMRI). Here, we recruited 62 Parkinson's disease patients and calculated the dynamic nodal efficiency networks based on rs-fMRI. With connectome-based predictive models using the least absolute shrinkage and selection operator, we demonstrated that the dynamic nodal efficiency properties predict drug therapy effect well. The contributed regions for the prediction include hippocampus, post-central gyrus, cingulate gyrus, and orbital gyrus. Specifically, the connections between hippocampus and cingulate gyrus, hippocampus and insular gyrus, insular gyrus, and orbital gyrus are positively related to the recovery (post-therapy severity level) after drug therapy. The analysis of these connection features may provide important information for clinical treatment of PD patients.

Keywords: fMRI, dynamic nodal efficiency, Parkinson's disease, drug treatment, prediction of post-therapy severity level

INTRODUCTION

Parkinson's disease (PD) is one of the most common neurodegenerative disorders. It is clinically characterized by some specific motor symptoms, including rigidity, slowness of movement, tremor at rest, bradykinesia, and postural instability and some other non-motor symptoms such as cognitive deficits, impaired olfaction, emotional problems (1, 2). PD can be considered as a

multi-systemic disease in the brain arising from dysfunction in several neural networks (3–5). The motor and cognitive impairments in PD have been related to abnormal functional connectivity and disrupted network integration in the brain (6–8).

Several graph theoretic studies revealed an abnormal topological organization of functional brain networks in PD patients. Specifically, Skidmore et al. combined fMRI and graph analysis to find a smaller global efficiency of brain networks in advanced PD patients (9). Wei et al. found that PD had significantly decreased efficiency in the cortico-basal ganglia motor pathway (10). In addition, Dubbelink et al. using magnetoencephalography and graph theory, reported that impaired local network efficiency and network decentralization are very early features of PD that continue to progress over time, along with reductions in global efficiency (6). In summary, the graph theory provides a powerful and general framework to characterize brain connectivity at global and local levels, and offers a collection of metrics that can quantify the segregation and integration of information within functional networks among the brain regions. However, most of the previous studies did not consider the important dynamic properties of FC over time, such as the dynamic nodal efficiency; instead, FC was usually assumed to be constant during the rs-fMRI experiment (8).

The graph theory-based approach applied to dynamic FC show that the variability in brain network may also provide important information on the underlying nature of neurodegeneration. In a study by Yu et.al., the reduced variability of local and global network efficiency was detected in a patient with schizophrenia (11). In a more recent PD study, dynamic topological properties of brain networks can characterize the underlying nature of Parkinson's disease and correlate with clinical features (8).

The dynamic property of fMRI can enrich the graph theory. We wonder if the dynamic nodal efficiency (dnE) can be used to predict the recovery effect after drug therapy (i.e., post-therapy severity level) of PD patients. If possible, it may provide useful guidance information for drug therapy. Connectome-based predictive modeling is a recently developed data-driven method for identifying the relationship between functional brain connectivity and the behavioral and cognitive variables of interest, and then predicting the behavior of patients (12–14). The predictive modeling procedure has been applied to analyze connectivity, such as attention control and temperament trait (14, 15). Its core idea is the cooperative analysis of the relationship between behavior and FC, finally finding the strong functional networks that are correlated to the behavior with statistical significance. It provides an effective way to explore the correlation between altered topological properties and clinical indexes of interest.

In the present study, we used rs-fMRI and sliding-window analysis to build the individual dnE network by computing each nodal efficiency of each sliding-window and predicted the post-therapy severity level of PD patients. The global efficiency is chosen to calculate the dnE, since it may reveal more PD properties than local efficiency, as indicated by Kim et al. whose study showed a significant difference in global efficiency between PD and the healthy control, but not in local efficiency (8). Specifically, we proposed a rigorous cross-validated prediction framework incorporating feature selection and regression techniques, to predict the drug therapy effect of levodopa (the most commonly used drug in PD treatment), which is evaluated by Unified Parkinson Disease Rating Scale III (UPDRS-III) (16) scores, using the rs-fMRI data from 62 PD patients. We aim to investigate the possibility of predicting individual after-therapy UPDRS-III scores using whole-brain dnE network. The post-therapy UPDRS-III scores for certain patients was estimated, and the potentially important connections that contribute to the recovery degree were predicted by the rs-fMRI data.

TABLE 1 | Participant demographic and clinical characteristics.

	Mean(±SD)
Age (years)	58.5(±10.1)
Disease duration (years)	10.4(±4.4)
MoCA	21.6(±5.5)
Depression score (BDI-II)	8.5(±10.0)
Levodopa equivalent daily dose (mg)	720.4(±295.7)
Hoehn and Yahr stage	3.7(±0.6)
Frame-wise displacement (mm)	0.33±(0.20)
Medication-off UPDRS-III	44.1(±12.0)
Medication-on UPDRS-III	22.2(±11.8)

Values are given as mean and SD. MoCA, Montreal Cognitive Assessment; BDI-II, Beck Depression Inventory-II; UPDRS-III, Unified Parkinson Disease Rating Scale III.

MATERIALS AND METHODS

Subjects

Sixty-two subjects (mean age, 58.5 ± 10.1 years; 31 females and 31 male patients) were recruited from Tsinghua University Yuquan Hospital, Beijing, China. Patients were told to stop taking drugs 12 h before the rs-fMRI scan (before therapy). Patients diagnosed with PD based on the UK Brain Bank criteria (17) were enrolled. Exclusion criteria includes a history of psychiatric or neurological disease other than PD, other major medical diseases, head injury, alcohol/drug dependency/abuse (8). Disease severity of each patient was evaluated by the UPDRS-III (16) scores given by an experienced specialist after taking levodopa, including the medication-on and medication-off states. These PD patients took different doses of levodopa, according to a widely used guidance (18) for each patient. None of them have taken other medicines. Details of the demographic information can be found in **Table 1**. All participants signed the informed consent form before the experiment. This research was approved by the Ethics Committee of Tsinghua University Yuquan Hospital.

MR IMAGE ACQUISITION

All data were collected on a 3T Philips Achieva MRI scanner (Philips Healthcare, Best, The Netherlands) with a

32-channel head coil. Head motion was controlled by fixing the head during scanning. Resting-state blood-oxygenation-level dependent (BOLD) signals were collected with following imaging parameters: 35 axial slices; repetition time (TR) = 2,000 ms; echo time (TE) = 30 ms; flip angle (FA) =90°; slice thickness =4.0 mm; slice gap =0.8 mm; acquisition matrix = 64 × 64; field of view = 224 × 224 mm^2. All the PD patients have only experienced one rs-fMRI scan, which was carried out before taking levodopa. During the scan, the participants were instructed to keep their eyes closed, relax their minds, and remain as motionless as possible but not to fall asleep. The rs-fMRI scan with 240 dynamic scans lasted for 8 min. High-resolution T1-weighted structural images in coronal view were acquired with slice thickness of 1 mm without slice gap. Other sequence parameters were: TR/TE = 7.64/3.73 ms, FOV = 256 × 256 mm^2 (acquisition matrix = 256 × 256 × 160).

Data Processing and Network Analysis

The pre-processing of rs-fMRI data was conducted using the SPM12 (http://www.fil.ion.ucl.ac.uk/spm) and GRETNA (19) software. The first four scans were discarded to allow for magnetization equilibration. Four subjects with the mean frame-wise displacement value exceeding the maximum displacement of 1 mm were excluded from either the above demographic information or subsequent data analysis. Data were realigned to the first volume to correct for head movement. A 0.01–0.10 Hz band-pass was used to reduce the effects of low frequency drift and high-frequency physiological noises. The nuisance signal regression (24-parameter head motion profiles, global signal, CSF signal, and WM signal) was performed. Data were spatially smoothed with a 4 mm full-width at half-maximum Gaussian kernel. In order to perform group analysis, the first scan of fMRI time series was co-registered to the same participant's T1-weighted images. The transformed T1 structural images were normalized to the Montreal Neurological Institute (MNI) template space, using the voxel size of 3 × 3 × 3 mm^3.

The flowchart of the subsequent data processing is shown in **Figure 1**. The GRETNA software was used to construct the whole-brain networks for each sliding-window (19). The human Brainnetome Atlas (http://atlas.brainnetome.org/) was applied to obtain 246 brain regions (i.e., nodes, with 123 in each hemisphere), including 210 cortical and 36 subcortical regions (20). The sliding-window approach was used to explore the time-varying changes of FC. The window was slided by 2 s along the 240 dyanmic scans (480 s). We chose the window size of 50 time points for the trade-off between the accuracy of capturing state transitions accurately and the number of overall state transitions (21), resulting in 191 consecutive windows across the entire scan. For each sliding window for a participant, the nodal efficiency was computed, resulting in a 191 nodal efficiency curve. For each patient, the dnE matrix (246 × 246) were calculated by computing the inter-node pearson correlation of the 191-time-point dynamic efficiency curve. The value of each element in the dynamic nodeal efficiency matrix ranges between −1 and 1.

Prediction Model

The least absolute shrinkage and selection operator (LASSO) method (14) was performed to select the features and build the model.

The least absolute shrinkage and selection operator (LASSO) is a regression analysis method that performs both variable selection and regularization in order to enhance the prediction accuracy and interpretability of the statistical model it produces. The object function is as below:

$$\min_{\beta} \|\mathbf{y} - \mathbf{x}\boldsymbol{\beta}\|_2^2 + \frac{1}{2}\lambda \|\boldsymbol{\beta}\|_1$$

where **x** denotes the dnE matrix and **y** donates the actual UPDRS-III scores. The objective of the whole regression process is to solve the matrix $\boldsymbol{\beta}$ by minimizing the loss function. This L1-norm regularization typically sets most coefficients to zero and retains one random feature among the correlated ones, the selection of parameter λ is a trade-off between the prediction error and L1-norm regularization we used $\lambda = 0.08$ in this study.

The prediction model was chosen to depict the correlation between the connectome-based feature and the UPDRS-III score. Considering the size of the dataset, it is not convincing if we only use part of the training-validate-test dataset. Therefore, the Leave-One-Out-Cross-Validation (LOOCV) was used to maximize the loss function (22, 23). In LOOCV, N-1 (N is number of subjects, $N = 62$) samples were used as training data and the remaining samples were used as validation data. The left subjects were used as the input to the training model which was derived with inner training data, generating the estimated UPDRS-III scores. This loop was repeated N times to test all subjects. Each time, the predicted UPDRS-III scores for the left-one-out subjects, the identified FCs, and their corresponding weights in the training model were obtained. By pulling all testing subjects across N loops together, we obtained the prediction results for all subjects. Thus, there were N regression models of the same type with the same parameters for learning and predicting different data. The prediction performance was assessed by the Pearson correlation (with Bonferroni correction) between the model predicted UPDRS-III scores and the actual scores. Permutation test (1,000 times) was carried out to access the significance (24). Mean Absolute Error (MAE) were used to measure the magnitude of the error between the predicted and the actual UPDRS-III scores.

FEATURE IDENTIFICATION

Since we applied a cross-validation strategy to estimate the UPDRS-III scores, in each iteration, slightly different connections were selected. The relative weights for all selected connections were determined by averaging the regression weights of all loops. For better interpretation and visualization (14, 15), we grouped the 246 FC nodes into 24 relatively large brain regions defined by the Brainnetome atlas (20), and estimated the inter-region contributing power by averaging the weights of all FCs connecting between two specific macroscale regions.

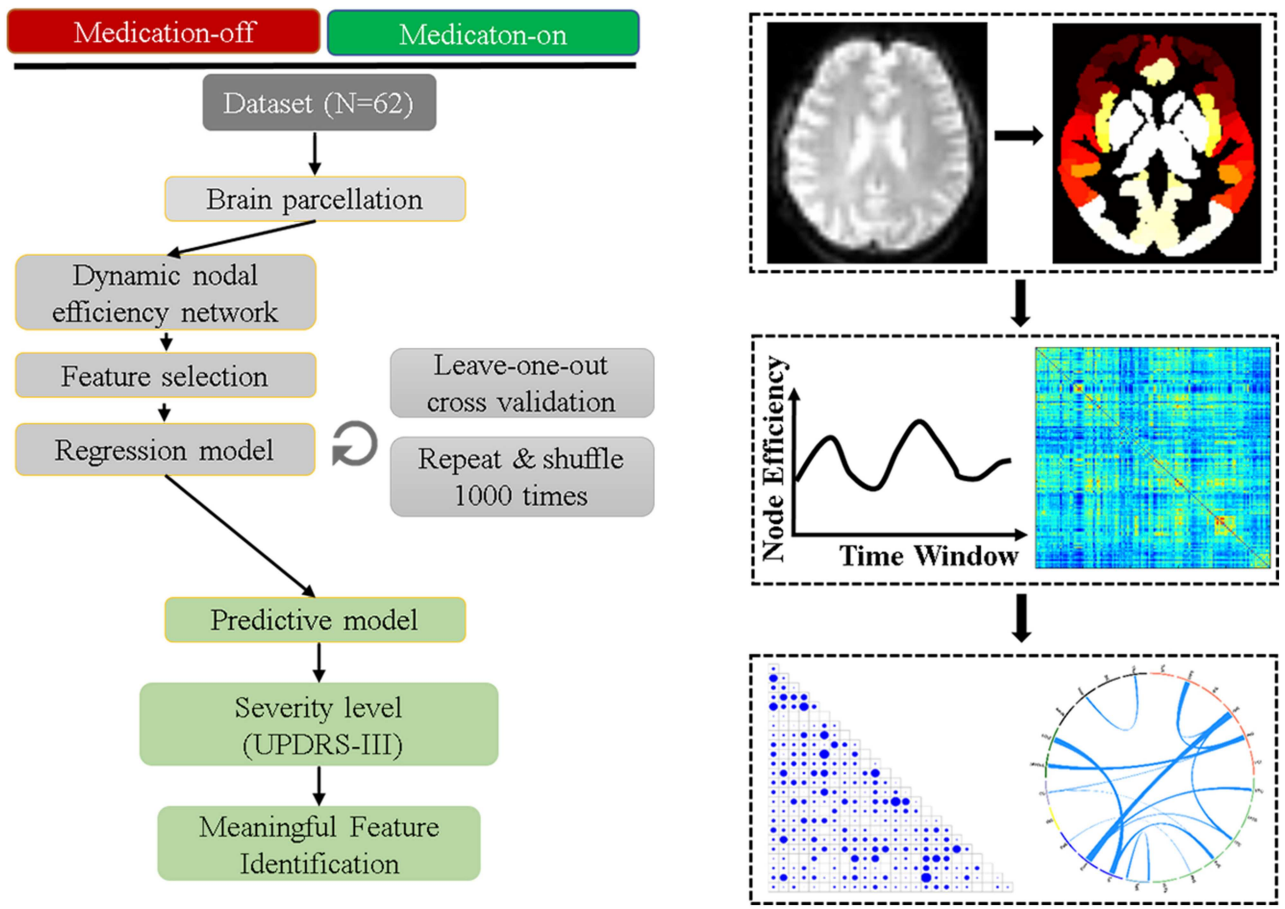

FIGURE 1 | The prediction and validation flowchart incorporating feature selection and regression analysis. **(A)** shows the detailed steps of the data preprocessing including parcellation, efficiency network computing, feature selection, regression model, and the final feature verification. **(B)** is the related information from the image preprocessing to feature identified.

RESULTS

Clinical Data

Firstly, we compared the UPDRS-III scores before and after levodopa therapy ("medication-off" and "medication-on," respectively). The paired t-test shows significant difference ($p < 0.0001$) of the UPDRS-III scores between medication-off (44.1 $\pm$ 12.0) and -on (22.2 $\pm$ 11.8), which demonstrates the efficacy of levodopa.

Feature Selection for Medication-off and Medication-on

The mean contributing weights of whole-brain dnE network are shown in **Figure 2**. For the medication-off status, MedioVentral Occipital Cortex (MVOcC), are the important regions. For the medication-on status, the important regions are frontal regions including the Inferior Frontal Gyrus (IFG), Middle Frontal Gyrus (MFG), Superior Frontal Gyrus (SFG) and Orbital Gyrus (OrG).

Prediction Performance

The dnE network based prediction models achieved significant correlation between the predicted and the true UPDRS-III scores of either medication-off or -on for the 62 PD patients (**Figure 3**). Specifically, Pearson correlation of $r = 0.54$ ($p = 4.56 \times 10^{-6}$, MAE = 9.49) and $r = 0.65$ ($p = 8.06 \times 10^{-9}$, MAE = 7.52) were obtained for medication-off and –on, respectively. All the results passed Bonferroni corrections for the multiple comparisons. The p-value of the permutation test is 0.004 and 0.001 for medication-off and –on, respectively.

Connections Identified

The relative weights of dnE network connecting between each pair of the 24 anatomically defined macro-scale areas are displayed in **Figure 4**. The identified features in the dnE network of either medication-off or -on include the negative connections (blue) and positive connections (red). The width of the inter-node lines represents the strength of the connections. For the negative connections, stronger connectivity reflects

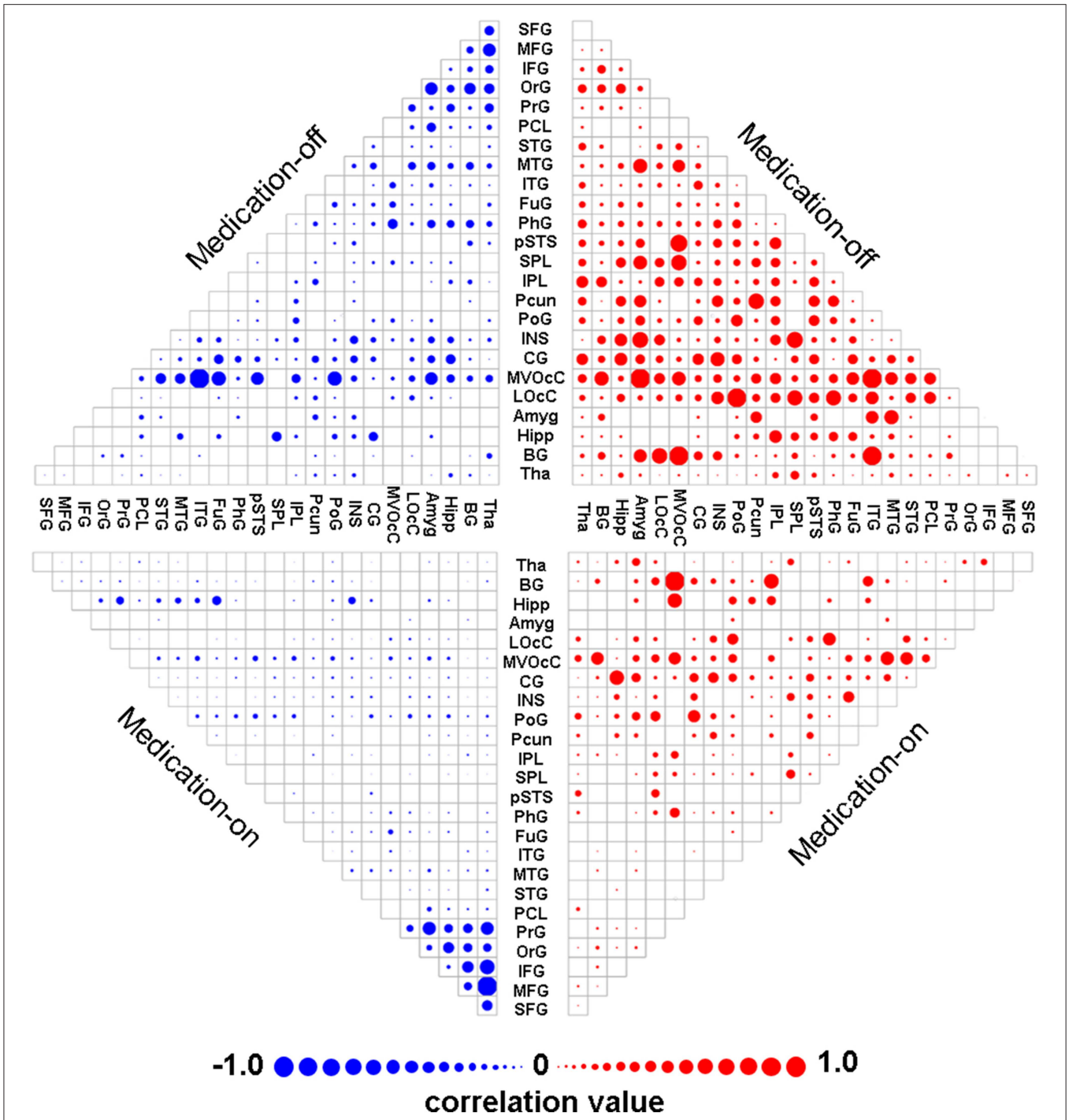

FIGURE 2 | Mean weights distribution of whole-brain dnE network for each of the two states including medication-off and medication-on. The mean contributing weights of whole-brain dnE network connections for medication-off and medication-on were calculated by computing the correlation between connections of each macro-scale with the traits of UPDRS-III. Blue represents negative correlation and red represents positive correlation. As shown in the matrix plot, the 246 FC nodes are grouped into 24 macro-scale brain regions that are anatomically defined by the Brainnetome atlas. For the matrix plots, rows and columns represent predefined macro-scale regions in the Brainnetome Atlas, and a bigger circle represents a higher predictive weight. Names of 24 macroscale regions were colored according to their lobe locations. dnE, dynamic nodal efficiency.

lower disease severity thus better recovery after drug therapy. The positive connection case reflects the contrary. Specifically, for medication-off, dnE network connections show more contributing power between Middle Temporal Gyrus (MTG) and STG, Postcentral Gyrus (PoG) and Superior Parietal Lobule (25). The stronger the connections, the better the recovery of PD.

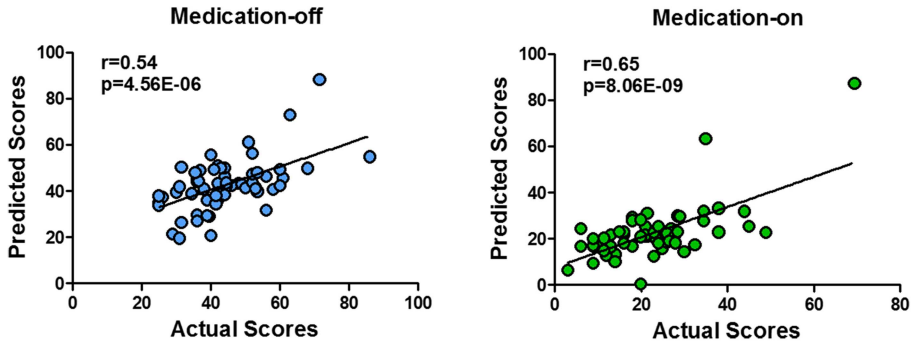

FIGURE 3 | Scatter plot of the predicted four states of the UPDRS-III scores with respect to their true values based on the prediction framework using whole-brain dnE network. With the connectome-based prediction framework, Pearson's correlation of $r = 0.54$ ($p = 4.56 \times 10^{-6}$) and $r = 0.65$ ($p = 8.06 \times 10^{-9}$) were achieved for medication-off and medication-on, respectively, in the nested cross-validation using whole-brain dynamic nodal efficiency network. The abbreviations of the brain areas are from the Brainnetome atlas (http://atlas.brainnetome.org/) (20).

There is a negative correlation between the strength of some connections and the UPDRS-III scores, such as the connections between Precuneus (Pcun) and Orbital Gyrus (OrG), Inferior Parietal Lobule (IPL), and lateral Occipital Cortex (LOcC), IPL, and Fusiform Gyrus (FuG). The stronger the connections, the worse the recovery of PD.

For medication-on, in terms of the feature analysis of predicting recovery effect after the drug therapy, the contributing power is mainly concentrated on hippocampus (Hipp), PoG, Pcun, Cingulate Gyrus (CG), Insular Gyrus (INS), and OrG. Particularly, the features of the connections between Hipp and CG, INS, Pcun, OrG, respectively, have much influence on the recovery after therapy. The stronger the connections, the better the recovery. For other regions, such as MFG and MTG, the stronger the connection between MFG and Inferior Temporal Gyrus (ITG) or the connection between MTG and SPL, the worse the recovery of PD. The prediction efficacy of each region is shown in **Figure 4C**. The results are from the regression model and are normalized to the range of 0 to 1.

DISCUSSION

Through analyzing the efficiency of correlation networks using rs-fMRI, the present study investigated the important features of connections that are correlated to the post-therapy disease severity (UPDRS-III scores) after taking levodopa in the 62 PD patients. Studying the effect of drug therapy is an important topic in PD research. Finding what influences the effect of drug therapy is of great significance. This work predicted the correlation between the dnE network and the actual effect of drug therapy by training a regression model. The major findings of the present study are as follows: (1) The connection efficiency of networks based on rs-fMRI can effectively depict the severity of PD (UPDRS-III scores), and further predict the recovery effect after drug therapy. (2) The Hipp region is an important area that indicates drug therapy effect in the dnE network. (3) Increased cortical functional connectivity from ITG and MTG has a negative effect on the recovery. As such, these findings provide new evidence that the rs-fMRI network connectivity strengthening or weakening within key functional networks in dnE network plays an important pathophysiological role in the recovery of PD patients.

The FC analysis of the brain network has revealed that the brain is organized according to a highly efficient small-world topology, combining a high level of segregation (local efficiency) with a high level of global integration (global efficiency) (26). Most of the previous studies did not consider the important dynamic properties of FC, as functional connectivity was assumed to be constant during rs-fMRI scanning. However, dynamic FC may yield novel insights into brain function and dysfunction (8). The sliding window approach is commonly used for examining dynamics in resting-state FC, resulting in quantification of the time-varying behavior of a chosen metric. In this study, we selected the nodal global efficiency (i.e., nodal efficiency) as the metric, then obtained the time-varying behavior of each nodal global efficiency. Global efficiency is a network attribute that quantifies how easily information can be exchanged over the network. It provides information on the communication efficiency of a network as a whole, with higher values indicating more efficient information transmission through the whole brain. We further calculated the inter-node correlation of the dnE, to further reveal the synchronization of the dynamic property of FC between two regions.

The prediction model analyses demonstrated that some specific subnetworks with decreased connectivity are correlated with the recovery effect after drug therapy. The regions mainly include parietal lobe, insular lobe, limbic lobe, and Hipp. The connections between these regions are directly positively correlated to the recovery after drug therapy: the stronger the connections, the better the recovery (lower UPDRS-III scores). Nonetheless, there are several key pathways in the SPL, ITG, MFG, MTG showed negative influence on the recovery of PD.

Previous studies showed that the decreased functional connectivity of the temporal cortex is related to the disease progression of PD (27, 28). We drew the similar conclusion here, especially for the connection between MTG and STG. In addition, we found that a distributed set of regions in the

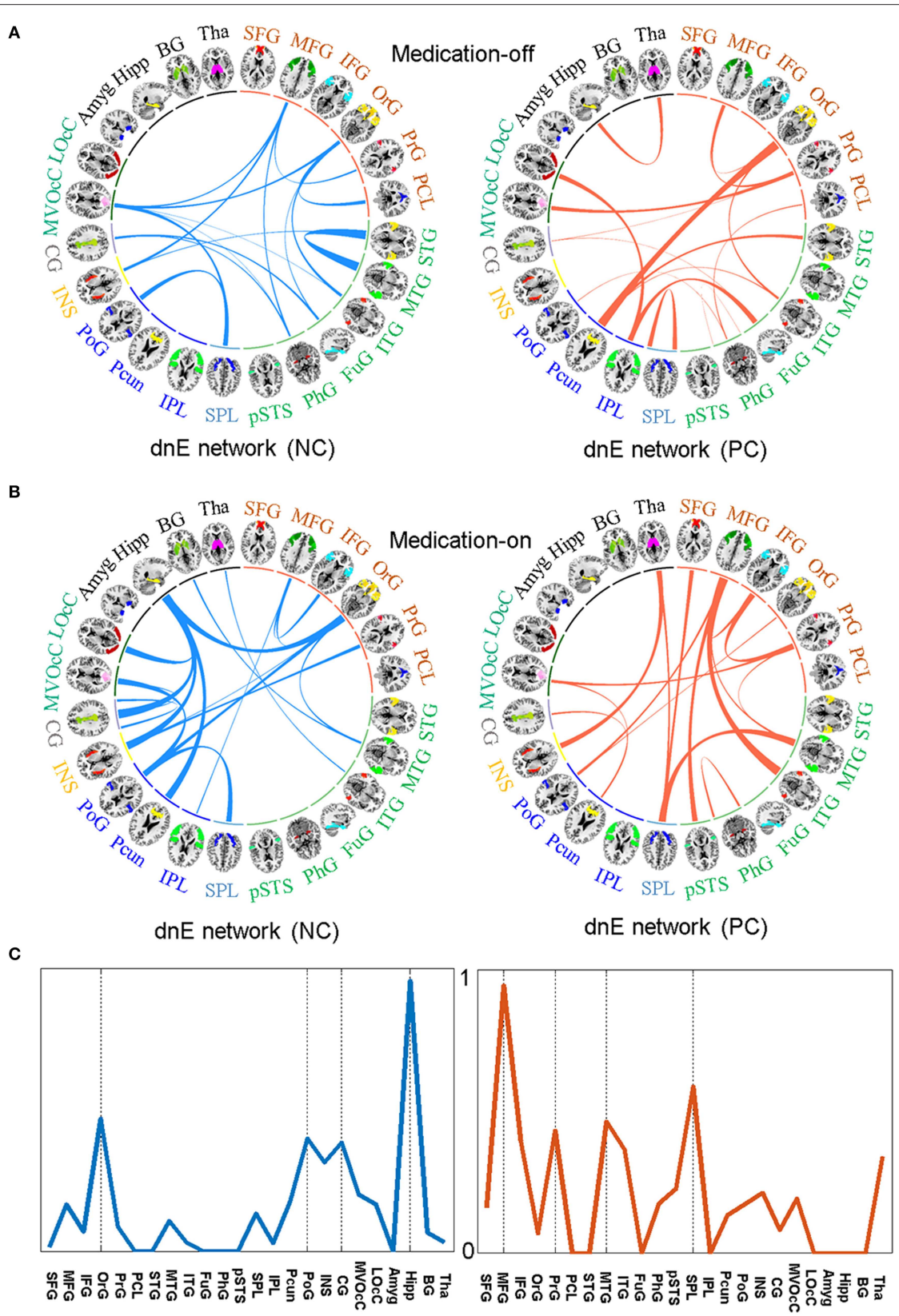

FIGURE 4 | Continued

FIGURE 4 | The identified features in the dnE network between medication-off **(A)** and medication-on **(B)**, respectively, including the negative connections (NC) represented by blue and the positive connections (PC) represented by red, respectively. The width of the inter-node lines represents the strength of connections. For the negative connections, stronger connectivity reflects smaller disease severity and better recovery after drug therapy. The positive connection case is on the contrary. The prediction efficacy of each node for medication-on is shown in **(C)**. The results are from the regression model and are normalized to the range of 0 to 1. As shown in the circle plots, the 246 FC nodes (inner circle) are grouped into 24 macro-scale brain regions (outer brain representations) that are anatomically defined by the Brainnetome atlas. Specifically, nodes incorporated in each of 24 macro-scale brain areas are plotted with different colors, which delineate their corresponding anatomy locations in the outer brain representations.

frontal lobe, temporal lobe, occipital lobe, and parietal lobe showed decreased inter-node correlation of dnE in these patients. The decreased correlation is related to the high post-therapy UPDRS-III scores of PD patients. It reveals that these regions are also related to the disease progression of PD. Among these important connections exist, such as the connection between the paracentral cortex and OrG. Some other studies have also reported that connections among these regions is related to cognitive decline (29).

This study shows that the Hipp region, which was previously reported to influence dementia (30), is also an important area to indicate drug therapy effect. Previous study also shows that there is a high correlation between PD and dementia, i.e., PD with dementia (31). This study reveals that individualized recovery effect after drug therapy can be influenced by the functional connections between Hipp and other areas, on which enough attention should be paid before therapy.

The selected features (**Figure 2**) are not necessarily useful for the following prediction. For example, the frontal area appears to be important in the feature selection, but the Hipp area is the dominant feature for prediction. Therefore, how to improve feature selection needs to be further studied. Reducing feature dimension while maintaining all of the connection information might need to be carefully considered.

There are several limitations of this study. First, the number of subjects was relatively small to draw firm conclusions. Second, the dynamic property of FC we investigated in this study is only the commonly used global efficiency. It should be noted that choosing the global efficiency does not mean less importance of other network properties. Other dynamic properties, such as local efficiency, may provide additional information and are worthwhile to be further investigated in future studies. Third, the long-term follow-up study should be carried out in the future to follow the outcome of patients.

CONCLUSION

In this study we studied a sample of 62 PD patients and calculated the dnE based on rs-fMRI. With connectome-based predictive models using LASSO, we demonstrated that the dnE properties can successfully predict the post-therapy severity level of PD patients after taking levodopa. The contributed regions for the prediction include hippocampus, post-central gyrus, cingulate gyrus, and orbital gyrus. Specifically, the connections between hippocampus and cingulate gyrus, hippocampus and insular gyrus, insular gyrus and orbital gyrus are positively related to the recovery after drug therapy. The analysis of these connectivity features can provide guidance information for clinical therapy in PD patients.

ETHICS STATEMENT

This study was carried out in accordance with The Nuremberg Code, World Medical Association Declaration of Helsinki and International Ethical Guidelines for Biomedical, Ethics Committee of Tsinghua University Yuquan Hospital. Research Involving Human Subjects, and with written informed consent from all subjects. All subjects gave written informed consent in accordance with the Declaration of Helsinki. The protocol was approved by the Ethics Committee of Tsinghua University Yuquan Hospital.

AUTHOR CONTRIBUTIONS

XL contributed to the experiments, data analysis, and writing of the manuscript. YX and SL contributed to performing the experiments and revising the manuscript. RZ and LH contributed to the data collection. ZH and YT revised the manuscript. ZN contributed to the manuscript revision. YM and HG are the guarantors of this study and had complete access to all data in the study. All authors are accountable for the contents of this research.

FUNDING

This work was supported by the Beijing Institute of Technology Research Fund Program for Young Scholars and the National Natural Science Foundation of China (Grant No. 61801026).

REFERENCES

1. Jankovic J. Parkinson's disease: clinical features and diagnosis. *J Neurol Neurosurg Psychiatry*. (2008) 79:368–76. doi: 10.1136/jnnp.2007.131045
2. Khoo TK, Yarnall AJ, Duncan GW, Coleman S, O'brien JT, Brooks DJ, et al. The spectrum of nonmotor symptoms in early Parkinson disease. *Neurology*. (2013) 80:276–81. doi: 10.1212/WNL.0b013e31827deb74
3. Brooks DJ, Pavese N. Imaging biomarkers in Parkinson's disease. *Progr Neurobiol*. (2011) 95:614–28. doi: 10.1016/j.pneurobio.2011.08.009
4. Luo C, Song W, Chen Q, Zheng Z, Chen K, Cao B, et al. Reduced functional connectivity in early-stage drug-naive Parkinson's disease: a resting-state fMRI study. *Neurobiol Aging*. (2014) 35:431–41. doi: 10.1016/j.neurobiolaging.2013.08.018

5. Ziegler E, Rouillard M, Andre E, Coolen T, Stender J, Balteau E, et al. Mapping track density changes in nigrostriatal and extranigral pathways in Parkinson's disease. *Neuroimage*. (2014) 99:498–508. doi: 10.1016/j.neuroimage.2014.06.033
6. Dubbelink KTEO, Hillebrand A, Stoffers D, Deijen JB, Twisk JWR, Stam CJ, et al. Disrupted brain network topology in Parkinson's disease: a longitudinal magnetoencephalography study. *Brain*. (2014) 137:197–207. doi: 10.1093/brain/awt316
7. Putcha D, Ross RS, Cronin-Golomb A, Janes AC, Stern CE. Altered intrinsic functional coupling between core neurocognitive networks in Parkinson's disease. *Neuroim Clin*. (2015) 7:449–55. doi: 10.1016/j.nicl.2015.01.012
8. Kim J, Criaud M, Cho SS, Diez-Cirarda M, Mihaescu A, Coakeley S, et al. Abnormal intrinsic brain functional network dynamics in Parkinson's disease. *Brain*. (2017) 140:2955–67. doi: 10.1093/brain/awx233
9. Skidmore F, Korenkevych D, Liu Y, He G, Bullmore E, Pardalos PM. Connectivity brain networks based on wavelet correlation analysis in Parkinson fMRI data. *Neurosci Lett*. (2011) 499:47–51. doi: 10.1016/j.neulet.2011.05.030
10. Wei L, Zhang J, Long Z, Wu GR, Hu X, Zhang Y, et al. Reduced topological efficiency in cortical-basal Ganglia motor network of Parkinson's disease: a resting state fMRI study. *PLoS ONE*. (2014) 9:e108124. doi: 10.1371/journal.pone.0108124
11. Yu QB, Erhardt EB, Sui J, Du YH, He H, Hjelm D, et al. Assessing dynamic brain graphs of time-varying connectivity in fMRI data: application to healthy controls and patients with schizophrenia. *Neuroimage*. (2015) 107:345–55. doi: 10.1016/j.neuroimage.2014.12.020
12. Shen X, Finn ES, Scheinost D, Rosenberg MD, Chun MM, Papademetris X, et al. Using connectome-based predictive modeling to predict individual behavior from brain connectivity. *Nat Protoc*. (2017) 12:506–18. doi: 10.1038/nprot.2016.178
13. Cui Z, Gong G. The effect of machine learning regression algorithms and sample size on individualized behavioral prediction with functional connectivity features. *Neuroimage*. (2018) 178:622–37. doi: 10.1016/j.neuroimage.2018.06.001
14. Jiang R, Calhoun VD, Zuo N, Lin D, Li J, Fan L, et al. Connectome-based individualized prediction of temperament trait scores. *Neuroimage*. (2018) 183:366–74. doi: 10.1016/j.neuroimage.2018.08.038
15. Rosenberg MD, Finn ES, Scheinost D, Papademetris X, Shen X, Constable RT, et al. A neuromarker of sustained attention from whole-brain functional connectivity. *Nat Neurosci*. (2016) 19:165–71. doi: 10.1038/nn.4179
16. Goetz CG, Tilley BC, Shaftman SR, Stebbins GT, Fahn S, Martinez-Martin P, et al. Movement disorder society-sponsored revision of the unified Parkinson's disease rating scale (MDS-UPDRS): scale presentation and clinimetric testing results. *Mov Disord*. (2008) 23:2129–70. doi: 10.1002/mds.22340
17. Defer GL, Widner H, Marie RM, Remy P, Levivier M. Core assessment program for surgical interventional therapies in Parkinson's disease (CAPSIT-PD). *Mov Disord*. (1999) 14:572–84.
18. Tomlinson CL, Stowe R, Patel S, Rick C, Gray R, Clarke CE. Systematic review of levodopa dose equivalency reporting in Parkinson's disease. *Mov Disord*. (2010) 25:2649–53. doi: 10.1002/mds.23429
19. Wang J, Wang X, Xia M, Liao X, Evans A, He Y. GRETNA: a graph theoretical network analysis toolbox for imaging connectomics. *Front Hum Neurosci*. (2015) 9:386. doi: 10.3389/fnhum.2015.00458
20. Fan L, Li H, Zhuo J, Zhang Y, Wang J, Chen L, et al. The human brainnetome atlas: a new brain atlas based on connectional architecture. *Cereb Cortex*. (2016) 26:3508–26. doi: 10.1093/cercor/bhw157
21. Shakil S, Lee CH, Keilholz SD. Evaluation of sliding window correlation performance for characterizing dynamic functional connectivity and brain states. *Neuroimage*. (2016) 133:111–28. doi: 10.1016/j.neuroimage.2016.02.074
22. Kohavi R. A study of cross-validation and bootstrap for accuracy estimation and model selection. In: *International Joint Conference on Artificial Intelligence*. Montreal, QC (1995). p. 1137–43.
23. Cui Z, Xia Z, Su M, Shu H, Gong G. Disrupted white matter connectivity underlying developmental dyslexia: a machine learning approach. *Hum Brain Mapp*. (2016) 37:1443–58. doi: 10.1002/hbm.23112
24. Cui Z, Su M, Li L, Shu H, Gong G. Individualized prediction of reading comprehension ability using gray matter volume. *Cereb Cortex*. (2018) 28:1656–72. doi: 10.1093/cercor/bhx061
25. Parnanzone S, Serrone D, Rossetti MC, D'onofrio S, Splendiani A, Micelli V, et al. Alterations of cerebral white matter structure in psychosis and their clinical correlations: a systematic review of Diffusion Tensor Imaging studies. *Riv Psichiatr*. (2017) 52, 49–66. doi: 10.1708/2679.27441
26. Achard S, Bullmore E. Efficiency and cost of economical brain functional networks. *PLoS Comput Biol*. (2007) 3:e17. doi: 10.1371/journal.pcbi.0030017
27. Dubbelink KTEO, Stoffers D, Deijen JB, Twisk JWR, Stam CJ, Hillebrand A, et al. Resting-state functional connectivity as a marker of disease progression in Parkinson's disease: a longitudinal MEG study. *Neuroim Clin*. (2013) 2:612–9. doi: 10.1016/j.nicl.2013.04.003
28. Suo X, Lei D, Li N, Cheng L, Chen F, Wang M, et al. Functional brain connectome and its relation to hoehn and yahr stage in Parkinson disease. *Radiology*. (2017) 285:904–13. doi: 10.1148/radiol.2017162929
29. Eidelberg D, Moeller JR, Dhawan V, Spetsieris P, Takikawa S, Ishikawa T, et al. The metabolic topography of Parkinsonism. *J Cereb Blood Flow Metab*. (1994) 14:783–801. doi: 10.1038/jcbfm.1994.99
30. Aarsland D, Creese B, Politis M, Chaudhuri KR, Ffytche DH, Weintraub D, et al. Cognitive decline in Parkinson disease. *Nat Rev Neurol*. (2017) 13:217–31. doi: 10.1038/nrneurol.2017.27
31. Shi M, Huber BR, Zhang J. Biomarkers for cognitive impairment in Parkinson disease. *Brain Pathol*. (2010) 20:660–71. doi: 10.1111/j.1750-3639.2009.00370.x

Conflict of Interest Statement: The authors declare that the research was conducted in the absence of any commercial or financial relationships that could be construed as a potential conflict of interest.

frontiers in Psychiatry

ORIGINAL RESEARCH
published: 12 July 2019
doi: 10.3389/fpsyt.2019.00484

Increased Temporal Dynamics of Intrinsic Brain Activity in Sensory and Perceptual Network of Schizophrenia

Youxue Zhang[1], Gang Guo[1] and Yuan Tian[2]*

[1] School of Psychology, Chengdu Normal University, Chengdu, China, [2] School of Foreign Languages, Chengdu Normal University, Chengdu, China

Schizophrenic subject is thought as a self-disorder patient related with abnormal brain functional network. It has been hypothesized that self-disorder is associated with the deficient functional integration of multisensory body signals in schizophrenic subjects. To further verify this assumption, 53 chronic schizophrenic subjects and 67 healthy subjects were included in this study and underwent resting-state functional magnetic resonance imaging. The data-driven methods, whole-brain temporal variability of fractional amplitude of low-frequency fluctuations and regional homogeneity (ReHo), were used to investigate dynamic local functional connectivity and dynamic local functional activity changes in schizophrenic subjects. Patients with schizophrenia exhibited increased temporal variability ReHo and fractional amplitude of low-frequency fluctuations across time windows within sensory and perception network (such as occipital gyrus, precentral and postcentral gyri, superior temporal gyrus, and thalamus). Critically, the increased dynamic ReHo of thalamus is significantly correlated with positive and total symptom of schizophrenic subjects. Our findings revealed that deficit in sensory and perception functional networks might contribute to neural physiopathology of self-disorder in schizophrenic subjects.

Keywords: schizophrenia, functional connectivity, temporal variability, self-disorder, sensory and perceptual network

OPEN ACCESS

Edited by:
Zaixu Cui,
University of Pennsylvania, United States

Reviewed by:
Jin Liu,
Beijing Normal University, China
Nan Zhang,
University of Science and Technology of China, China

****Correspondence:***
Youxue Zhang
yx_zhang06@163.com

Specialty section:
This article was submitted to Neuroimaging and Stimulation, a section of the journal Frontiers in Psychiatry

Received: *02 December 2018*
Accepted: *19 June 2019*
Published: *12 July 2019*

Citation:
Zhang Y, Guo G and Tian Y (2019) Increased Temporal Dynamics of Intrinsic Brain Activity in Sensory and Perceptual Network of Schizophrenia. Front. Psychiatry 10:484. doi: 10.3389/fpsyt.2019.00484

INTRODUCTION

About 1% of the whole adult population suffer from schizophrenia, which is one of the costliest mental disorders. Schizophrenic subject is typically considered as a self-disorder (1). Self-disorder could be associated with several positive symptoms. The major point of schizophrenic subjects' positive symptom is unable to efficiently distinguish self and others. This symptom would lead to a worse deficit that the schizophrenic patients could not confirm their actions and thoughts are related to external information or stimulation. Importantly, in schizophrenia, the symptoms related to self-disorder have been considered a crucial factor to identify whether the psychiatric patient is schizophrenic or not (2).

There are many neuroimaging studies that have been employed in investigating the neuropathological mechanism of schizophrenia (3–5). Although many functional connectivity studies of schizophrenia focused on the abnormal long-range functional connectivity among spatially distributed brain regions (6, 7), few studies paid attention on local functional information of blood oxygen level dependence and functional interaction between spatially adjacent regions (8, 9). Thus, to quantify local or short-range functional connectivity in human brain, several measures were commonly employed in neuroimaging

studies, including regional homogeneity (ReHo) (10), local power of blood oxygen level dependence [low-frequency fluctuations (fALFF)] (11), and functional connectivity strength (12) derived from resting-state functional magnetic resonance imaging (fMRI). Several studies have reported that there are significant relationships between static ReHo/fALFF and several factors, such as age, gender, and intelligence in healthy subjects (13, 14). These findings have revealed that the static local neural activity and short-range functional connectivity have been linked with the physiological and psychological factors in human brain.

In schizophrenia, multi-site resting-state fMRI study has shown that schizophrenic subjects exhibited decreased static fALFF in cuneus, middle temporal gyrus, and posterior cingulate cortex compared with healthy subjects (15). Guo et al. has also found that the schizophrenic patients showed both decreased static fALFF in the posterior cingulate cortex and decreased gray matter volume in medial prefrontal cortex, indicating that the changes of brain function and anatomy within default model network might contribute separately to the pathophysiology of schizophrenia (16). Besides, recent studies have indicated that schizophrenic patients have shown reduced static functional connectivity density in primary sensory network of schizophrenia and decreased static ReHo in visual and sensorimotor networks compared with healthy controls (17). Furthermore, the symptomatology (e.g., auditory hallucinations) in schizophrenia has been proved to be related to abnormal multisensory static functional connectivity (18). In conclusion, the deficit static functional connectivity of sensory and perceptual systems may potentially contribute to physiopathology of schizophrenia. While these studies have implicitly revealed that functional connectivity is a stable characteristic across the entire resting scan period, recent studies have indicated that functional connectivity is not stationary and changes over time (19, 20).

Assessing brain dynamic functional connectivity from resting-state fMRI has advanced our knowledge of the brain (21). Specifically, a recent neuroimaging study has stated that functional connectivity variability seems to be a reliable feature, partly dependent on functional relationships among distributed brain regions (22). Dynamic functional connectivity analysis could provide a novel method to sensitively capture the abnormal functional connectivity related with psychiatric disorders (23–26). The results of dynamic functional connectivity analyses also revealed transient states of dysconnectivity in schizophrenia (27, 28), which support and expand current knowledge regarding dysconnectivity in schizophrenia. Moreover, a recent study demonstrated that the feature of dynamic functional connectivity significantly outperforms the static connectivity in classification analysis (29). These findings reveal that static functional analysis may obscure important dynamic features of network behavior.

During recent years, few studies have focused on altered local temporal variability of functional activity or short-range functional connectivity in schizophrenia, which could reveal information that is not from static functional connectivity (30). Thus, we sought to determine whether altered temporal variability of regional neural activity was associated with symptom of schizophrenia in this study. The dynamic neural activity analysis used in this study includes dynamic ReHo and fALFF, which allow us to identify voxel-level dynamic functional alterations in schizophrenia compared with healthy subjects. On the basis of previous results about abnormal static functional connectivity in primary motor and perception networks, we hypothesize that abnormal dynamic neural activity in schizophrenia would locate in primary perceptual systems, such as primary sensory-motor cortex and related visual and thalamus regions. In addition, schizophrenic subjects are expected to show significant association between altered variability of these network and symptom of schizophrenic subjects.

MATERIALS AND METHODS

Subjects Selection and Schizophrenic Patients' Clinical Symptoms

Fifty-three chronic schizophrenic subjects and 67 healthy controls are included in this study. Related resting-state fMRI data are collected from the Center for Biomedical Research Excellence. The patients with schizophrenia are diagnosed according to Diagnostic and Statistical Manual of Mental Disorders, 4th Edition, diagnostic. The psychiatric symptom severity is measured using positive and negative syndrome scale (PANSS) assessment. Healthy subjects are also recruited, those who do not have schizophrenia and not exhibiting Axis I symptoms. These research procedures were in accordance with institutional review boards of the USA. Written informed consent was obtained from each subject before the study. Details of demographic characteristics of both groups are shown in **Table 1**.

Data Acquisition and Image Preprocessing

Functional imaging scan was performed on a 3T MRI scanner (Siemens Trio). Resting-state functional image are collected with single-shot full k-space echo-planar imaging (EPI) (repetition time = 2,000 ms, echo time = 29 ms, number of slices = 32, slice thickness = 3 mm, matrix size: 64 × 64, flip angle = 7°, field of view = 256 × 256 mm^2). Subjects underwent 6-min scan. A total of 180 volumes of EPI images were obtained.

The preprocessing steps of functional image were performed using commonly processing steps [Data Processing and Analysis

TABLE 1 | Dataset (The Center for Biomedical Research Excellence, chronic).

	Patients with Schizophrenia	Healthy controls	*p*
Sample size	53	67	–
Gender (Male/Female)	42/11	46/21	0.192[a]
Age (years)	36.75 ± 13.67	34.82 ± 11.28	0.398[b]
Education level (years)	13.20 ± 1.82	14.02 ± 1.86	0.024[b]
Handedness (both/right/left)	1/42/10	1/65/1	0.004[a]
FD	0.15 ± 0.07	0.14 ± 0.08	0.433[b]
Disease duration (years)	14.94 ± 4.60	–	–
PANSS-positive score	14.94 ± 4.61	–	–
PANSS-negative score	14.43 ± 5.26	–	–
PANSS-global score	30.07 ± 8.28	–	–

Indicated values are shown as mean ± standard deviation. PANSS, positive and negative symptom scale; FD, Framewise displacement.

[a]*Indicates the p values from the comparison analysis (Chi-square test).*

[b]*Indicates the p values from the comparison analysis (two-sample t-test).*

of Brain Imaging (DPABI) (31), http://rfmri.org/dpabi] and briefly described here. First, temporal and spatial corrections were performed, including slice time and head motion correction, furthermore normalized (voxel size: 3 mm) into EPI template. Any subjects who had a maximum translation in any of the cardinal directions larger than 3 mm or a maximum rotation larger than 3° were excluded from subsequence analysis. Moreover, framewise displacement (FD) was evaluated in two groups as suggested by Power et al. (32). Second, detrending analysis was performed on the normalized data to minimize the effect of linear trend. Third, several nuisance signals were regressed out from functional image through linear regression analysis. The nuisance signals include six motion parameters and their first temporal derivative, white matter and cerebrospinal fluid signals. In this study, the global signal was not removed from the functional image (33, 34).

Temporal Variability Analysis

Two widely used approaches, including ReHo and fALFF, were used to measure voxel-level functional maps (35). We calculated dynamic ReHo and fALFF through sliding window analysis (**Figure 1A**). Based on the "rule of thumb," which is $1/f_{min}$ of data should be equal or less than the length of window (36), the whole-run time series of each voxel was segmented into 50 TR windows and sliding the onset of these windows by one TR. Then, within each window, we calculated ReHo and fALFF at each voxel in whole-brain mask.

In the ReHo analysis, the frequency band passing (0.01–0.08 Hz) was done on fMRI data. Then, Kendall's W value was calculated for each voxel, between the time series of the target voxels and the series of their nearest voxels (26 voxels) in the whole-brain mask (10). In the fALFF analysis, fALFF is defined as the percentage of the power within the low-frequency range (0.01–0.08 Hz) in total power of whole frequency range (0–0.25 Hz) (11).

Across n window, we calculated the coefficient of variation (CV) maps of ReHo and fALFF for each subject. We define the CV of a voxel k as:

$$CV_k = \frac{\sqrt{\sum_{t=1}^{n}\left(x_t - x_{mean}\right)^2 / n}}{x_{mean}}$$

where x_t is ReHo or fALFF score of voxel k over time window t, $t = 1,2,\ldots,n$; x_{mean} is mean score of x_t across time window t. Finally, individual voxel-wise ReHo and fALFF CV maps were

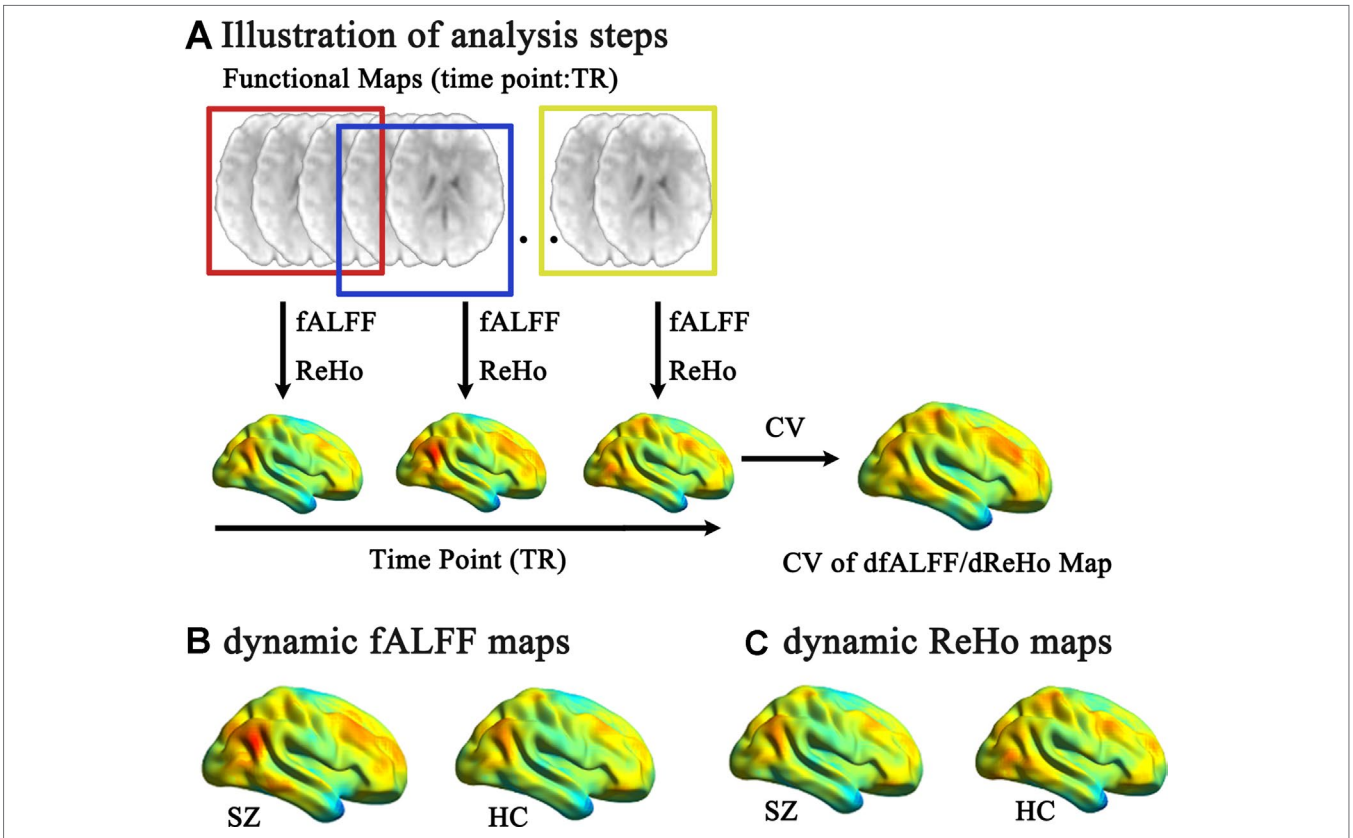

FIGURE 1 | Illustration of analysis steps and temporal variability of dynamic fALFF and ReHo pattern. **(A)** The preprocessed full-length blood oxygen level-dependent fMRI maps were segmented into several sliding windows (50 TR). Within each window, the fALFF and ReHo were computed for each voxel. The sliding window was systematically shifted by one TR, and the corresponding fALFF and ReHo were computed. Then, the temporal variability of the dynamic fALFF and ReHo were defined as the CV maps across the sliding windows. The pattern of temporal variability of the fALFF **(B)** and ReHo **(C)** of the schizophrenic subjects/healthy controls were shown.

standardized by dividing the whole-brain mean values and, furthermore, spatially smoothed (6-mm full width at half maximum of the Gaussian kernel). Then, two-sample t-tests were performed for ReHo and fALFF CV maps, respectively (DPABI, http://rfmri.org/dpabi), between schizophrenic and healthy subjects with age, gender, education level, handedness, and FD as covariates, with a statistical significance level corrected by false discovery rate ($p < 0.05$).

Correlations With Pathological Factors

We assessed the association between the score of clinical score and significant changes of temporal variability in regional functional measurements in patients with schizophrenia. We extract the mean CV score from the peak voxel and its nearest voxels (26 voxels) for each significant cluster. Then, the partial correlation analysis was performed between ReHo and fALFF CV scores and patients' PANSS scores with age, gender, education level, handedness, medication dosage, and FD as covariates ($p < 0.05$).

Validation Analysis

Recent fMRI study has indicated that sliding window-based dynamic functional connectivity could be largely explained by head motion (37). Patient is chronic schizophrenic subjects in this study. The antipsychotic treatment might have an effect on dynamic local neural activity of schizophrenic subjects. Thus, we preformed the validation analysis to investigate the influence of these factors on dynamic temporal variability of regional functional measurements in schizophrenic subjects.

First, spike-regression-based scrubbing was performed to take into account transient head motion (38, 39). We defined the "bad points" with high FD (above 0.5 mm) and their adjacent time points (1 back and 2 forward) for each subject. These "bad points" were modeled as separate regressor in the nuisance regression models in the preprocessing analysis. Then, for new preprocessed fMRI data, we reevaluated the temporal variability of ReHo and fALFF through sliding window analysis. Two-sample t-tests were also performed between two groups with age, gender, education level, handedness, and FD as covariates. Second, to take account of antipsychotic treatment, we calculated the relationship between altered temporal variability of fALFF/ReHo and medication dosage in schizophrenia group by using correlation analysis ($p < 0.05$).

RESULTS

Temporal Variability of fALFF/ReHo Between Schizophrenic and Healthy Groups

Temporal variability of dynamic fALFF and ReHo were shown at each voxel for each subject (**Figures 1B**, **C**) with the BrainNet viewer (http://www.nitrc.org/projects/bnv/) (40). The variability of these dynamic local neural activity displayed a nonuniform spatial distribution across the brain. The lowest variability was located in the limbic system. The largest variability was mainly located in the heteromodal association region, including the temporal–parietal junction, prefrontal and posteromedial cortex. The primary sensory and visual cortices showed a moderate level of variability. Furthermore, using two-sample *t* test, schizophrenic subjects showed increased temporal variability in both dynamic fALFF and ReHo compared with healthy controls (**Table 2**, **Figure 2**) with the DPABI viewer (41). Within temporal variability of fALFF, increased dynamic fALFF were observed in thalamus, super temporal gyrus, precentral/postcentral gyrus, and lingual gyrus in schizophrenic subjects. Similar increased dynamic ReHo were also being found in patients with schizophrenia, including super temporal gyrus, thalamus, postcentral gyrus, middle cingulum cortex, and cuneus. Furthermore, these findings were observed by using spike-regression-based scrubbing procedure (**SFigure 1**).

Correlations With Pathological Factors

We observed positive correlation between PANSS scores and the increased temporal variability of ReHo in schizophrenic subjects: PANSS-positive score and thalamus within basal ganglia network (BGN) ($r = 0.317$, $p = 0.021$, **Figure 3A**) and PANSS-total score and thalamus within BGN ($r = 0.369$, $p = 0.006$, **Figure 3B**). The relationship was observed between PANSS-total score and thalamus within BGN by using spike-regression-based scrubbing procedure (**SFigure 2**). Moreover, no other significant correlations were found between the altered temporal variability of fALFF/ReHo and medication dosage in schizophrenia group.

DISCUSSION

This study has presented some new insights in alterations of dynamic temporal variability of ReHo and fALFF in schizophrenia through sliding window analysis. Consistent with our hypothesis, increased dynamic temporal variability of ReHo and fALFF were observed in sensory and perceptual networks in schizophrenic subjects. Critically, the psychiatric symptom analysis has indicated that increased temporal variability of ReHo showed significantly positive relationship with the positive symptoms of schizophrenic subjects. These findings provide evidence that there is deficient temporal variability of local neural activity in low-level perceptual processing in schizophrenic subjects.

While these are well known about the abnormal higher-order brain function in schizophrenia, such as memory and cognitive (42, 43), neuroimaging studies have also documented some basic sensory processing deficits in schizophrenic subjects. The perceptual deficits have been increasingly observed in the sensory networks, including primary motor and visual regions (44, 45). A recent study has also revealed that schizophrenic subjects has shown increased resting-state functional connectivity variability in sensory and perceptual networks (46). Most of these locations were in line with the meta-analysis' results of schizophrenia (47). Increased variability of local neural activity of sensorimotor regions might reflect the deficits in the integration of multisensory stimuli in schizophrenia (48). Moreover, enhanced dynamic local neural activity might indicate that the abnormal bottom–up processing is associated with the pathological mechanism of schizophrenia (46). In this study, we observed increased temporal variability of

TABLE 2 | Significant increased dynamic fALFF and ReHo in schizophrenic subjects.

Regions	MNI coordinates			Peak t-score	Cluster voxels
	x	y	z		
Dynamic fALFF					
Left postcentral gyrus	−57	−12	21	5.992	763
Left precentral gyrus					
Left superior temporal gyrus					
Right postcentral gyrus	48	−21	60	5.097	452
Right precentral gyrus					
Left postcentral gyrus	−18	−42	75	5.844	228
Left precuneus					
Left superior parietal gyrus					
Right lingual gyrus	9	−81	−9	3.921	60
Left Thalamus	−9	−12	0	3.970	33
Dynamic ReHo					
Left postcentral gyrus	−30	−39	66	5.549	1,363
Left superior parietal gyrus					
Right cuneus					
Left cuneus					
Left precentral gyrus					
Left superior temporal gyrus					
Left temporal gyrus					
Right postcentral gyrus	39	−30	48	6.401	1,326
Right precentral gyrus					
Right superior temporal gyrus					
Right rolandic operculum					
Right insula					
Right heschl gyrus					
Left Middle temporal gyrus					
Middle cingulum cortex	−6	0	42	4.727	121
Supplementary motor area					
Left thalamus	−6	−12	6	4.899	108
Right thalamus					

ReHo and fALFF in sensory and perceptual system across time windows in schizophrenic subjects. These increased local temporal variabilities might provide some new evidences to support deficient dynamic neural activity in primary sensorimotor, as well as the abnormal dynamic bottom–up processing in schizophrenia.

Furthermore, schizophrenic patients could be commonly considered as a self-disorder with abnormal functional network (49). Recent studies have revealed that the processing and integration of multisensory bodily signals underlay a coherent self-experience in healthy controls (50, 51). In the "rubber-hand illusion" experiment, Botvinick and Cohen pointed out that the subjects would have true self-experience when they saw the fake hand was stroked, synchronous individual's unseen hand (50). Disturbances in self-experiences were also reported by Ehrsson; they found that visual perception was not match with proprioceptive information (51). These studies have provided the evidence that the sense of self-experiences depend on multisensory information that arose from the body, such as proprioceptive, spatial, and temporal sensorimotor signals. In schizophrenia, the deficits of visual and motor networks appear to be related to self-disorder (46, 52, 53). Besides, the neurobiological model of self-disorder has also indicated that deficient sense of self in schizophrenia is largely related to the abnormal multisensory signals integration from body and external stimuli (54, 55). Thalamus is a very crucial key role in gating and in integrating multisensory and cognitive information in human brain. Thus, previous studies have indicated that the altered static function of the thalamus is an important feature related to the schizophrenic subjects' self-disorder symptom (56, 57). In this study, we found increased temporal variability of ReHo and fALFF in primary visual and somatosensory area in schizophrenic patients. These increased dynamic neural activity across time may be related to the high interaction within regional sensorimotor functional network in schizophrenia. Increased temporal variability of thalamus was also observed in schizophrenic subjects, which may suggest that abnormal dynamic functional integration across time in schizophrenia exists between multisensory regions and higher order cognitive functional system. A significant relationship was observed between increased dynamic ReHo of thalamus and PANSS-positive score. These findings indicated that schizophrenic subjects have altered dynamic local functional connectivity and local dynamic neural activity in thalamus regions. Moreover, increased local dynamic functional connectivity of the thalamus maybe related with a positive symptom of schizophrenic subjects. Therefore, the abnormal dynamic local neural activity within the visual, sensorimotor, and thalamus areas might provide more evidence about abnormal self-processing in schizophrenia.

While our results provide a new insight of dynamic functional activity for understanding the self-disorder in schizophrenia, several main methodological points of this study should be further addressed. First, dynamic temporal

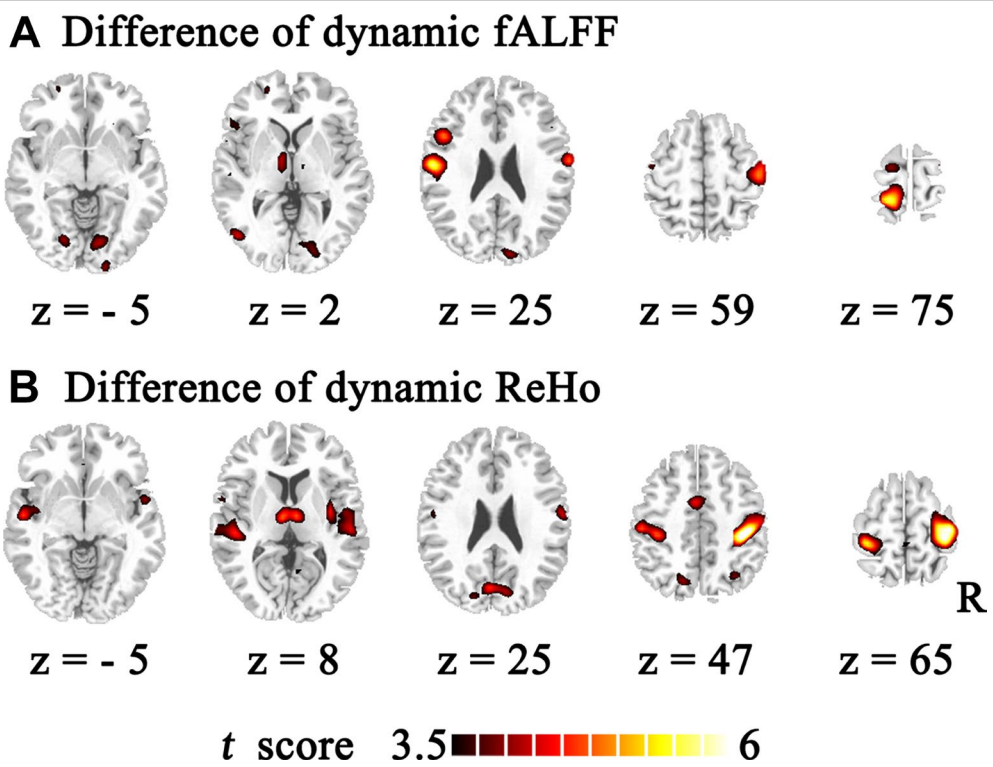

FIGURE 2 | Group difference of temporal variability of the dynamic fALFF and ReHo. Temporal variability of the dynamic fALFF and ReHo between schizophrenic and healthy subjects were identified using two-sample *t* tests. The significance level was set $P_{FDR} < 0.05$. **(A)** The increased dynamic fALFF in schizophrenic subjects were compared with those of healthy controls. **(B)** The enhanced dynamic ReHo in patients with schizophrenia.

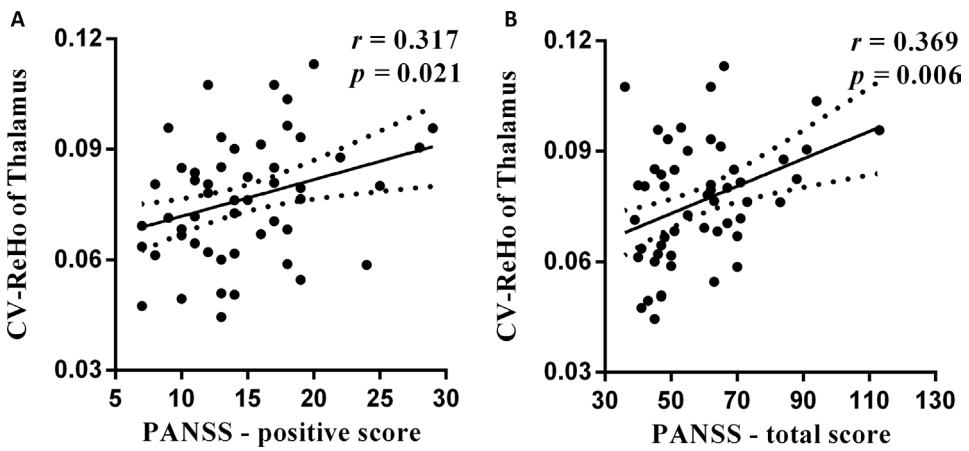

FIGURE 3 | The relationship between altered temporal variability of dynamic ReHo and PANSS scores. **(A)** The positive association is observed between increased CV score of thalamus region and PANSS-positive score in schizophrenic subjects. **(B)** The PANSS-total score was also positively related with CV score of thalamus region in patients.

variability of ReHo and fALFF were calculated through sliding window correlation analysis. The size of window length is one parameter that does not have formal consensus, although we selected it based on the frequency of preprocessed data. Second, the patient we chose is chronic schizophrenic subjects. The antipsychotic treatment might have an effect on dynamic local neural activity of patients. We should validate our findings in the first-episode schizophrenic subjects in further study. Third, self-experience assessment is not included in the current study. We should measure it and investigate the relationship between self-experience score and static/dynamic local neural activity in schizophrenic subjects.

CONCLUSION

In conclusion, this study has combined resting-state fMRI and dynamic functional analysis. Our findings have revealed an increased temporal variability of ReHo and fALFF in primary visual and sensorimotor networks, as well as in the thalamus in schizophrenia patients. It has been showed that the increased dynamic neural activity of the thalamus was significantly related with a positive symptom of schizophrenic subjects. Thus, our findings might have potential interpretation for the neural physiopathology of self-disorder in schizophrenia.

AUTHOR CONTRIBUTIONS

YZ made a substantial contribution to the conception and drafting and revising of the article. YZ, GG, and YT made a substantial contribution to the analysis and interpretation of the data, and gave final approval of the version to be published.

FUNDING

This scientific work was supported by grants from the National Nature Science Foundation of China (grant number: 81801775) and Advanced Talents Introduction Program of Chengdu Normal University (YJRC2017-4).

SUPPLEMENTARY MATERIAL

The Supplementary Material for this article can be found online at: https://www.frontiersin.org/articles/10.3389/fpsyt.2019.00484/full#supplementary-material

REFERENCES

1. Sass LA, Parnas J. Schizophrenia, consciousness, and the self. *Schizophr Bull* (2003) 29(3):427–44. doi: 10.1093/oxfordjournals.schbul.a007017
2. Waters FA, Badcock JC. First-rank symptoms in schizophrenia: reexamining mechanisms of self-recognition. *Schizophr Bull* (2010) 36(3):510–7. doi: 10.1093/schbul/sbn112
3. Liu F, Zhuo C, Yu C. Altered cerebral blood flow covariance network in schizophrenia. *Front Neurosci* (2016) 10:308. doi: 10.3389/fnins.2016.00308
4. Zhu J, Zhuo C, Xu L, Liu F, Qin W, Yu C. Altered coupling between resting-state cerebral blood flow and functional connectivity in schizophrenia. *Schizophr Bull* (2017) 43(6):1363–74. doi: 10.1093/schbul/sbx051
5. Liu F, Tian H, Li J, Li S, Zhuo C. Altered voxel-wise gray matter structural brain networks in schizophrenia: association with brain genetic expression pattern. *Brain Imaging Behav* (2019) 13(2):493–502. doi: 10.1007/s11682-018-9880-6
6. Minzenberg MJ, Laird AR, Thelen S, Carter CS, Glahn DC. Meta-analysis of 41 functional neuroimaging studies of executive function in schizophrenia. *Arch Gen Psychiatry* (2009) 66(8):811–22. doi: 10.1001/archgenpsychiatry.2009.91
7. He H, Luo C, Luo Y, Duan M, Yi Q, Biswal BB, et al. Reduction in gray matter of cerebellum in schizophrenia and its influence on static and dynamic connectivity. *Hum Brain Mapp* (2018) 40(2):517-28. doi: 10.1002/hbm.24391
8. Liu H, Liu Z, Liang M, Hao Y, Tan L, Kuang F, et al. Decreased regional homogeneity in schizophrenia: a resting state functional magnetic resonance imaging study. *Neuroreport* (2006) 17(1):19–22. doi: 10.1097/01.wnr.0000195666.22714.35
9. Hoptman MJ, Zuo XN, Butler PD, Javitt DC, D'Angelo D, Mauro CJ, et al. Amplitude of low-frequency oscillations in schizophrenia: a resting state fMRI study. *Schizophr Res* (2010) 117(1):13–20. doi: 10.1016/j.schres.2009.09.030
10. Zang Y, Jiang T, Lu Y, He Y, Tian L. Regional homogeneity approach to fMRI data analysis. *Neuroimage* (2004) 22(1):394–400. doi: 10.1016/j.neuroimage.2003.12.030
11. Zou QH, Zhu CZ, Yang Y, Zuo XN, Long XY, Cao QJ, et al. An improved approach to detection of amplitude of low-frequency fluctuation (ALFF) for resting-state fMRI: fractional ALFF. *J Neurosci Methods* (2008) 172(1):137–41. doi: 10.1016/j.jneumeth.2008.04.012
12. Jiang Y, Luo C, Li X, Duan M, He H, Chen X, et al. Progressive reduction in gray matter in patients with schizophrenia assessed with MR imaging by using causal network analysis. *Radiology* (2018) 287(2):729. doi: 10.1148/radiol.2018184005
13. Wang L, Song M, Jiang T, Zhang Y, Yu C. Regional homogeneity of the resting-state brain activity correlates with individual intelligence. *Neurosci Lett* (2011) 488(3):275–8. doi: 10.1016/j.neulet.2010.11.046
14. Xiang Y, Kong F, Wen X, Wu Q, Mo L. Neural correlates of envy: regional homogeneity of resting-state brain activity predicts dispositional envy. *Neuroimage* (2016) 142:225–30. doi: 10.1016/j.neuroimage.2016.08.003
15. Turner JA, Damaraju E, van Erp TG, Mathalon DH, Ford JM, Voyvodic J, et al. A multi-site resting state fMRI study on the amplitude of low frequency fluctuations in schizophrenia. *Front Neurosci* (2013) 7:137. doi: 10.3389/fnins.2013.00137
16. Guo W, Liu F, Xiao C, Zhang Z, Yu M, Liu J, et al. Dissociation of anatomical and functional alterations of the default-mode network in first-episode, drug-naive schizophrenia. *Clin Neurophysiol* (2015) 126(12):2276–81. doi: 10.1016/j.clinph.2015.01.025
17. Wang S, Zhang Y, Lv L, Wu R, Fan X, Zhao J, et al. Abnormal regional homogeneity as a potential imaging biomarker for adolescent-onset schizophrenia: a resting-state fMRI study and support vector machine analysis. *Schizophr Res* (2018) 192:179–84. doi: 10.1016/j.schres.2017.05.038
18. Javitt DC. Sensory processing in schizophrenia: neither simple nor intact. *Schizophr Bull* (2009) 35(6):1059–64. doi: 10.1093/schbul/sbp110
19. Chang C, Glover GH. Time-frequency dynamics of resting-state brain connectivity measured with fMRI. *Neuroimage* (2010) 50(1):81–98. doi: 10.1016/j.neuroimage.2009.12.011
20. Hansen EC, Battaglia D, Spiegler A, Deco G, Jirsa VK. Functional connectivity dynamics: modeling the switching behavior of the resting state. *Neuroimage* (2015) 105:525–35. doi: 10.1016/j.neuroimage.2014.11.001
21. Allen EA, Damaraju E, Plis SM, Erhardt EB, Eichele T, Calhoun VD. Tracking whole-brain connectivity dynamics in the resting state. *Cereb Cortex* (2014) 24(3):663–76. doi: 10.1093/cercor/bhs352
22. Hutchison RM, Womelsdorf T, Allen EA, Bandettini PA, Calhoun VD, Corbetta M, et al. Dynamic functional connectivity: promise, issues, and interpretations. *Neuroimage* (2013) 80:360–78. doi: 10.1016/j.neuroimage.2013.05.079
23. Sakoglu U, Pearlson GD, Kiehl KA, Wang YM, Michael AM, Calhoun VD. A method for evaluating dynamic functional network connectivity and task-modulation: application to schizophrenia. *MAGMA* (2010) 23(5-6):351–66. doi: 10.1007/s10334-010-0197-8
24. Ma S, Calhoun VD, Phlypo R, Adali T. Dynamic changes of spatial functional network connectivity in healthy individuals and schizophrenia patients using independent vector analysis. *Neuroimage* (2014) 90:196–206. doi: 10.1016/j.neuroimage.2013.12.063
25. Du YH, Pearlson GD, Yu QB, He H, Lin DD, Sui J, et al. Interaction among subsystems within default mode network diminished in schizophrenia patients: a dynamic connectivity approach. *Schizophr Res* (2016) 170(1):55–65. doi: 10.1016/j.schres.2015.11.021
26. Liu F, Wang Y, Li M, Wang W, Li R, Zhang Z, et al. Dynamic functional network connectivity in idiopathic generalized epilepsy with generalized

tonic-clonic seizure. *Hum Brain Mapp* (2017) 38(2):957–73. doi: 10.1002/hbm.23430
27. Damaraju E, Allen EA, Belger A, Ford JM, McEwen S, Mathalon DH, et al. Dynamic functional connectivity analysis reveals transient states of dysconnectivity in schizophrenia. *Neuroimage Clin* (2014) 5:298–308. doi: 10.1016/j.nicl.2014.07.003
28. Rashid B, Damaraju E, Pearlson GD, Calhoun VD. Dynamic connectivity states estimated from resting fMRI Identify differences among Schizophrenia, bipolar disorder, and healthy control subjects. *Front Hum Neurosci* (2014) 8:897. doi: 10.3389/fnhum.2014.00897
29. Rashid B, Arbabshirani MR, Damaraju E, Cetin MS, Miller R, Pearlson GD, et al. Classification of schizophrenia and bipolar patients using static and dynamic resting-state fMRI brain connectivity. *Neuroimage* (2016) 134:645–57. doi: 10.1016/j.neuroimage.2016.04.051
30. Fu Z, Tu Y, Di X, Du Y, Pearlson GD, Turner JA, et al. Characterizing dynamic amplitude of low-frequency fluctuation and its relationship with dynamic functional connectivity: an application to schizophrenia. *Neuroimage* (2018) 180(Pt B):619–31. doi: 10.1016/j.neuroimage.2017.09.035
31. Yan CG, Wang XD, Zuo XN, Zang YF. DPABI: Data Processing & Analysis for (Resting-State) Brain Imaging. Neuroinformatics (2016) 14(3):339–51. doi: 10.1007/s12021-016-9299-4
32. Power JD, Barnes KA, Snyder AZ, Schlaggar BL, Petersen SE. Spurious but systematic correlations in functional connectivity MRI networks arise from subject motion. *Neuroimage* (2012) 59(3):2142–54. doi: 10.1016/j.neuroimage.2011.10.018
33. Yang GJ, Murray JD, Repovs G, Cole MW, Savic A, Glasser MF, et al. Altered global brain signal in schizophrenia. *Proc Natl Acad Sci U S A* (2014) 111(20):7438–43. doi: 10.1073/pnas.1405289111
34. Liu F, Guo W, Fouche JP, Wang Y, Wang W, Ding J, et al. Multivariate classification of social anxiety disorder using whole brain functional connectivity. *Brain Struct Funct* (2015) 220(1):101–15. doi: 10.1007/s00429-013-0641-4
35. Bueno APA, Pinaya WHL, Rebello K, de Souza LC, Hornberger M, Sato JR. Regional dynamics of the resting brain in amyotrophic lateral sclerosis using fractional amplitude of low-frequency fluctuations and regional homogeneity analyses. *Brain Connect* (2019) 9(4):356–64. doi: 10.1089/brain.2019.0663
36. Leonardi N, Van De Ville D. On spurious and real fluctuations of dynamic functional connectivity during rest. Neuroimage (2015) 104:430–6. doi: 10.1016/j.neuroimage.2014.09.007
37. Laumann TO, Snyder AZ, Mitra A, Gordon EM, Gratton C, Adeyemo B, et al. On the stability of BOLD fMRI correlations. *Cereb Cortex* (2017) 27(10):4719–32. doi: 10.1093/cercor/bhw265
38. Yan CG, Cheung B, Kelly C, Colcombe S, Craddock RC, Di Martino A, et al. A comprehensive assessment of regional variation in the impact of head micromovements on functional connectomics. *Neuroimage* (2013) 76:183–201. doi: 10.1016/j.neuroimage.2013.03.004
39. Power JD, Schlaggar BL, Petersen SE. Recent progress and outstanding issues in motion correction in resting state fMRI. *Neuroimage* (2015) 105:536–51. doi: 10.1016/j.neuroimage.2014.10.044
40. Xia M, Wang J, He Y. BrainNet Viewer: a network visualization tool for human brain connectomics. *PLoS One* (2013) 8(7):e68910. doi: 10.1371/journal.pone.0068910
41. Yan CG, Wang XD, Zuo XN, Zang YF. DPABI: data processing & analysis for (Resting-State) brain imaging. *Neuroinformatics* (2016) 14(3):339–51. doi: 10.1007/s12021-016-9299-4
42. Weinberger DR, Gallhofer B. Cognitive function in schizophrenia. *Int Clin Psychopharmacol* (1997) 12 Suppl 4:S29–36. doi: 10.1097/00004850-199709004-00006
43. Achim AM, Bertrand MC, Sutton H, Montoya A, Czechowska Y, Malla AK, et al. Selective abnormal modulation of hippocampal activity during memory formation in first-episode psychosis. *Arch Gen Psychiatry* (2007) 64(9):999–1014. doi: 10.1001/archpsyc.64.9.999
44. Li CS. Impaired detection of visual motion in schizophrenia patients. *Prog Neuropsychopharmacol Biol Psychiatry* (2002) 26(5):929–34. doi: 10.1016/S0278-5846(02)00207-5
45. Martinez A, Hillyard SA, Dias EC, Hagler DJ, Jr., Butler PD, Guilfoyle DN, et al. Magnocellular pathway impairment in schizophrenia: evidence from functional magnetic resonance imaging. *J Neurosci* (2008) 28(30):7492–500. doi: 10.1523/JNEUROSCI.1852-08.2008
46. Dong D, Duan M, Wang Y, Zhang X, Jia X, Li Y, et al. Reconfiguration of dynamic functional connectivity in sensory and perceptual system in schizophrenia. *Cereb Cortex* (2018). doi: 10.1093/cercor/bhy232
47. Xu Y, Zhuo C, Qin W, Zhu J, Yu C. Altered spontaneous brain activity in schizophrenia: a meta-analysis and a large-sample study. *Biomed Res Int* (2015) 2015:204628. doi: 10.1155/2015/204628
48. Chen X, Duan MJ, Xie QK, Lai YX, Dong L, Cao WF, et al. Functional disconnection between the visual cortex and the sensorimotor cortex suggests a potential mechanism for self-disorder in schizophrenia. *Schizophr Res* (2015) 166(1-3):151–7. doi: 10.1016/j.schres.2015.06.014
49. Sass LA. Self-disturbance and schizophrenia: structure, specificity, pathogenesis (Current issues, New directions). *Schizophr Res* (2014) 152(1):5–11. doi: 10.1016/j.schres.2013.05.017
50. Botvinick M, Cohen J. Rubber hands 'feel' touch that eyes see. *Nature* (1998) 391(6669):756. doi: 10.1038/35784
51. Ehrsson HH. The experimental induction of out-of-body experiences. *Science* (2007) 317(5841):1048. doi: 10.1126/science.1142175
52. Brenner CA, Lysaker PH, Wilt MA, O'Donnell BF. Visual processing and neuropsychological function in schizophrenia and schizoaffective disorder. *Psychiatry Res* (2002) 111(2-3):125–36. doi: 10.1016/S0165-1781(02)00139-7
53. Bordier C, Nicolini C, Forcellini G, Bifone A. Disrupted modular organization of primary sensory brain areas in schizophrenia. *Neuroimage Clin* (2018) 18:682–93. doi: 10.1016/j.nicl.2018.02.035
54. Postmes L, Sno HN, Goedhart S, van der Stel J, Heering HD, de Haand L. Schizophrenia as a self-disorder due to perceptual incoherence. *Schizophr Res* (2014) 152(1):41–50. doi: 10.1016/j.schres.2013.07.027
55. Borda JP, Sass LA. Phenomenology and neurobiology of self disorder in schizophrenia: primary factors. *Schizophr Res* (2015) 169(1-3):464–73. doi: 10.1016/j.schres.2015.09.024
56. Anticevic A. Understanding the role of thalamic circuits in schizophrenia neuropathology. *Schizophr Res* (2017) 180:1–3. doi: 10.1016/j.schres.2016.11.044
57. Li T, Wang Q, Zhang J, Rolls ET, Yang W, Palaniyappan L, et al. Brain-wide analysis of functional connectivity in first-episode and chronic stages of schizophrenia. *Schizophr Bull* (2017) 43(2):436–48. doi: 10.1093/schbul/sbw099

Conflict of Interest Statement: The authors declare that the research was conducted in the absence of any commercial or financial relationships that could be construed as a potential conflict of interest.

frontiers in Neurology

ORIGINAL RESEARCH
published: 01 October 2019
doi: 10.3389/fneur.2019.01052

Dynamic Alterations of Spontaneous Neural Activity in Parkinson's Disease: A Resting-State fMRI Study

Chao Zhang[1†], Binru Dou[1†], Jiali Wang[1], Kai Xu[1], Haiyan Zhang[2], Muhammad Umair Sami[1], Chunfeng Hu[1], Yutao Rong[1], Qihua Xiao[3], Nan Chen[4] and Kuncheng Li[4]*

[1] Department of Radiology, Affiliated Hospital of Xuzhou Medical University, Xuzhou, China, [2] Department of Radiology, Affiliated 2 Hospital of Xuzhou Medical University, Xuzhou, China, [3] Department of Neurology, Affiliated Hospital of Xuzhou Medical University, Xuzhou, China, [4] Department of Radiology, Xuanwu Hospital, Capital Medical University, Beijing, China

Objective: To investigate the dynamic amplitude of low-frequency fluctuations (dALFFs) in patients with Parkinson's disease (PD) and healthy controls (HCs) and further explore whether dALFF can be used to test the feasibility of differentiating PD from HCs.

Methods: Twenty-eight patients with PD and 28 demographically matched HCs underwent resting-state functional magnetic resonance imaging (rs-fMRI) scans and neuropsychological tests. A dynamic method was used to calculate the dALFFs of rs-fMRI data obtained from all subjects. The dALFF alterations were compared between the PD and HC groups, and the correlations between dALFF variability and disease duration/neuropsychological tests were further calculated. Then, the statistical differences in dALFF between both groups were selected as classification features to help distinguish patients with PD from HCs through a linear support vector machine (SVM) classifier. The classifier performance was assessed using a permutation test (repeated 5,000 times).

Results: Significantly increased dALFF was detected in the left precuneus in patients with PD compared to HCs, and dALFF variability in this region was positively correlated with disease duration. Our results show that 80.36% ($p < 0.001$) subjects were correctly classified based on the SVM classifier by using the leave-one-out cross-validation method.

Conclusion: Patients with PD exhibited abnormal dynamic brain activity in the left precuneus, and the dALFF variability could distinguish PD from HCs with high accuracy. Our results showed novel insights into the pathophysiological mechanisms of PD.

Keywords: Parkinson's disease, resting-state fMRI, dynamic brain activity, amplitude of low-frequency fluctuations, support vector machine

OPEN ACCESS

Edited by:
Wenbin Guo,
Central South University, China

Reviewed by:
Xiuqin Jia,
Capital Medical University, China
Tianmei Si,
Peking University Sixth Hospital, China
Li Wang,
Capital Medical University, China

****Correspondence:***
Kai Xu
xukaixz@163.com

[†]These authors have contributed equally to this work

Specialty section:
This article was submitted to Applied Neuroimaging, a section of the journal Frontiers in Neurology

Received: *07 June 2019*
Accepted: *17 September 2019*
Published: *01 October 2019*

Citation:
Zhang C, Dou B, Wang J, Xu K, Zhang H, Sami MU, Hu C, Rong Y, Xiao Q, Chen N and Li K (2019) Dynamic Alterations of Spontaneous Neural Activity in Parkinson's Disease: A Resting-State fMRI Study. Front. Neurol. 10:1052. doi: 10.3389/fneur.2019.01052

INTRODUCTION

Parkinson's disease (PD) is a common neurodegenerative disorder characterized by progressive impairment of motor function and widespread non-motor symptoms, which affects patients' quality of life and is, hence, a significant social burden (1–3). At present, the pathophysiological mechanism of PD is not fully understood, and it is still a neuroimaging challenge to form a

definitive diagnosis at the early stage of the disease (1). Magnetic resonance imaging (MRI) has made great contributions in the clinical evaluation of PD (4, 5). Conventional MRI has been used to exclude secondary parkinsonism caused by neoplasms, vascular parkinsonism, and multiple sclerosis among others. The common imaging features of primary PD include iron deposition and substantia nigra atrophy (6, 7). However, several new reports have revealed that the cerebral region is widely involved in patients with PD. Therefore, it is important to explore novel imaging features that could help effectively identify PD.

In recent years, advanced neuroimaging techniques have allowed us to noninvasively explore the nature of the human brain in an efficient manner (8–10). Resting-state functional MRI (rs-fMRI) is an established tool to investigate the intrinsic neuronal activity of the human brain by measuring the amplitude of spontaneous low-frequency fluctuations (ALFFs) of blood-oxygen-level dependent (BOLD) signals (11–13). ALFF has been widely used to investigate regional brain activity in neurological diseases. Abnormal ALFFs in PD have been detected in extensive brain regions and act as an important characteristic related to subtypes of motor symptom or comorbidities (14). When compared with healthy controls (HCs), patients with tremor-dominant PD exhibited increased ALFF in the right cerebellar posterior lobe, while those with PD with postural instability/gait difficulty exhibited decreased ALFF in the bilateral putamen and cerebellar posterior lobe (15). PD patients with depression had significantly lower ALFF in the prefrontal cortex and anterior cingulated cortex than PD patients without depression (16). PD patients with apathy showed lower ALFF in the left orbital middle frontal gyrus and bilateral superior frontal gyrus (17) than PD patients without apathy. Further, PD patients with visual hallucinations showed lower ALFF in both lingual gyrii/cunei and greater ALFF in the temporo-parietal regions, medial temporal gyrus, and cerebellum than those with non-visual hallucinations and HCs (18). By measuring the local spontaneous brain activities, these studies provided satisfactory evidence that widespread cerebral regions were involved in PD, which greatly contributed to the understanding the neurobiological foundations of such disorders. However, the results of these studies were limited in that their focus on abnormal brain activities in PD with different motor/non-motor symptoms was based solely on group-level analysis; thus far, to our best knowledge, no study has used these abnormal features to distinguish PD with specific symptoms at an individual level.

Previous studies on aberrant static ALFF in PD are inconsistent as they report both lower and higher local brain activity in various cerebral areas. However, a static state analysis of ALFF ignores the dynamic characteristics of brain activity during the whole scanning period. Evidences from rs-fMRI that employ a sliding window approach have effectively detected dynamic functional connectivity features with higher sensitivity than the static state method (12, 19, 20). Recent studies reported that dynamic rs-fMRI analysis strategy not only made good contributions to human-brain exploration but also played an important role in studying the pathogenesis of schizophrenia (21–23). Nevertheless, few reports have focused on time-varying local spontaneous neuronal activity in PD, as ALFF itself exists with substantial fluctuations either (24, 25). Furthermore, support vector machine (SVM) is one of the most widely used supervised machine-learning approaches that can enable individual-level classification and prediction with high accuracy (26, 27). Uddin et al. (28) applied SVM to distinguish patients with autism from normal individuals with a classifier accuracy of over 80%. Accordingly, SVM has been proposed as an effective tool for diagnostic application in the clinic.

To date, no studies have evaluated the combined effects of dynamic ALFF and supervised machine-learning approaches on PD. Based on previous findings that a static ALFF has greater heterogeneity in PD and the proven property of dynamic methods, we hypothesized that dynamic intrinsic local spontaneous neuronal activity will show greater variability in subjects with PD than HCs, and that it may be another powerful index of rs-fMRI in exploring the underlying mechanisms of PD. We aimed to identify the cerebral regions that displayed abnormal dynamic local neuronal activity based on the voxel level of the whole brain. Furthermore, we applied SVM to observe whether the aberrant dALFF could be used as a feature to distinguish PD from HCs. This study may improve our understanding of the potential pathophysiological mechanism of PD. Moreover, we hope that this research can contribute to the clinical diagnosis of PD at an individual level.

MATERIALS AND METHODS

Subjects

This study was carried out in accordance with the tenets of the Helsinki Declaration and approved by the local ethics committee of Xuzhou Affiliated Hospital, Xuzhou Medical University. Written informed consent was obtained from all subjects before participation in the study.

The project used a convenience sample of 31 hospitalized patients with PD who met the UK Bank diagnostic criteria for PD (29). All patients underwent neuropsychological tests such as the Mini Mental Status Examination (MMSE) and the Montreal Cognitive Assessment (MoCA) and motor impairment evaluation including the Unified Parkinson's Disease Rating Scale (UPDRS) and the Hoehn and Yahr (H-Y) stage when patients were off medication. The included patients had no history of mental illness or other neurological diseases. The exclusion criteria of the participants were MRI-confirmed brain abnormalities such as trauma, stroke, tumor, and infection and contraindications to MRI such as claustrophobia and implanted metal devices. In addition, the subjects with a history of drug and/or alcohol abuse and syncope were also excluded. All patients underwent routine treatment, and none of them received any other relevant interventions. Thirty-two age- and sex-matched healthy volunteers were included as HCs. Three patients and four HCs were excluded because of head motion artifacts. Finally, 28 patients with PD (15 male and 13 female, 59.17 $\pm$ 9.72 years old) and 28 HCs (14 male and 14 female, 58.18 $\pm$ 6.46 years old) were included for analysis. There were no significant intergroup differences with respect to age and sex (**Table 1**). All patients underwent functional MRI scanning when they were off medication; all the HCs also underwent the same protocol

TABLE 1 | Demographics and clinical data.

Variable	PD ($N = 28$)	HCs ($N = 28$)	P
Sex (M/F)	15/13	14/14	0.789[#]
Age (years)	59.17 ± 9.72	58.18 ± 6.46	0.794*
Duration of PD (years)	8.46 ± 2.92	N/A	N/A
UPDRS-III	29.1 ± 8.70	N/A	N/A
H-Y	2.02 ± 0.71	N/A	N/A
MoCA	24.39 ± 2.52	25.86 ± 1.73	0.015*
MMSE	27.64 ± 1.25	27.71 ± 1.24	0.831*
CV values	0.18 ± 0.04	0.13 ± 0.12	<0.001*

PD, Parkinson's disease; HCs, healthy controls; M, male; F, female; UPDRS-III, unified Parkinson's disease rating scale; H-Y, Hoehn and Yahr disability scale; MoCA, Montreal Cognitive Assessment; MMSE, Mini-Mental Status Examination.
Data are presented as the range and mean ± SD.
[#]The p-value was obtained using a chi-square test.
**The p-value was obtained by a general linear mode analysis.*

for MRI scanning and neuropsychological tests. All subjects were right-handed.

MRI Data Acquisition

All participants were scanned in a 3.0 Tesla MRI scanner (GE Medical Systems, Signa HD, Waukesha, WI) with an eight-channel head coil. During the scan, comfortable foam pads were used to stabilize the head of each subject to minimize head motion, and all subjects wore earplugs to reduce the noise from the MRI machine. Then, an echo-planar imaging sequence was employed to acquire resting BOLD images. The parameters of the protocol are as follows: time of repetition, 2,000 ms; time of echo, 30 ms; field of view, 220 mm × 220 mm; slice thickness, 3 mm; slice gap, 1 mm; voxel size, 3.4 mm × 3.4 mm × 4.0 mm; number of slices, 36; flip angle, 90°; and total volume of each subject, 185.

Preprocessing of rs-fMRI Data

The rs-fMRI data preprocessing were carried out using data Processing and Analysis for (Resting-State) Brain Imaging (DPABI) (http://www.rfmri.org/dpabi) (30). The first 10 time points of each subject were excluded to stabilize the status and allow participants to adapt to the scanning condition. Slice timing was carried out on the remaining 175 volumes to correct time differences. Realignment was performed to correct head motion by using a Friston-24 model for individual-level correction, and any subject with a head maximum displacement >2 mm, maximum rotation >2.0°, or mean framewise displacement (FD) >0.3 was excluded. In our study, mean FD was set as a covariate for further group-level statistics to minimize the potential influences of head motion. Several covariates such as the Friston 24 head-motion parameters, cerebrospinal fluid signal, and white matter signal were regressed. Then, the processed volumes were normalized to the standard Montreal Neurological Institute (MNI) echo planar imaging (EPI) template with a voxel size of 3 mm × 3 mm × 3 mm. Finally, functional volumes were smoothed with 6-mm full width at half maximum. We did not carry out global signal regression of our data given that there is still some controversy regarding removal of the global signal (31–33).

Dynamic ALFF Analysis

The analysis of dynamic amplitude of low-frequency fluctuations (dALFF) was carried out using Temporal Dynamic Analysis (TDA) toolkits based on DPABI (34). Before dALFF calculation, functional volumes were bandpass filtered (0.01–0.08 Hz) to minimize the influences of low-frequency drifts and fluctuations of the signal. The sliding window is an important parameter to capture dynamic spontaneous neural activities, and the proper window length is critical for dynamic analysis. Too small a window length may not allow robust estimation of dynamic changes, and too long a window length may not be able to detect dynamic activity. Previous studies provided the range of the appropriate window length as 10–75 TR, step = 1 TR) (12, 35). To maximize the statistical power, a moderate sliding window length of 50 TR (step = 1 TR) was selected. The post-processed 175 volumes of each subject were segmented into 126 windows in all. The ALFF was calculated in each sliding window. The standard deviation (SD) of ALFF values of each voxel across 126 windows was further calculated to assess the variability of ALFF. We also calculated the static ALFF containing the whole sliding window.

Statistical Analysis

Two-sample t-test was used to observe intergroup differences in age and MoCA/MMSE scores. Sex-based group difference was evaluated using the chi-square test. A general linear mode (GLM) with age, sex, and mean FD as covariates was used to compare the difference of dALFF/ALFF between the PD and HC groups. Multiple comparisons were corrected using Gaussian Random-Field (GRF) method (voxel level, $p < 0.001$; cluster level, $p < 0.05$).

Partial correlation analysis was calculated between dALFF variability and disease duration/MoCA/MMSE/UPDRS/H-Y with age and sex as covariates ($p < 0.05$). All statistical analyses were performed using SPSS version 16 (SPSS Inc., Chicago, IL, USA).

Support Vector Machine Analysis

The intergroup dALFF difference was used as the classification feature in this study. We then trained the SVMs by providing labeled observations, for which the classification results were known. To overcome the limitations of our samples, the leave-one-out cross-validation (LOOCV) method was applied to estimate the generalization ability of our classifier. To verify the ability of the validation strategy, we also made a classification comparison by introducing 10-fold cross-validations. Then, the total accuracy, sensitivity, and specificity were obtained to assess classifier performance.

A permutation test was used to evaluate the statistical significance of this classification accuracy (36). The permutation test was repeated 5,000 times, and during each time, the classifier randomly reallocated labels of PD and HC to the training subjects and repeated the entire classification process. The p-value was obtained after the total permutation was accomplished.

RESULTS

Demographics and Clinical Data

The details of age, sex, and MoCA/MMSE scores are listed in **Table 1**. The results showed no significant difference in age ($p = 0.652$), sex ($p = 0.789$), and MMSE ($p = 0.831$) between the PD and HC groups. However, the MoCA score of the PD group was significantly lower than that of the HCs ($p < 0.05$).

Differences in ALFF/Dynamic ALFF and Correlational Analysis

The intergroup differences in dALFF are shown in **Figure 1** and **Tables 1**, **2**. Compared with HCs, significantly increased coefficient of variation (CV) of dALFF was noted in the left precuneus of PD patients ($p < 0.001$). In addition, we found that the CV of dALFF was positively correlated with disease duration ($p < 0.001$, $r = 0.800$) (**Figure 1**), and no significant correlation was found between dALFF variability and MoCA/MMSE/UPDRS/H-Y scores (**Supplementary Material**). There were no significant intergroup differences in ALFF.

Classification Results

Classification results are shown in **Figure 2**. The accuracy of linear SVM classifier using LOOCV achieved an accuracy of 80.36%, sensitivity of 85.71%, and specificity of 75% ($p < 0.001$, non-parametric permutation approach). The receiver operating characteristic (ROC) curve of the classifier was 0.82. A 10-fold validation was also employed in our study to verify the reliability of the classification method, which generated a classifier accuracy of 71.43%.

DISCUSSION

Upon literature review, we observed that only few studies employed a TDA method to explore the neural-activity characteristics of PD. The present study showed the following findings: (1) the dALFF of patients with PD compared to HCs was notably different in the left precuneus; (2) a significant correlation between CV of dALFF in the left precuneus and the course of the disease was found in PD; (3) dALFF in the left precuneus showed high accuracy in distinguishing between patients with PD and HCs.

Prior studies have noted the importance of cerebral static local neural activities in PD (4, 14, 15). To our best knowledge, dynamic changes in spontaneous neural activity has been very

TABLE 2 | dALFF alterations between PD groups and HCs.

Region	Cluster size (voxel)	MNI (x,y,z)	*t*-value
Left Precuneus	94	(−12, −42, 60)	4.34

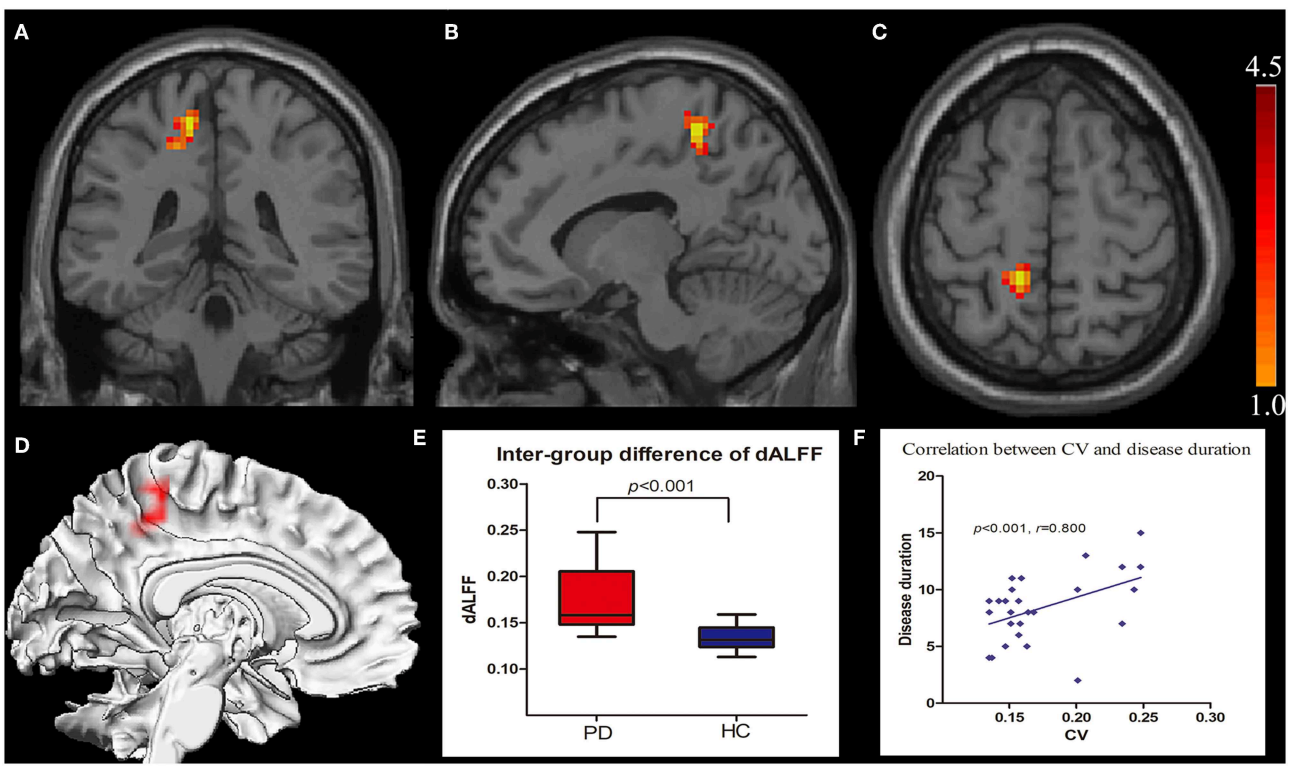

FIGURE 1 | Increased CV of dALFF in the left precuneus displayed in coronal **(A)**, sagittal **(B)**, transverse **(C)**, and three-dimensional view **(D)**. Box plots with Whiskers (min–max) show the CV values in the left precuneus of the two groups **(E)**, and scatterplots show the relationship between the CV in the precuneus of the PD group and the disease duration **(F)**. CV, coefficient of variation; dALFF, dynamic spontaneous low-frequency fluctuation.

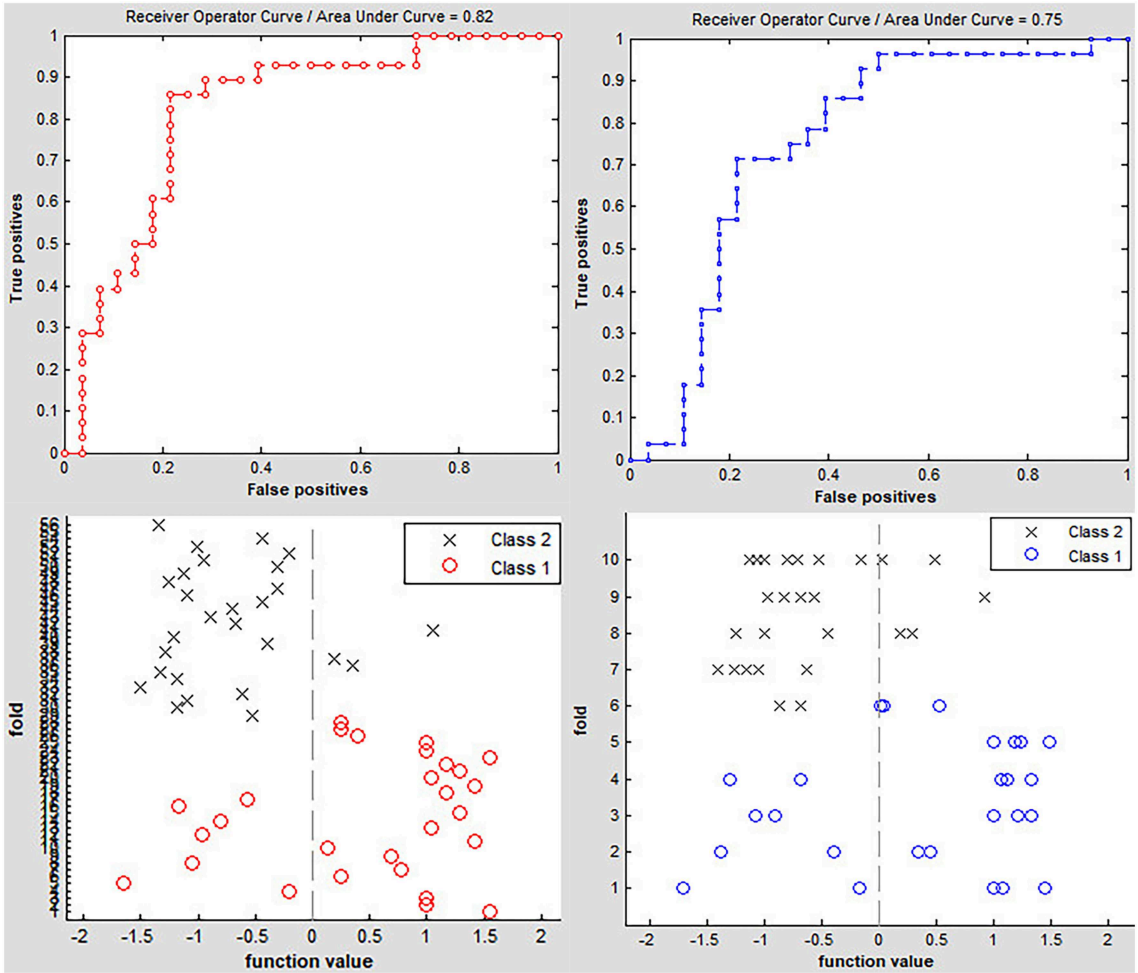

FIGURE 2 | Classification accuracy of altered dynamic ALFF in the left precuneus obtained by the leave-one-out (red line) and nested 10-fold (blue line) cross validation methods in PD groups, respectively.

poorly researched. The rs-fMRI analysis was based on the hypothesis that brain activity was in a stationary state during the entire scanning period; thus, the dynamic characteristics could not be identified. Dynamic algorithm was proven to represent the time-dependent characteristics of brain activity under the given scanning period. A recent study captured abnormal dALFF/ Regional Homogeneity (ReHo) in stroke patients by using TDA and compared it with HCs; they further found that variability in brain activity could be used to evaluate patients' motor function (24). Liu et al. (12) found abnormal functional network connection (FNC) through dynamic instead of static state. Dynamic FNC was significantly correlated with the frequency of epileptic seizures and the course of the disease. Furthermore, dynamic FNC could distinguish patients with idiopathic generalized epilepsy with generalized tonic–clonic seizures from controls with an accuracy of 77.91% through linear SVM classifier ($p < 0.001$). Dynamic algorithm showed the capability to characterize neural activity of the human brain by identifying specific function signatures.

Our dynamic algorithm showed that the dALFF in the left precuneus in PD was notably different than HCs. The result was partially consistent with previous reports that the left precuneus was a key cerebral region in patients with PD. Precuneus, which mainly constitutes the medial and posterior part of the parietal lobe, contributes to motor and cognitive tasks, and has been reported as displaying the highest resting metabolic rate among all cerebral regions (37). Interestingly, the precuneus consumed 35% more glucose than other brain regions in the resting brain (38). Perfusion single photon-emission computed tomography (SPECT) and [^{18}F]fluorodeoxyglucose positron emission tomography ([^{18}F]FDG-PET) proved that the precuneus was the most remarkable area of hypometabolism in the posterior cortical region (39). Another [^{18}F]FDG-PET-based study on PD found that the metabolic capability of the left precuneus decreased with disease progression (40). Similarly, a more recent research using the arterial spin labeling (ASL) technique showed that cerebral blood flow (CBF) in the left precuneus significantly reduced in the PD group when compared with HCs (41). These functional imaging studies supported the view that the left precuneus might be more prone to attack in neuropsychiatric disorders. Additional rs-fMRI studies showed that the left precuneus was closely

associated with motor and non-motor symptoms in PD. Hu et al. (42) found that increased local brain activity in the left precuneus was related to the Hamilton Depression Rating Scale score, by using static brain activity analysis. Thibes et al. (43) used a brain connection algorithm and showed that the left precuneus was a critical node connecting with specific cerebral regions in PD. In addition, morphological changes of the left precuneus were also found in PD with cognitive impairment and isolated apathy through voxel-based morphometry (44, 45). Therefore, the left precuneus is undoubtedly an important and vulnerable structure in patients with PD.

In our study, the higher variability of dynamic local brain activity level in the left precuneus was positively correlated with the course of PD. This meant that the degree of variation was significantly increased with an extended disease course, which reflected the increased or decreased brain activity at different sliding windows during the whole scanning period. These findings revealed a localized brain function impairment over time in PD. However, the abnormal dALFF did not correlate with UPDRS/H-Y scores in the present findings, likely because the heterogeneous motor symptoms in PD were associated with integration of multiple cerebral region function, rather than being determined by a single brain region impairment (46, 47). Unlike previous reports, the present study did not find significant intergroup differences with respect to ALFF, either because the sample size in our study was relatively small or because the result was not powerful enough to pass the multiple comparison correction of the present statistical methods. In fact, the dynamic features were concealed under the static analysis that represented a measure of the average amplitude of local activity across different scanning time points within the whole scan (12). Thus, static rs-fMRI may not be as sensitive as dynamic analysis to detect neural-activity changes. Our study indicated that dynamic analysis could completely unearth information of brain activity. In addition, the present result suggested that the left precuneus was an important structure involved in PD, and higher dALFF in this region was a promising imaging marker reflecting the disease duration. Besides, our findings did not show a correlation between dALFF and MoCA/MMSE tests. This may be because the MoCA and MMSE scales were mainly appropriate for cognitive screening, and our study lacked detailed assessment of cognitive performance compared to previous studies (48).

The imaging diagnosis of PD remains a challenge even now, as a confirmed diagnosis in most patients is still made depending on the clinical symptoms (49). An assessment of the iron content and volume of substantia nigra may be useful indicators to identify PD and evaluate the disease progression (6, 7). However, this approach has not been widely applied in the clinical management of patients with PD. Previous reports demonstrated that SVM was a powerful tool utilizing imaging features to distinguish PD patients from HCs. In our study, we tested the inter-group difference of dALFF in the left precuneus as a classification feature to discriminate PD from HCs through a linear SVM classifier. The accuracy of this classification was 80.36% when an LOOCV method was employed (non-parametric permutation correction, $p < 0.001$). Further, to compare the performance of SVM using LOOCV, a nested 10-fold cross-validation method was used to assess the classifier's performance; the accuracy was 71.43%. These findings showed that SVM could achieve better classification capability with LOOCV, and the results also provided evidence that patients with PD could be distinguished from HCs at the individual level when using dALFF variation in the left precuneus. These results support the hypothesis that the dALFF could identify individual PD patients.

Our study has some limitations. First, all patients were on medication. Although patients underwent fMRI scanning while they were off medication, the effects of the long-term treatment could not be completely ruled out. Second, the classification power based on the 28 PD patients was still not strong enough, and we just used SVM in the same sample to testify the classification accuracy. Third, the patients did not undergo comprehensive cognitive scales testing, which could have prevented a more accurate detection of cognitive performance. Future research should include a larger sample size and another independent test sample should be recruited for testifying classification accuracy.

CONCLUSION

To our best knowledge, this is the first study to attempt to investigate the dynamic spontaneous neural activities in patients with PD. Our results provided evidence that dynamic analysis was more sensitive to detect alteration of brain activity than a static method. In addition, the CV of dALFF was found to be correlated with the course of the disease, which may ultimately contribute to identifying PD at the individual level. Thus, our results provide novel insights on the pathophysiological mechanisms of PD.

DATA AVAILABILITY STATEMENT

The datasets generated for this study are available on request to the corresponding author.

ETHICS STATEMENT

The studies involving human participants were reviewed and approved by Ethical committee of Xuzhou Affiliated Hospital. The patients/participants provided their written informed consent to participate in this study.

AUTHOR CONTRIBUTIONS

CZ and BD contributed equally to this work for the conception/design of the study, the acquisition, analysis, interpretation of data, drafting of the manuscript, final approval of the version to be published, and agreement to be accountable for all aspects of the research. JW, CH, YR, HZ, and MS were responsible for data analysis, drafting of the manuscript, final approval of the version to be published, and agreement to be accountable for all aspects of the research. QX, NC, and KL were responsible for revision of the manuscript, final approval of the version to be published, and agreement to be accountable for

all aspects of the work. KX was responsible for design of the study, revision of the work, final approval of the version to be published, and agreement to be accountable for all aspects of the work.

FUNDING

This study was supported by the National Natural Science Foundation of China (No. 81871339; No. 81271556) and Xuzhou Science and Technology Project (No. KC18051).

ACKNOWLEDGMENTS

We thank all the volunteers who participated in this research.

SUPPLEMENTARY MATERIAL

The Supplementary Material for this article can be found online at: https://www.frontiersin.org/articles/10.3389/fneur.2019.01052/full#supplementary-material

REFERENCES

1. Kalia LV, Lang AE. Parkinson's disease. *Lancet*. (2015) 386:896–912. doi: 10.1016/S0140-6736(14)61393-3
2. Sveinbjornsdottir S. The clinical symptoms of Parkinson's disease. *J Neurochem*. (2016) 139(Suppl. 1):318–24. doi: 10.1111/jnc.13691
3. Tysnes OB, Storstein A. Epidemiology of Parkinson's disease. *J Neural Transm*. (2017) 124:901–5. doi: 10.1007/s00702-017-1686-y
4. Kahan J, Urner M, Moran R, Flandin G, Marreiros A, Mancini L, et al. Resting state functional MRI in Parkinson's disease: the impact of deep brain stimulation on 'effective' connectivity. *Brain*. (2014) 137(Pt 4):1130–44. doi: 10.1093/brain/awu027
5. Vanegas-Arroyave N, Lauro PM, Huang L, Hallett M, Horovitz SG, Zaghloul KA, et al. Tractography patterns of subthalamic nucleus deep brain stimulation. *Brain*. (2016) 139(Pt 4):1200–10. doi: 10.1093/brain/aww020
6. Wu SF, Zhu ZF, Kong Y, Zhang HP, Zhou GQ, Jiang QT, et al. Assessment of cerebral iron content in patients with Parkinson's disease by the susceptibility-weighted MRI. *Eur Rev Med Pharmacol Sci*. (2014) 18:2605–8
7. Zhang J, Zhang Y, Wang J, Cai P, Luo C, Qian Z, et al. Characterizing iron deposition in Parkinson's disease using susceptibility-weighted imaging: an *in vivo* MR study. *Brain Res*. (2010) 1330:124–30. doi: 10.1016/j.brainres.2010.03.036
8. Guo WB, Liu F, Xue ZM, Xu XJ, Wu RR, Ma CQ, et al. Alterations of the amplitude of low-frequency fluctuations in treatment-resistant and treatment-response depression: a resting-state fMRI study. *Prog Neuropsychopharmacol Biol Psychiatry*. (2012) 37:153–60. doi: 10.1016/j.pnpbp.2012.01.011
9. Liu F, Guo W, Fouche JP, Wang Y, Wang W, Ding J, et al. Multivariate classification of social anxiety disorder using whole brain functional connectivity. *Brain Struct Funct*. (2015) 220:101–15. doi: 10.1007/s00429-013-0641-4
10. Zhang C, Zhang H, Xu K, Yang H, Liu C, Yu T, et al. Impaired prefrontal cortex-thalamus pathway in intractable temporal lobe epilepsy with aberrant executive control function: MRI evidence. *Clin Neurophysiol*. (2019) 130:484–90. doi: 10.1016/j.clinph.2018.12.007
11. Liu F, Guo W, Liu L, Long Z, Ma C, Xue Z, et al. Abnormal amplitude low-frequency oscillations in medication-naive, first-episode patients with major depressive disorder: a resting-state fMRI study. *J Affect Disord*. (2013) 146:401–6. doi: 10.1016/j.jad.2012.10.001
12. Liu F, Wang Y, Li M, Wang W, Li R, Zhang Z, et al. Dynamic functional network connectivity in idiopathic generalized epilepsy with generalized tonic-clonic seizure. *Hum Brain Mapp*. (2017) 38:957–73. doi: 10.1002/hbm.23430
13. Zang YF, He Y, Zhu CZ, Cao QJ, Sui MQ, Liang M, et al. Altered baseline brain activity in children with ADHD revealed by resting-state functional MRI. *Brain Dev*. (2007) 29:83–91. doi: 10.1016/j.braindev.2006.07.002
14. Pan P, Zhang Y, Liu Y, Zhang H, Guan D, Xu Y. Abnormalities of regional brain function in Parkinson's disease: a meta-analysis of resting state functional magnetic resonance imaging studies. *Sci Rep*. (2017) 7:40469. doi: 10.1038/srep40469
15. Chen HM, Wang ZJ, Fang JP, Gao LY, Ma LY, Wu T, et al. Different patterns of spontaneous brain activity between tremor-dominant and postural instability/gait difficulty subtypes of Parkinson's disease: a resting-state fMRI study. *CNS Neurosci Ther*. (2015) 21:855–66. doi: 10.1111/cns.12464
16. Wen X, Wu X, Liu J, Li K, Yao L. Abnormal baseline brain activity in non-depressed Parkinson's disease and depressed Parkinson's disease: a resting-state functional magnetic resonance imaging study. *PLoS ONE*. (2013) 8:e63691. doi: 10.1371/journal.pone.0063691
17. Shen YT, Li JY, Yuan YS, Wang XX, Wang M, Wang JW, et al. Disrupted amplitude of low-frequency fluctuations and causal connectivity in Parkinson's disease with apathy. *Neurosci Lett*. (2018) 683:75–81. doi: 10.1016/j.neulet.2018.06.043
18. Yao N, Pang S, Cheung C, Chang RS, Lau KK, Suckling J, et al. Resting activity in visual and corticostriatal pathways in Parkinson's disease with hallucinations. *Parkinsonism Relat Disord*. (2015) 21:131–7. doi: 10.1016/j.parkreldis.2014.11.020
19. Duncan ES, Small SL. Changes in dynamic resting state network connectivity following aphasia therapy. *Brain Imaging Behav*. (2018) 12:1141–9. doi: 10.1007/s11682-017-9771-2
20. Liu J, Liao X, Xia M, He Y. Chronnectome fingerprinting: identifying individuals and predicting higher cognitive functions using dynamic brain connectivity patterns. *Hum Brain Mapp*. (2018) 39:902–15. doi: 10.1002/hbm.23890
21. Damaraju E, Allen EA, Belger A, Ford JM, McEwen S, Mathalon DH, et al. Dynamic functional connectivity analysis reveals transient states of dysconnectivity in schizophrenia. *NeuroImage Clin*. (2014) 5:298–308. doi: 10.1016/j.nicl.2014.07.003
22. Fong AHC, Yoo K, Rosenberg MD, Zhang S, Li CR, Scheinost D, et al. Dynamic functional connectivity during task performance and rest predicts individual differences in attention across studies. *NeuroImage*. (2019) 188:14–25. doi: 10.1016/j.neuroimage.2018.11.057
23. Menon SS, Krishnamurthy K. A comparison of static and dynamic functional connectivities for identifying subjects and biological sex using intrinsic individual brain connectivity. *Sci Rep*. (2019) 9:5729. doi: 10.1038/s41598-019-42090-4
24. Chen J, Sun D, Shi Y, Jin W, Wang Y, Xi Q, et al. Dynamic alterations in spontaneous neural activity in multiple brain networks in subacute stroke patients: a resting-state fMRI study. *Front Neurosci*. (2018) 12:994. doi: 10.3389/fnins.2018.00994
25. Liao X, Yuan L, Zhao T, Dai Z, Shu N, Xia M, et al. Spontaneous functional network dynamics and associated structural substrates in the human brain. *Front Hum Neurosci*. (2015) 9:478. doi: 10.3389/fnhum.2015.00478
26. Liu F, Wee CY, Chen H, Shen D. Inter-modality relationship constrained multi-modality multi-task feature selection for Alzheimer's disease and mild cognitive impairment identification. *Neuroimage*. (2014) 84:466–75. doi: 10.1016/j.neuroimage.2013.09.015
27. Vergun S, Deshpande AS, Meier TB, Song J, Tudorascu DL, Nair VA, et al. Characterizing functional connectivity differences in aging adults using machine learning on resting state fMRI data. *Front Comput Neurosci*. (2013) 7:38. doi: 10.3389/fncom.2013.00038
28. Uddin LQ, Menon V, Young CB, Ryali S, Chen T, Khouzam A, et al. Multivariate searchlight classification of structural magnetic resonance imaging in children and adolescents with autism. *Biol Psychiatry*. (2011) 70:833–41. doi: 10.1016/j.biopsych.2011.07.014

29. Hughes AJ, Daniel SE, Kilford L, Lees AJ. Accuracy of clinical diagnosis of idiopathic Parkinson's disease: a clinico-pathological study of 100 cases. *J Neurol Neurosurg Psychiatry*. (1992) 55:181–4. doi: 10.1136/jnnp.55.3.181
30. Yan CG, Wang XD, Zuo XN, Zang YF. DPABI: data processing and analysis for (Resting-State) brain imaging. *Neuroinformatics*. (2016) 14:339–51. doi: 10.1007/s12021-016-9299-4
31. Chai XJ, Castanon AN, Ongur D, Whitfield-Gabrieli S. Anticorrelations in resting state networks without global signal regression. *Neuroimage*. (2012) 59:1420–8. doi: 10.1016/j.neuroimage.2011.08.048
32. Scholvinck ML, Maier A, Ye FQ, Duyn JH, Leopold DA. Neural basis of global resting-state fMRI activity. *Proc Natl Acad Sci USA*. (2010) 107:10238–43. doi: 10.1073/pnas.0913110107
33. Zhang C, Yang H, Qin W, Liu C, Qi Z, Chen N, et al. Characteristics of resting-state functional connectivity in intractable unilateral temporal lobe epilepsy patients with impaired executive control function. *Front hum Neurosci*. (2017) 11:609. doi: 10.3389/fnhum.2017.00609
34. Yan CG, Yang Z, Colcombe S, Zuo XN, Milham M. Concordance among indices of intrinsic brain function: insights from inter-individual variation and temporal dynamics. *Sci Bull*. (2017) 23:1572–84. doi: 10.1016/j.scib.2017.09.015
35. Zalesky A, Breakspear M. Towards a statistical test for functional connectivity dynamics. *Neuroimage*. (2015) 114:466–70. doi: 10.1016/j.neuroimage.2015.03.047
36. Liu F, Guo W, Yu D, Gao Q, Gao K, Xue Z, et al. Classification of different therapeutic responses of major depressive disorder with multivariate pattern analysis method based on structural MR scans. *PLoS ONE*. (2012) 7:e40968. doi: 10.1371/journal.pone.0040968
37. Cavanna AE, Trimble MR. The precuneus: a review of its functional anatomy and behavioural correlates. *Brain*. (2006) 129(Pt 3):564–83. doi: 10.1093/brain/awl004
38. Gusnard DA, Akbudak E, Shulman GL, Raichle ME. Medial prefrontal cortex and self-referential mental activity: relation to a default mode of brain function. *Proc Natl Acad Sci USA*. (2001) 98:4259–64. doi: 10.1073/pnas.071043098
39. Nobili F, Abbruzzese G, Morbelli S, Marchese R, Girtler N, Dessi B, et al. Amnestic mild cognitive impairment in Parkinson's disease: a brain perfusion SPECT study. *Mov Disord*. (2009) 24:414–21. doi: 10.1002/mds.22381
40. Tang CC, Poston KL, Dhawan V, Eidelberg D. Abnormalities in metabolic network activity precede the onset of motor symptoms in Parkinson's disease. *J Neurosci*. (2010) 30:1049–56. doi: 10.1523/JNEUROSCI.4188-09.2010
41. Syrimi ZJ, Vojtisek L, Eliasova I, Viskova J, Svatkova A, Vanicek J, et al. Arterial spin labelling detects posterior cortical hypoperfusion in non-demented patients with Parkinson's disease. *J Neural Transm*. (2017) 124:551–7. doi: 10.1007/s00702-017-1703-1
42. Hu X, Song X, Li E, Liu J, Yuan Y, Liu W, et al. Altered resting-state brain activity and connectivity in depressed Parkinson's disease. *PLoS ONE*. (2015) 10:e0131133. doi: 10.1371/journal.pone.0131133
43. Thibes RB, Novaes NP, Lucato LT, Campanholo KR, Melo LM, Leite CC, et al. Altered functional connectivity between precuneus and motor systems in Parkinson's disease patients. *Brain Connect*. (2017) 7:643–7. doi: 10.1089/brain.2017.0534
44. Chen B, Wang S, Sun W, Shang X, Liu H, Liu G, et al. Functional and structural changes in gray matter of Parkinson's disease patients with mild cognitive impairment. *Eur J Radiol*. (2017) 93:16–23. doi: 10.1016/j.ejrad.2017.05.018
45. Shin JH, Shin SA, Lee JY, Nam H, Lim JS, Kim YK. Precuneus degeneration and isolated apathy in patients with Parkinson's disease. *Neurosci Lett*. (2017) 653:250–7. doi: 10.1016/j.neulet.2017.05.061
46. Barbagallo G, Caligiuri ME, Arabia G, Cherubini A, Lupo A, Nistico R, et al. Structural connectivity differences in motor network between tremor-dominant and nontremor Parkinson's disease. *Hum Brain Mapp*. (2017) 38:4716–29. doi: 10.1002/hbm.23697
47. Canu E, Agosta F, Sarasso E, Volonte MA, Basaia S, Stojkovic T, et al. Brain structural and functional connectivity in Parkinson's disease with freezing of gait. *Mol Neurobiol*. (2015) 36:5064–78. doi: 10.1002/hbm.22994
48. Jia X, Li Y, Li K, Liang P, Fu X. Precuneus dysfunction in Parkinson's disease with mild cognitive impairment. *Front Aging Neurosci*. (2018) 10:427. doi: 10.3389/fnagi.2018.00427
49. Ascherio A, Schwarzschild MA. The epidemiology of Parkinson's disease: risk factors and prevention. *Lancet Neurol*. (2016) 15:1257–72. doi: 10.1016/S1474-4422(16)30230-7

Conflict of Interest: The authors declare that the research was conducted in the absence of any commercial or financial relationships that could be construed as a potential conflict of interest.

Advantages of publishing in Frontiers

OPEN ACCESS
Articles are free to read for greatest visibility and readership

FAST PUBLICATION
Around 90 days from submission to decision

HIGH QUALITY PEER-REVIEW
Rigorous, collaborative, and constructive peer-review

TRANSPARENT PEER-REVIEW
Editors and reviewers acknowledged by name on published articles

Frontiers
Avenue du Tribunal-Fédéral 34
1005 Lausanne | Switzerland

Visit us: www.frontiersin.org
Contact us: info@frontiersin.org | +41 21 510 17 00

REPRODUCIBILITY OF RESEARCH
Support open data and methods to enhance research reproducibility

DIGITAL PUBLISHING
Articles designed for optimal readership across devices

FOLLOW US
@frontiersin

IMPACT METRICS
Advanced article metrics track visibility across digital media

EXTENSIVE PROMOTION
Marketing and promotion of impactful research

LOOP RESEARCH NETWORK
Our network increases your article's readership